Investigation of machining forces during constant velocity drilling in SACE (Spark Assisted Chemical Engraving) Technology

Nandkishor Motiram Dhawale

A Thesis

in

the Department

of

Mechanical and Industrial Engineering

Presented in partial fulfillment of the requirements
for the Degree of Master of Applied Science (Mechanical Engineering) at
Concordia University
Montreal, Quebec, Canada
November 2009

Your file Votre référence
ISBN: 978-0-494-67096-5
Our file Notre référence
ISBN: 978-0-494-67096-5

ABSTRACT

Investigation of machining forces during constant velocity drilling in SACE (Spark Assisted Chemical Engraving) Technology

Nandkishor Dhawale

***S**park **A**ssisted **C**hemical **E**ngraving (SACE)* is a non conventional technology used for micro machining and drilling in non-conductive materials like glass, quartz and ceramics. The drilling can be done by penetrating the tool in work-piece. The penetrating strategies could be gravity feed drilling, *constant velocity drilling* and feedback based drilling. To optimize the material removal rate, without damaging the drill-hole quality, all of these strategies are investigated for practical applications, out of which gravity feed is found well characterized by now.

Investigation and characterization of *constant velocity drilling*, still remains one of the underdeveloped areas in *SACE*. It is certainly presumed that investigation on forces acting at the tool-work piece contact point can be a potential tool in characterizing a *constant velocity drilling* process for *SACE*. It is also understood that studying such forces exerted on the tool during *constant velocity drilling*, can help in identifying and implementing the finest feedback control strategies for *SACE* drilling technology.

This thesis report presents the outcome on investigated real-time forces, acting at the tool-work piece contact point during various constant velocity drilling experiments for *SACE* Technology.

ACKNOWLEDGMENTS

The project has been carried out at Concordia University Montreal (Quebec, Canada) in the Department of Mechanical & Industrial Engineering. The work of this thesis represents the concerted efforts of many individuals. The research work includes involving a very wide area of technical domain such as mechatronics, chemical and electronics engineering where different features are treated.

So it is that I begin my thanks to all those who encouraged and supported me with their expertise during the process of my work on this thesis. Firstly I begin by thanking my supervisor - Associate Professor at Concordia University, Dr. Rolf Wüthrich, without his help, support and guidance the research couldn't have been possible. I am indebted to him for his constant support and motivation which inspired me to undertake this work. I would also express my sincere gratitude and thanks to Mr. Dan Juras, Mr. Gilles Huard and Mr. Robert Oliver for guiding me to build the setup parts and certain prototypes for my experiment.

And lastly and most importantly I want to thank my father who has been my source of encouragement and inspiration throughout.

Words can never express how grateful I will ever be to all these people.

Thank you so much.

DEDICATION

To my family and friends I dedicate this.

Table of Contents

Table of contents detailed

List of Figures

List of Tables

List of symbols

Notation	Interpretation
μ	Micro-meters
a	Area of flexible structure
A	Area of tool tip.
B	Viscous damping
b	Breadth of work-piece
C_v	Voice coil coefficient
d	Damping of flexible structure
E	Youngs modulus of glass (Work-piece)
e_s	Error signal
F	Force
f	Typical force value
$F^{v\text{-}c}$	Force due to voice coil
$F_a(t)$	Force from SACE drilling model
F^{ext}	External force
f_{max}	Maximum force due to gas film
F^r	Friction force
h	Height of tool
i	Current in voice coil
I_A	Inertial moment of a horizontal rode from the clumping point
I_M	Inertial moment of flexible structure
I_m	Inertial mass of work-piece
k	Mechanical stiffness of flexible structure
K_0	Non-machining stiffness in model
k_0	Non machining stiffness in data
K_1	Stiffness due to tool-machine head assembly
k_1	Initial stiffness in classified types
K_2	Stiffness due to work-piece assembly
k_2	Later stiffness in classified trends
K_D	Derivative Gain
K_{eq}	Equivalent stiffness of drilling model
K_I	Integral Gain
K_P	Proportional Gain
K_u	Ultimate Gain
K_z	Angular rigidity of flexible structure
l	Length of mass M_1
LO_t	Original length of tool
LO_w	Original Height of work Piece
L_t	Final length of tool
L_w	Final height of work-piece
m	Inertial mass of tool-head assembly
M	Mass of flexible structure

M_1	Horizontal mass of the flexible structure
M_2	Vertical mass of flexible structure
N	Constant
P	Pressure
Pi	Constant
P_{max}	Maximum pressure in gas film (bubble)
R	Radius
T	Time
T	Time
T_D	Time for derivative
T_I	Time for integral
T_m	Temperature in work-piece molten zone.
T_t	Integrator reset time
T_u	Ultimate period
U^{crit}	Critical voltage
V	Velocity
V/I	Voltage to current converter
V_{lim}	Limiting speed
W_{max}	Maximum deflection for work-piece
$Wt.$	Weight
X_0	Distance of Z stage from datum
X_1	Distance of flexible structure from datum
X_2	Distance of Work-piece surface from datum
Z	Displacement in Z direction
z_0	Work-piece surface touching distance for non-machining experiments
z_1	Work-piece surface touching distance for drilling experiments
z_e	Error in surface touching distance
α_t	Thermal expansion coefficient for tool material
α_w	Thermal expansion coefficient for work-piece material
ΔL_t	Change in toll length due to thermal expansion
ΔL_w	Change in Work-piece height due to thermal expansion
ΔT	Change in temperature
ΔT_t	Change in temperature for tool
ΔT_w	Change in temperature for work-piece
H	Viscosity in molten zone
Ξ	Damping ratio
Π	Constant
T	Time constant in drilling model
Φ	Diameter
Φ	Diameter of tool
ωn	Natural frequency of flexible structure

Chapter 1

Introduction and literature review

Introduction

This master's thesis takes place in the scope of research on development of a real-time force measurement setup and investigation's of machining forces during SACE (Spark Assisted Chemical Engraving) constant feed drilling, an unconventional machining technology.

Spark Assisted Chemical Engraving (SACE) is a promising technology for micro-machining several types of materials like glass quartz, polymers and some ceramics [1-5]. The foundation for SACE emerges from electrical chemical discharges, first developed by Kurafuji and Suda [10].

Using SACE machining, it is possible to drill holes with a diameter in the order of 100 μm to 1 mm diameter. The two most familiar drilling strategies are constant feed and gravity feed [5]. Constant feed involves pushing the tool-electrode into the work piece at a constant velocity, while gravity involves penetrating the tool into the work piece with a constant force. In both cases the voltage between the two electrodes is kept constant. These are both open loop strategies, and usually, it is not always possible to generate reproducible results by using SACE in open loop. Thus implementing a well designed closed loop controller for the process could fix this issue. An important step toward designing a controller is to model the dynamics of the SACE machining system [43].

To the author's best knowledge, before the work presented in this report, very few closed loop controllers, has been attempted on SACE. One known attempt was to reduce the

variability in drilling, for gravity feed. In [39] for the first time, a proportional feedback controller was applied, on SACE. A decrease in the standard deviation in the depth evolution of the process was reported. Such a lessening in the standard deviation of the depth evolution is essential because the variability of the quality and the variability of the depth evolution are linked [40]. The strong results obtained with a proportional controller indicate more study is desirable. To enhance such studies, characterization of the fundamentals involved in SACE drilling technologies can be an essential step.

1.1 Principle of SACE

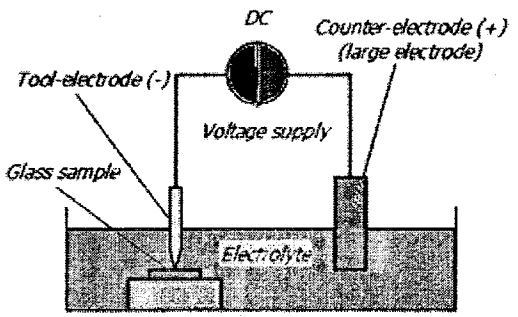

Figure 1.1- General SACE Setup.

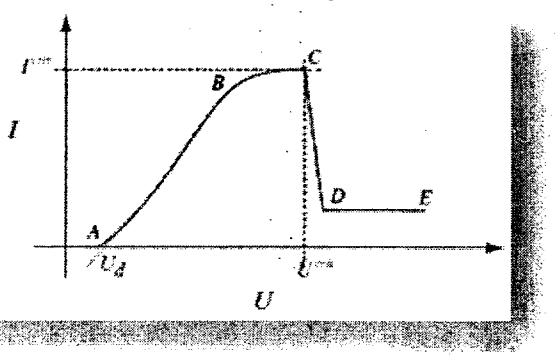

Figure 1.2 - Current-Voltage characteristic [41].

Figure 1.1 shows the general set up of a SACE drilling apparatus [5]. The process takes place in an electrochemical cell with two electrodes in an electrolyte (figure 1.1). The electrolyte solution is typically sodium hydroxide (30 % wt.) or potassium hydroxide (30 % wt.). In general the cathode is used as tool-electrode and the anode as counter-electrode. The surface ratio (counter electrode/tool-electrode) has to be high enough so the electro chemical discharges can take place.

When the applied voltage is higher than a critical value (typically around 30V, depending on the electrolyte and the tool-electrode geometry) bubbles develop so dense on the

electrode surface that they coalesce into a gas film [6]. This voltage, written U^{crit} (figure 1.3), depends on the electrolyte composition and the work-piece material.

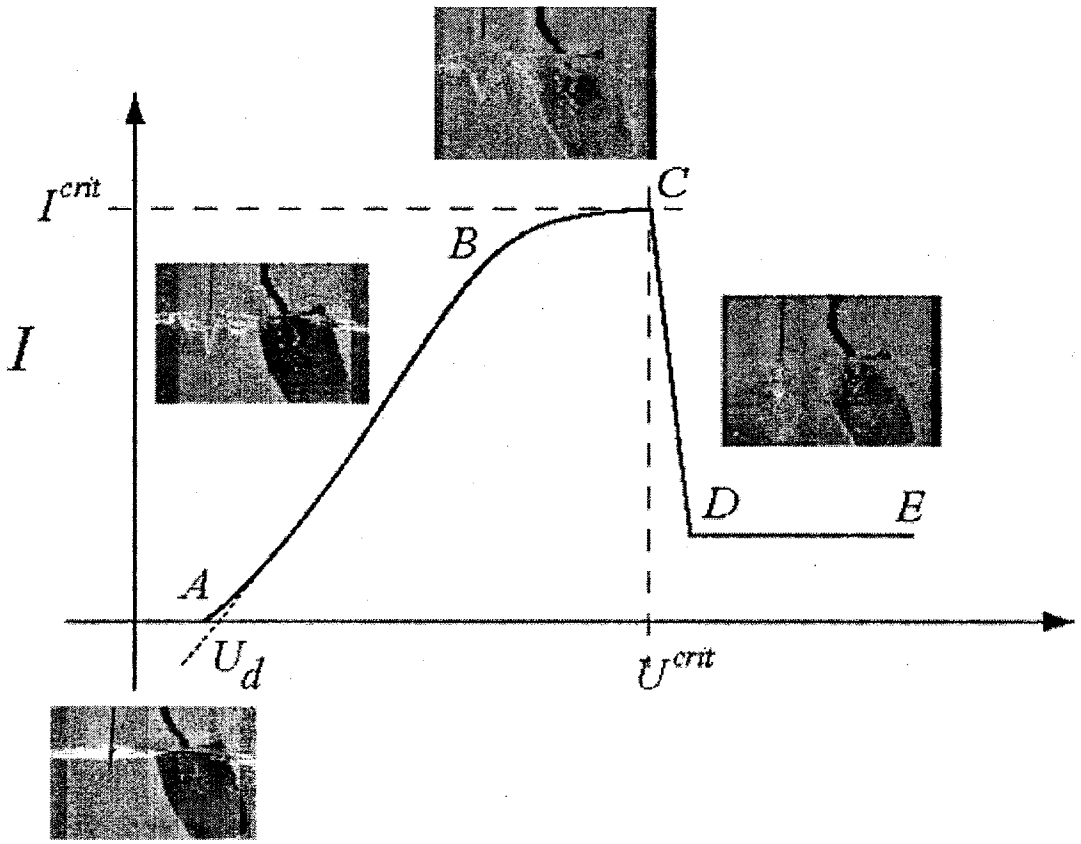

Figure 1.3- Detailed current-voltage characteristic [41].

Electrical discharges occur between the electrode and the electrolyte. The discharges are what cause the glass sample to be machined. Currently, the machining mechanism is believed to be a combination of local melting and chemical etching [7]. Machining starts if the electrode is placed close enough, in general not greater that 25 μm for glass, above the work-piece [7]. The heat produced by the discharges locally melts the work sample [7]. Chemical effects also do probably take place. The process can be put into practice on

a table top machine [7] and does not need any expensive clean room environment or facilities.

1.2 The machined material

Since the machining takes place in a chemical environment, it is interesting to learn further about the work pieces material in order for a better understanding about the outcome of machining. Work-pieces used in this study are standard microscope slides produced by "Menzel Glaser", (softening littleton point 720°C) whose approximate chemical composition is presented in the Table 1.1 [35].

Silicon Dioxide	SiO_2	72.20%
Sodium Oxide	Na_2O	14.30%
Potassium Oxide	K_2O	1.20%
Calcium Oxide	CaO	6.40%
Magnesium Oxide	MgO	4.30%
Aluminum Oxide	$AL2O_3$	1.20%
Ferric Oxide	Fe_2O_3	0.03%
Sulfur Trioxide	SO_3	0.30%

Table 1.1- Chemical composition of sample (according to the manufacturer Menzel Glaser).

When immersed in alkaline solutions, glass is susceptible to chemical modifications. Such modifications manifest a change of the surface composition [9]. These changes depend on the glass material itself and the nature of the alkaline solution. The mechanism which is associated with above mentioned paragraph is called etching, in which the alkaline solution attacks the glass, where it is hydrated and totally dissolved by breaking the Si-O-Si bond on the surface of the glass (figure 1.5).

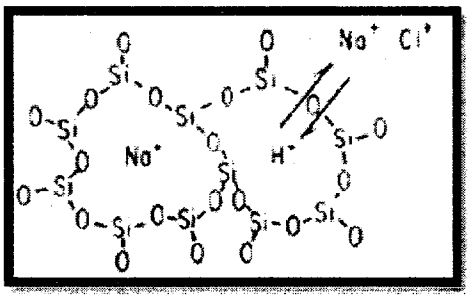

Figure 1.4-Leaching of glass [35].

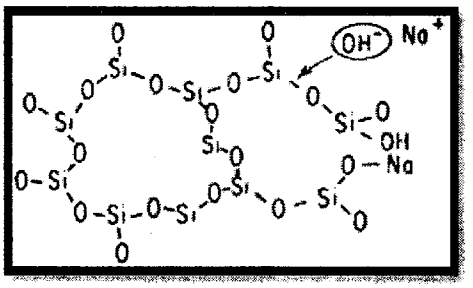

Figure 1.5- Etching of glass [35].

The reaction is

$$OH^- + \equiv Si - O - Si \equiv \rightarrow \equiv SiO^- + \equiv SiOH \qquad (1.1)$$

The reaction with NaOH can be written as follows:

$$2xNaOH + xSiO_2 \rightarrow xNa_2\,SiO_3 + xH_2O \qquad (1.2)$$

The chemical attack rate varies essentially with the temperature and the pH of the solution.

1.3 Micro-machining with SACE

Machining with SACE is a multifaceted process influenced by several parameters most of them not independent [28]. Several experimentations have been reported in order to understand the process and showed that it depends on chemical, mechanical and electrical parameters. Influence of several parameters, like electrolyte properties, applied voltage and others was reported in [3]. The material removal rate increases with the applied voltage [11, 12] and electrolyte temperature [3, 12, 13].

Figure 1.6 and 1.7 show prototype devices built, using simple glass slides. These glass slides are *2D* machined using SACE technology. [38]

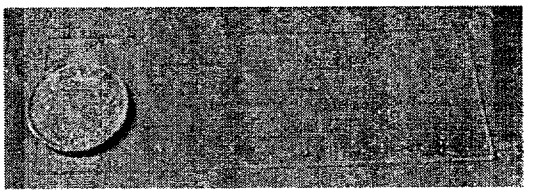

Figure 1.6- Micro-reactor to be used as a cultivation chamber for biosensor cell, machined by SACE glass[38].

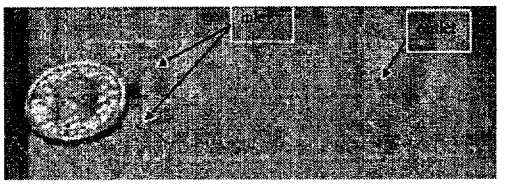

Figure 1.7-Micro-rector for chemical applications can be machined by SACE in diffusion mimicked [38].

1.4 Micro-hole drilling with SACE.

So far mainly two drilling strategies (gravity feed and constant velocity feed) are used for SACE. Both of these strategies are investigated in more details for useful applications.

1.4.1 Gravity feed drilling

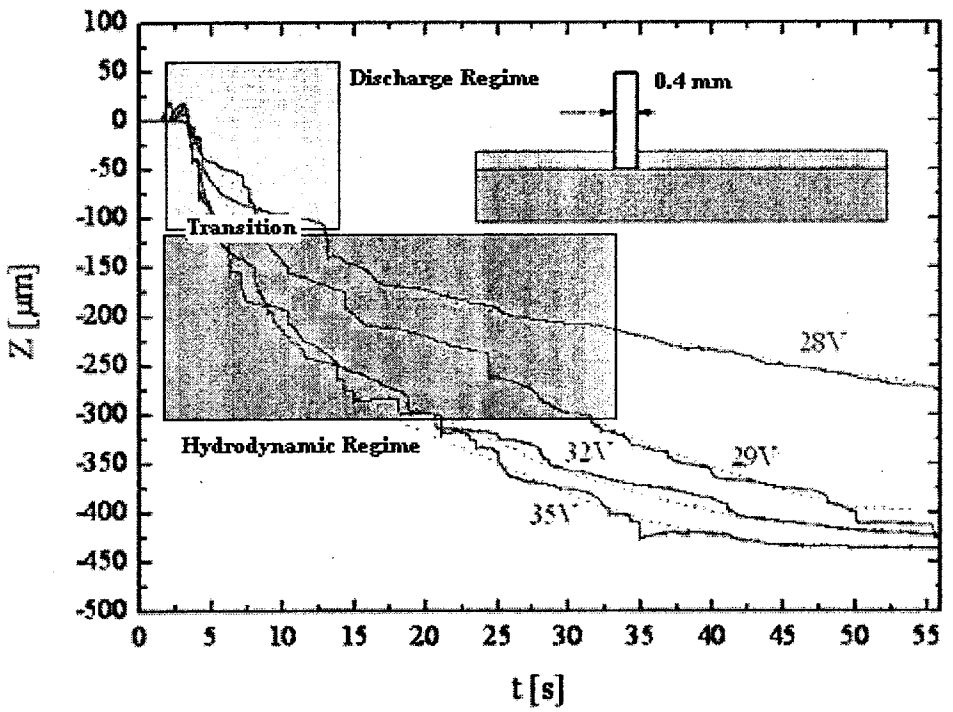

Figure 1.8- Evolution for gravity feed drilling [40].

Details on characterizations for gravity feed strategies can be found in [16-19]. It was found that gravity-feed drilling is characterized by two regimes (figure 1.9). During the discharge regime, in the first 100-200 microns, the drilling is fast (up to 100 μm/s) and controlled by the number of discharges (applied voltage). For higher depth, in the hydrodynamic region, drilling becomes slower (typically around 1 to 1.5 μm/s) and is nearly independent of applied voltage.

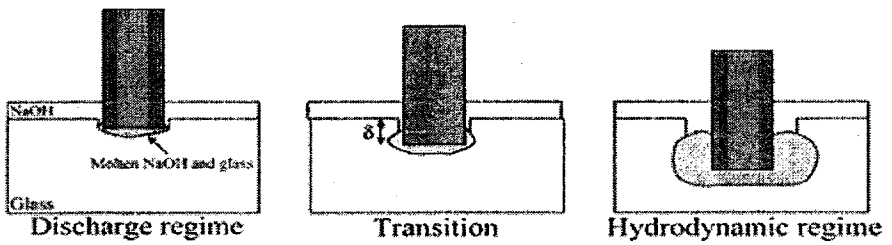

Figure 1.9-Characterization of gravity feed drilling [40].

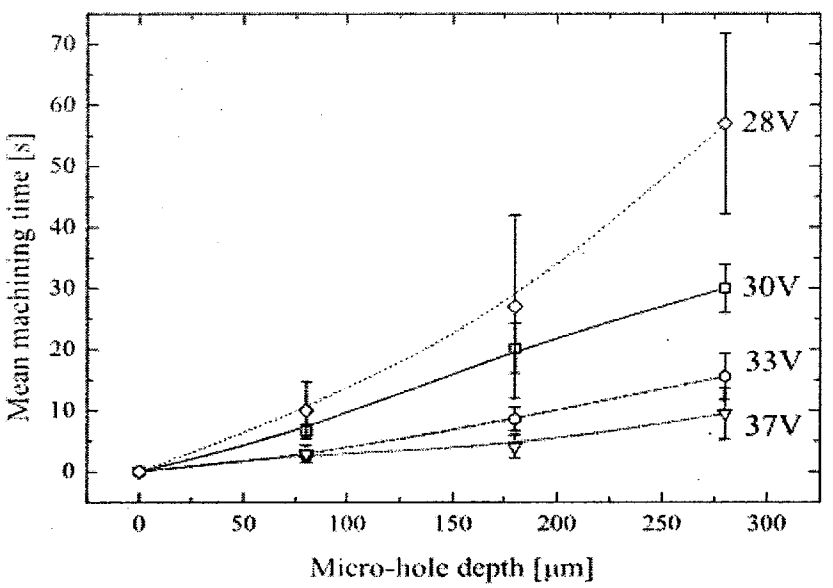

Figure 1.10- Drilling time in SACE glass gravity-feed drilling for a 0.4mm cylindrical S.S tool-cathode in 30 % wt. NaOH [36].

In the hydrodynamic regime, the machining rate is probably controlled by the ability of the electrolyte to reach the tool-electrode tip and the ability of removing the melted material.

Drilling time in gravity-feed machining is mainly determined by the drilling depth of the hole and the machining voltage as shown in figure 1.10 (0.4mm cylindrical stainless steel tool-cathode in 30%wt NaOH [18, 19]). Typical drilling times for glass are a few seconds for micro-holes of about 200-300 μm. For deeper holes, the machining switches to the hydro-dynamic regime and drilling times increases significantly.

1.4.2 Example of samples

Figure 1.11 and 1.12 shows an illustration of micro holes drilled in glass using gravity feed [35]. The quality of gravity-feed drilling has been characterized [18]. It shows that four different kinds of holes can be distinguished depending on the applied voltage and drilling depth (figure 1.12).

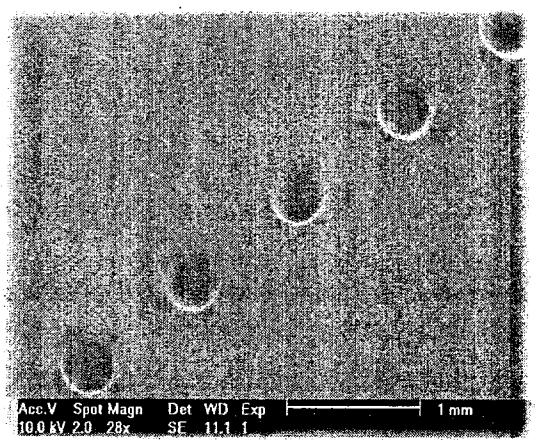

Figure 1.11- Micro holes drilled in glass [35].

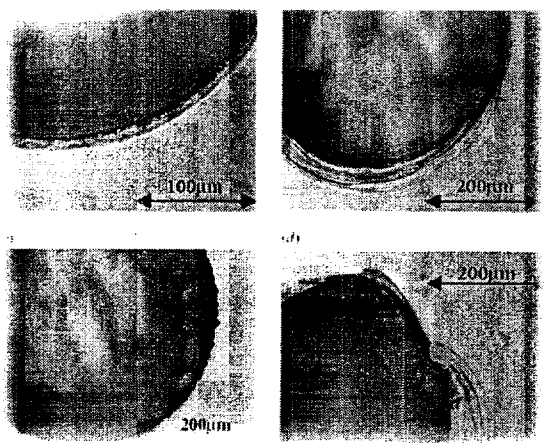

Figure 1.12- 4 different qualities of drilled holes [35].

The best quality of hole is found mostly at lower voltages giving a drawback of low material removal rate.

1.4.3 Mechanism

Figure 1.13, show, heat generated by electrochemical discharges, increases locally the temperature of the glass up to typically T_m=550° C, lowering its viscosity. Chemical etching by OH radicals removes the melted material [1]

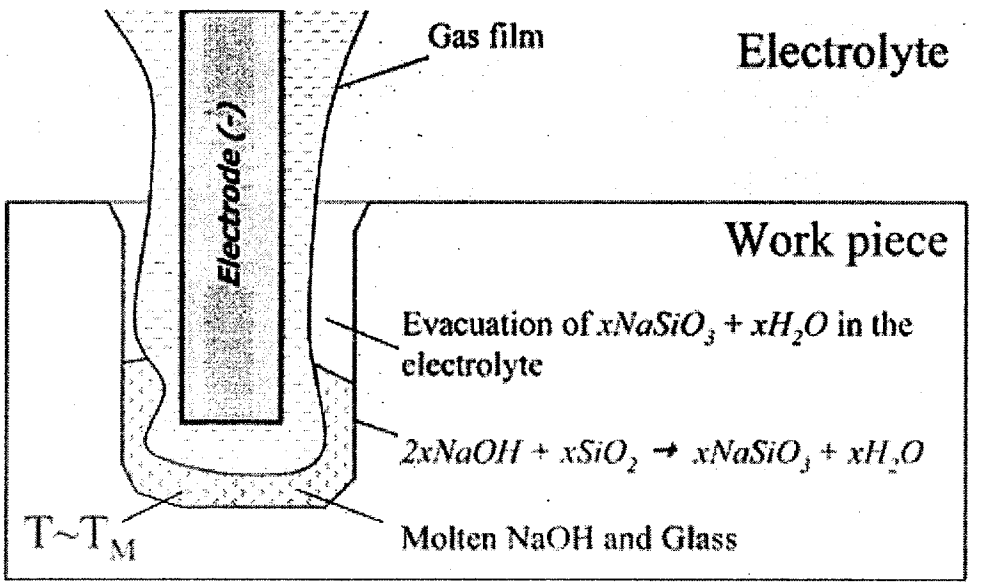

Figure 1.13- Temperature distribution and machining mechanism [36].

1.5 Constant feed drilling

From the literature review it is clear that so far no systematic work has been done in characterizing constant velocity drilling for SACE. Constant velocity differs to gravity feed by avoiding any mechanical contact between tool-electrode and work-piece [36]. Using this strategy the problem of electrode bending can be avoided, however it can be hard to control the gap between the same, resulting to inability for online monitoring of

the drilling progress. Constant feed drilling is advantageous towards having control on the tool-electrode motion, giving the capability to drill much complex shapes than simple cylindrical holes. [36]

The tool feed rate is the key parameter to be selected earlier, depending on the material removal rate of the process to avoid any heat affected zones around the micro-hole or breaking of tool and work-piece [36]. So far only few studies on optimal feed rate were conducted. Depending on the tool diameter the typical values are reported to be around 5-15 μm/s [7]. These values can be slightly higher than the limiting speed reached in the hydrodynamic regime during gravity feed drilling.

As in gravity feed drilling, the mean drill-hole diameter increases with drilling depth [7]. It is found that high enough depths are succeeded with maximal drill-hole diameter. This can be associated with lack of electrolyte reaching the machining zone, consequently shifting the discharge activity to the upper part of tool-electrode resulting to enlargement of drill hole at the entrance.

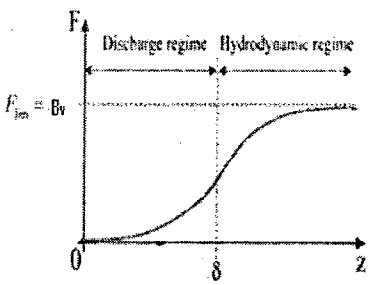

Figure 1.14- Assumption of the behavior of machining force [35].

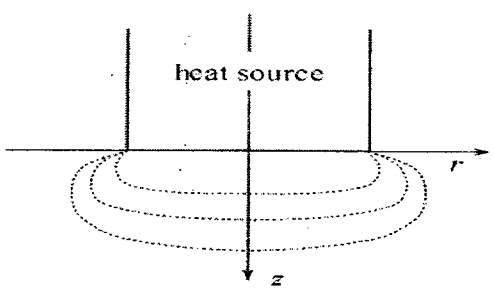

Figure 1.15- Tool as heat source model [35].

Based on the understandings obtained from gravity feed drilling, the behavior of constant velocity drilling can be presumed. Figure 1.14 shows a typical guess on, machining forces acting on the tool in function of the drilling depth.

The tool (figure 1.15 and 1.12) is assumed to be a heat source, of generating a heat due to electrochemical discharges. The temperature is estimated to be 550°C. At this high temperature the work piece could be melted in vicinity area around the tool due to heat, the viscosity of molten work-piece-electrolyte at this temperature is expected to be around a typical value of $\eta = 1.4 \times 10^8\ Pa.s$ [35]. The force acting on the tool is assumed to be the viscous forces acting in the molten zone. The forces are in function of the drilling depth and are expected to be low during the discharge regime and to grow until a limiting value in the hydrodynamic regime. The reason for such behavior is assumed to be due to the electrolyte's inability to reach the machining zone, (see figure 1.12) during the drilling at high depths.

Using the same setup of gravity feed drilling, constant velocity drilling strategy can be implemented, by changing the motion stage software and adding a separate digitally realized, real-time position feed-back controller.

1.6 Feedback systems

Feedback is used to control machines. Feedback is both a mechanism process and signal that is looped back to a control system within itself. This loop is called a feedback loop. A control system usually has a input and output to the system, when the output of the system is fed back into the system as part of its input it is called the feedback [34]. Feedback and regulation are self related. The negative feedback helps to maintain

stability in a system in spite of external changes. It is related to homeostasis. Positive feedback amplifies possibilities of divergence (evolution change of goals). It is the condition to change, evolution, growth; it gives the system the ability to access new points of equilibrium.

The most common general-purpose controller using a control-loop feedback mechanism is a Proportional-Integral-Derivative (PID) controller. A PID controller is a simple three-term controller.

The letters P, I and D stand for:

- P - Proportional
- I - Integral
- D – Derivative

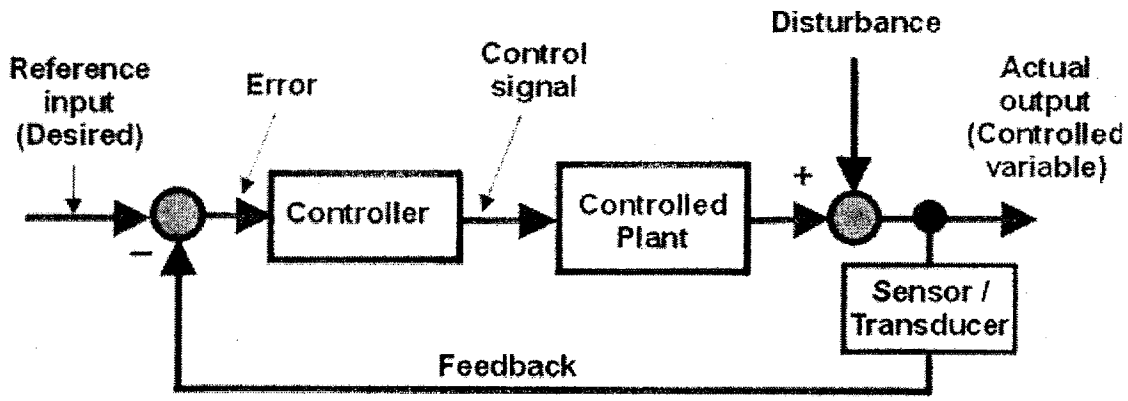

Figure 1.16- General feedback control scheme [44].

Each term of the PID controller copes with time. The proportional term handles the present state of the system, the integral term handles its past, and the derivative or slope term tries to predict and handle the future

The transfer function of the most basic form of PID controller is given as

$$C_S = K_p + \frac{K_I}{s} + K_D S = \frac{K_D S^2 + K_p S + K_I}{S} \quad (1.3)$$

Where, K_P = proportional gain, K_I = integral gain and K_D = derivative gain

All are most interested in four major characteristics of the closed-loop step response, which are.

1. **Rise Time**: the time it takes for the plant output y to rise beyond *90%* of the desired level for the first time.

2. **Overshoot**: how much the peak level is higher than the steady state, normalized against the steady state.

3. **Settling Time**: the time it takes for the system to converge to its steady state.

Response Rise	Time	Overshoot	Settling Time [S]	S-S Error
K_P	Decrease	Increase	NT	Decrease
K_I	Decrease	Increase	Increase	Eliminate
K_D	NT	Decrease	Decrease	NT

Table 1.2- Closed loop system response affected by change in PID parameters [34].

* NT stands for no definite trend or minor change.

4. **Steady-state Error**: the difference between the steady-state output and the desired output.

The change in each of the controller parameters K_P, K_I and K_D can be summarized as in table1.2

1.7 Why force measurement can help to develop constant velocity feedback strategies?

Figure 1.18 shows the interacting parameters in a typical SACE drilling technology where, it can be clearly seen that the process is very complex due to interaction of many

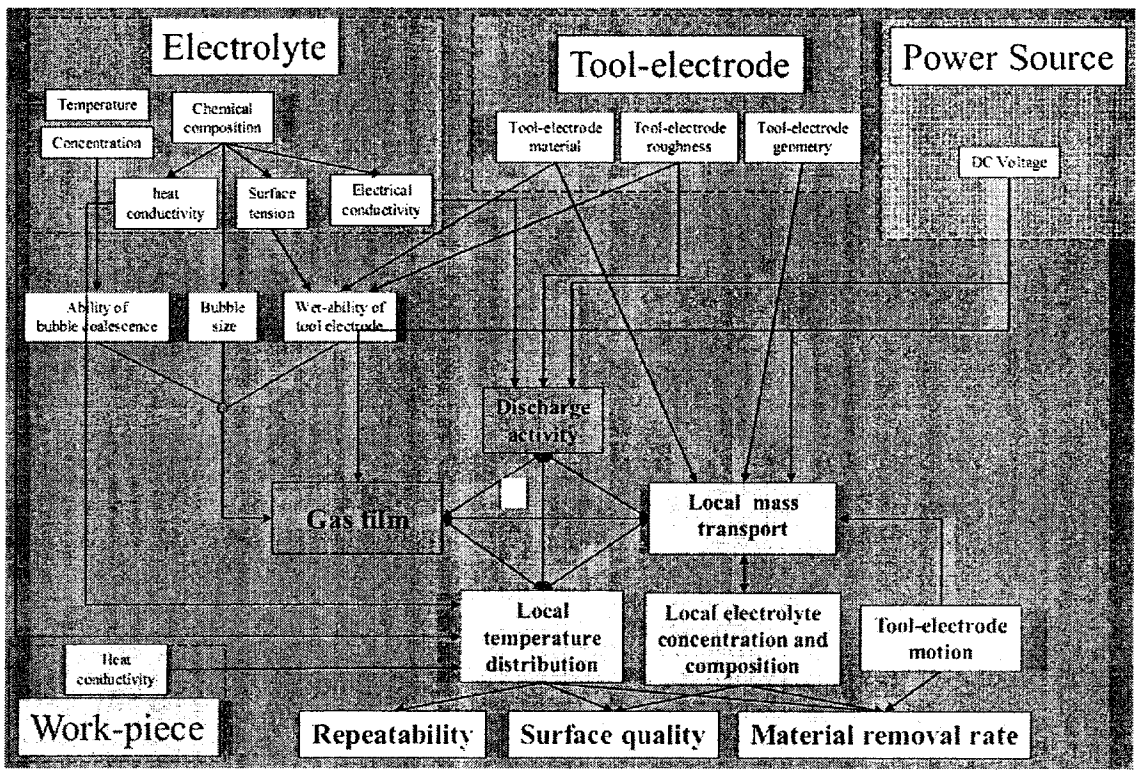

Figure 1.17-Interactions between different parameters in SACE drilling [3].

parameters. Keeping in mind, to have quality of hole as controlled parameter, then study on the parameters governing the quality of hole might be essential. The effects of most of the top parameters were systematically studied until now and good understanding is available, keeping the tool-electrode motion as one interesting parameter. Few experiments, investigating the effects of tool vibration and tool rotation, conclude that the

flow of the electrolyte inside holes during drilling can be promoted by appropriate tool-vibration and rotation [14].

Use of force-feedback control for SACE could be an interesting possibility, a systematic study on the machining forces during constant velocity drilling, could be a better step towards characterization of constant velocity drilling process, and implementing the force feedback drilling control strategies.

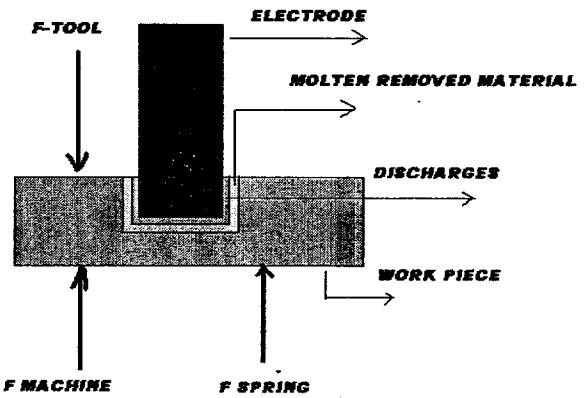

Figure 1.18-Forces acting on the work piece.

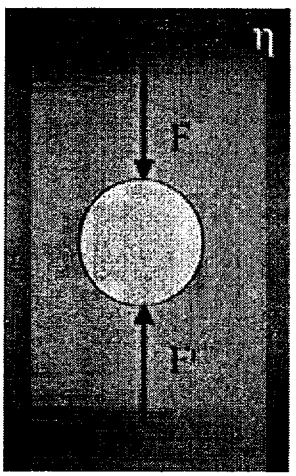

Figure 1.19-Forces acting on the work piece (simplified) [35].

Figure 1.18 and 1.19 show the general SACE drilling setup, forces like viscous damping and tool/work-piece bending are assumed to be present during the drilling process.

To measure the force acting on the tool electrode during drilling or machining process can be possible [14]. By using the measured force signal, starting with simple feedback based drilling strategies to wide complex, model based controller can be developed in future. The knowledge gained from the characterization of the force acting on the tool during constant velocity drilling process could be integrated in developing feedback based drilling methods. Such strategies are expected to improve the quality of hole while

keeping high material removal rate in SACE drilling. As example, knowing the behavior of forces as a function of drilling depths could be used to develop variable speed drilling processes. Investigations on behavior and trends of the various drilling parameters might help in developing a model based controller to speed up the drilling process.

1.8 Thesis objective and overview

The main objective of this thesis is to investigate the force exerted on the tool during a constant velocity drilling process for SACE technology.

To achieve this objective, the remaining of the thesis is divided as follows:

- Development and implementation of the force measurement setup, its characterization and its functional validation.
- Development of a model for the force exerted on the tool, during constant velocity drilling.
- Analysis of the experimental data and the results obtained.

1.8.1 Originality of work

The originality of work is defined, based on literature reviews. It is found that less efforts or mostly no work has been done towards the following approach on SACE. Successfully implementing of a real-time force measurement setup for SACE drilling technology, model of the force exerted on the tool during constant velocity SACE drilling and experimental investigations on the forces acting on the tool during constant velocity drilling using SACE technology.

1.8.2 Contribution to the field of SACE

The principal contributions of this thesis work are

- Development of a successful real-time force measurement setup.
- Model of the force exerted on the tool during constant velocity drilling.
- New findings on early force detection and its probable reasons.
- Experimental investigations on the forces acting on the tool during constant velocity drilling.

Chapter 2

Development and implementation of a real time force measurement system for SACE technology

2.1 Chapter overview

This chapter highlights the details on the available laboratory SACE machining setup, including the assembly parts and modeling of force exerted on machine head assembly followed by the techniques used in developing the real-time force measurement sensor. Summary on the parameters of the position control setup will be presented at the end.

2.2 The SACE laboratory machining setup

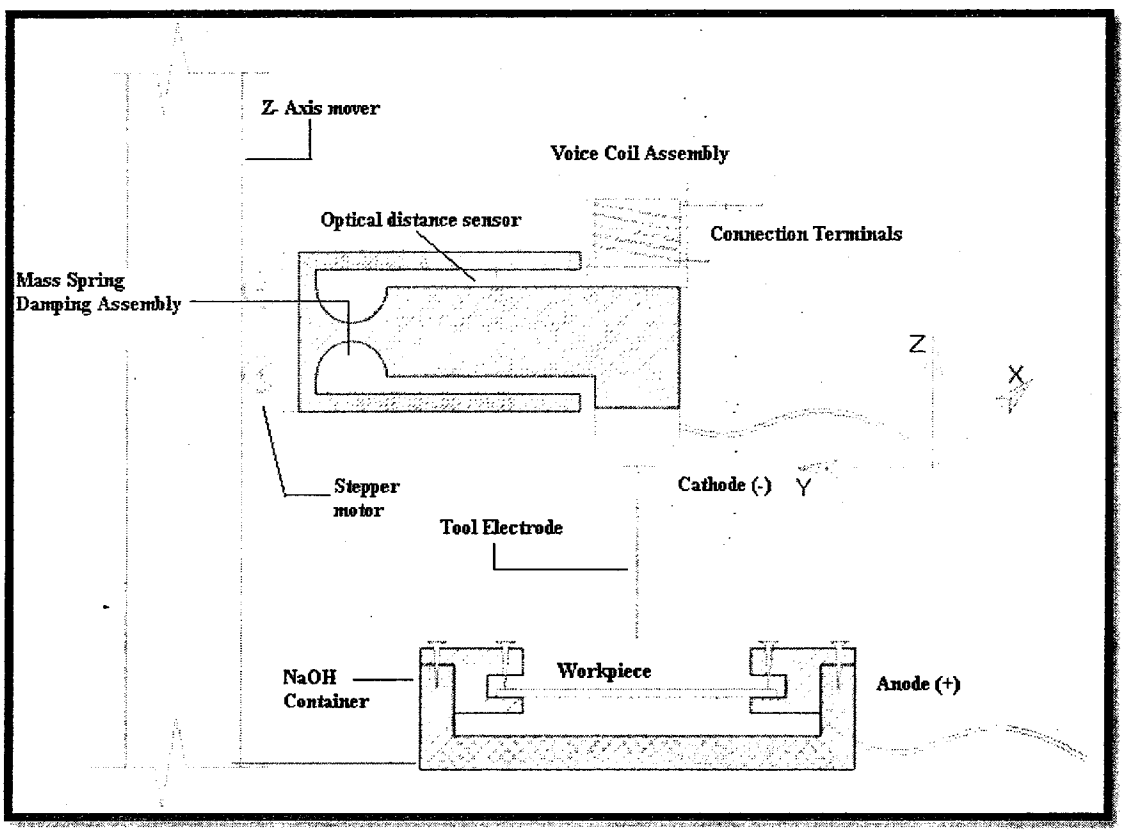

Figure 2.1- Drawing of the "SACE" Machining Setup.

As discussed previously, a real-time force measurement system can be used to develop feedback controlled drilling strategies. Knowing the future benefits, a real-time force measurement system is constructed using the available machining head assembly (figure 2.1). The desired tool-head position is controlled using a voice-coil actuator. The position is read using an optical sensor, and compared with the desired position. This error signal is fed to a PID controller.

Thus a zero displacement force measurement principle (figure 2.2), is implemented using a setup consisting of the pre-made machine head assembly, a pre-mounted optical position sensor & signal conditioning, a pre-mounted voice coil actuator, a V/I converter unit, a box for I/O connections, a computer system including a DAQ card its drivers and a real-time OS kernel called RTWT package from Matlab/Simulink. The PID control software is realized using Matlab/Simulink block models in a real time windows target environment.

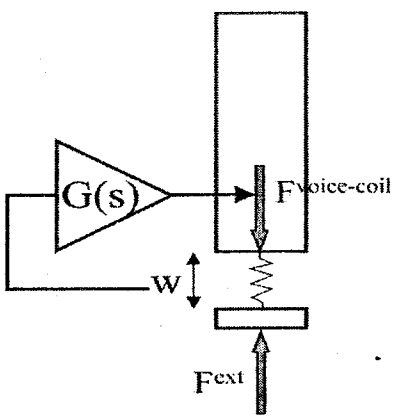

Figure 2.2 -Zero for displacement [35].

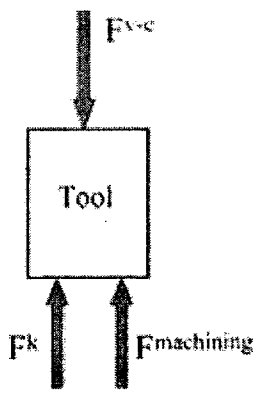

Figure 2.3- Forces acting on the tool during the machining [35].

The machine head assembly consists of position measurement sensor and signal conditioner circuitry as mounted (figure 2.1), which acts in a linear range of about 700

microns and gives an appropriate position value with a resolution better than 1 microns. The position sensor value is fed to an analog input channel of the DAQ card (12 bit resolution). The control system software calculates the appropriate output signal which is written on the analog output channel of the DAQ card and given to the voice coil assembly through a V/I converter unit.

2.3 Position control system for the machining head

The desired tool-head position (within the sensor linear range of 700 μm) can be controlled using a voice coil actuator providing a force proportionally to the driving current($f = i \times Cv$). This current is provided by a servo amplifier which also works as voltage to current converter. The voltage input to the servo amplifier is a command signal given by the digitally implemented controller. The position control is done to satisfy the need of zero displacement force measurement, discussed in the previous section. The Position control system for the flexible machine head assembly is developed using following course of action.

1. Experiment to check the linear and adequate sensitive region of the optical position sensor.
2. Experiment to identify the system using time response analysis.
3. Finally realization of position control, using Ziegler Nicholas tuning method.

2.3.1 Sensor output

As mentioned earlier any displacement of the machine head in Z direction is monitored, using an optical sensor. The output of the optical sensor is in volts. Figure 2.4- shows response of the optical sensor output in volts with respect to the actual position moved by

the flexible structure. It can be observed that, the sensor output is linear between 400-1150 μm of the flexible structure displacement. In this region the sensitivity of the optical sensor is very good (6 mV/μm).

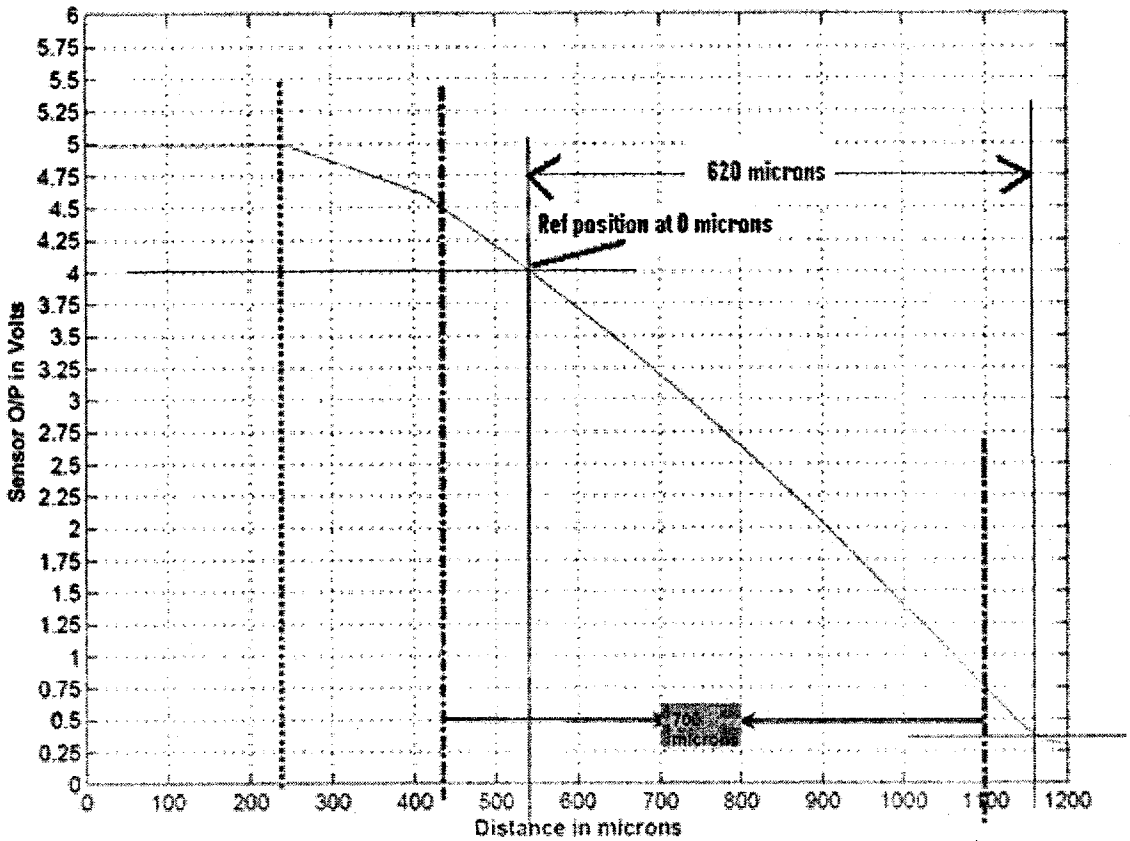

Figure 2.4-Optical sensor o/p to flexible structure movement in - Z direction (upwards).

2.3.2 Step input

The value of current in amperes, needed to lift the flexible structure is identified experimentally. Figure 2.5 shows all color coded, I/O signals. A ramp input (blue) is given to the voice coil and output (red) from optical sensor is observed. The response of the voice coil-flexible structure to ramp input is studied. It is observed that the response is

divided in to three regions, dead band, uncompensated-gravity region and finally the sensitive or active region. It is clearly visible that, the dead band can be compensated by providing 1 V and the gravity can be compensated by providing 4 V. For drilling experiments, at least 400 μm displacements is expected, thus the so called sensitive or active region is used as the range for position control.

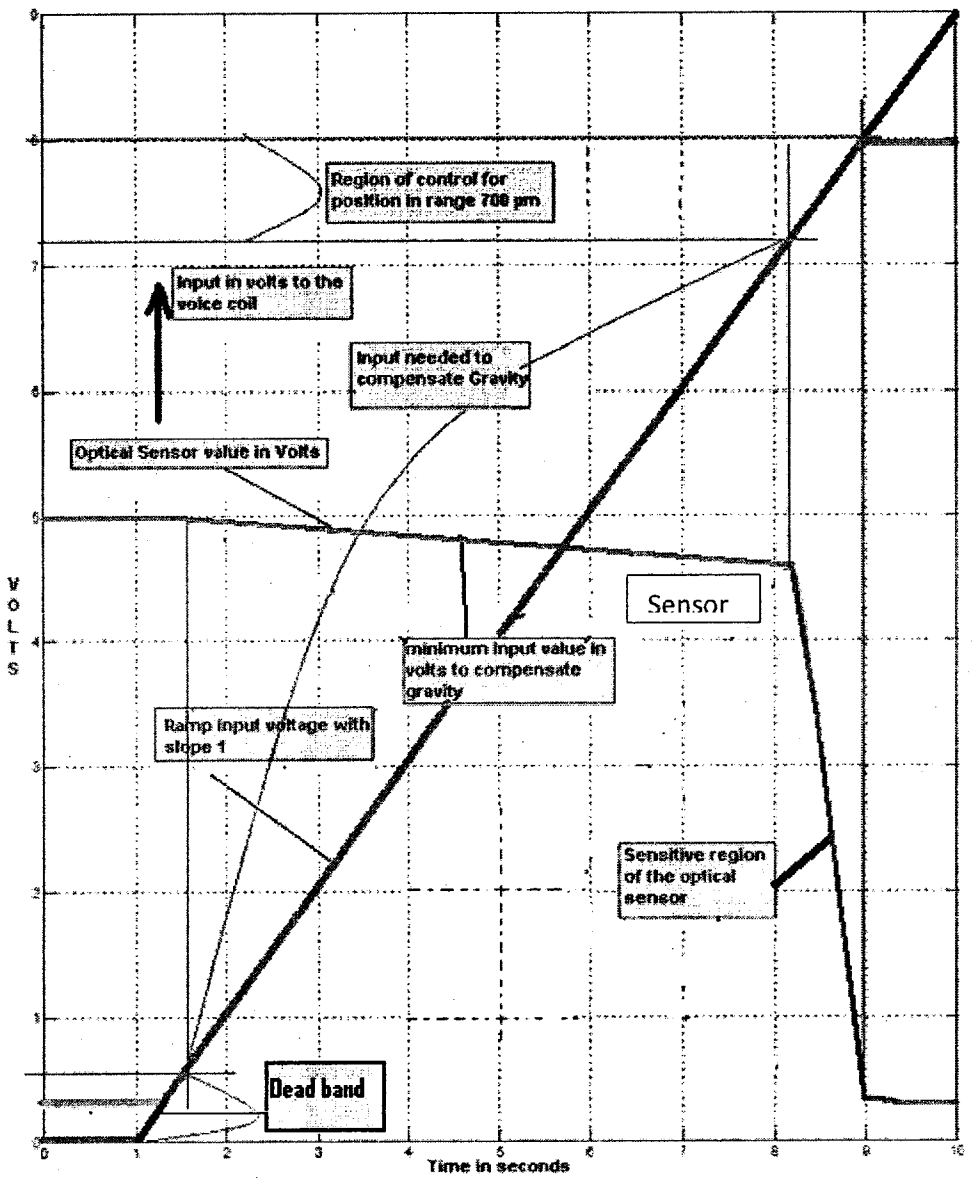

Figure 2.5-Input command in volts to voice coil Vs flexible structure movement in - Z direction (upwards).

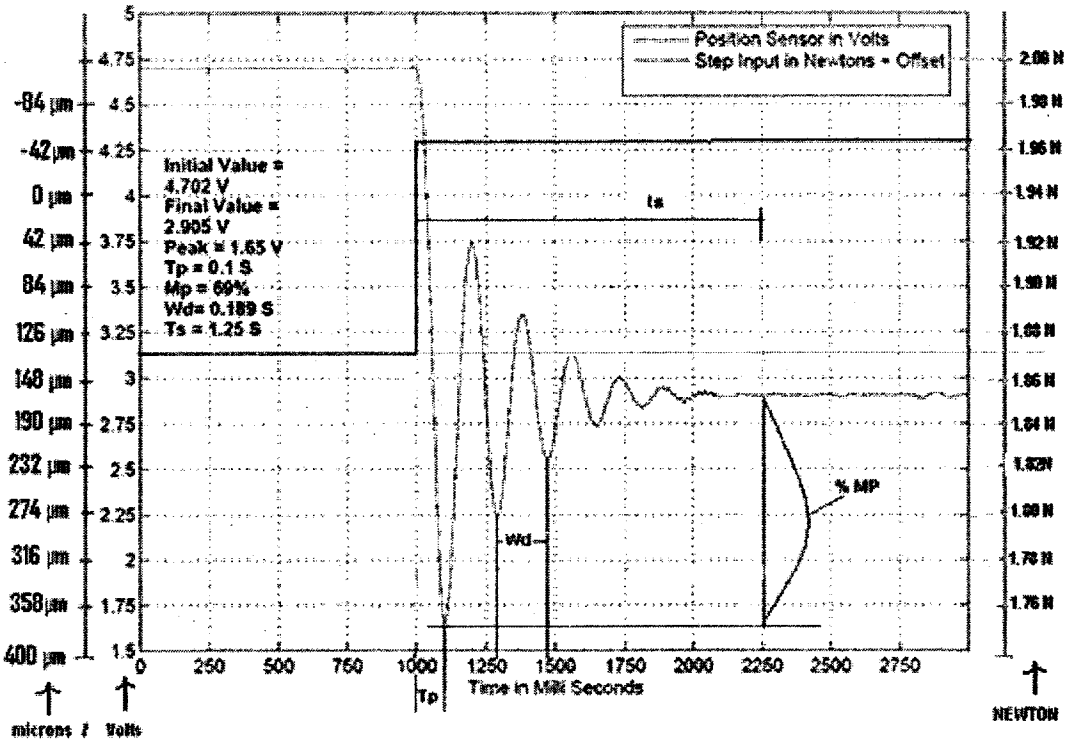

Fig 2.6- Step response for time response analysis.

2.3.3 System identification

Figure 2.6 shows the step response of the flexible structure.

The natural frequency ω_n and the damping ratio ξ are determined from the system's step response by assuming a second order system.

Percentage Peak Overshoot = $100 \times e^{-\pi(\xi/\sqrt{1-\xi^2})}$ (2.1)

Similarly we find the value for ω_n using

$$\omega_n = \omega d / \sqrt{1-\xi^2} \qquad (2.2)$$

Considering the intermediate gains and the second order system equations below

$$\frac{\omega n^2}{s^2+2\xi\omega ns+\omega n^2} \qquad (2.3)$$ Equation for second order system

Equation of the flexible structure with the considered elements

The identified system parameters are shown in table 2.2.

Parameter	**Symbol**	**Typical Value**	**Units**
Damaping Ratio	ζ	*0.12*	N/A
Natural frequency	ωn	*32.54*	*Rad/s*
Inertial Mass	*m*	*0.187*	*Kg*
Damping	*d*	*1.49*	*N-s/m*
Mechanical Stiffness	*k*	*312.55*	*N/m*

Table 2.1- Parameters after system identification.

2.3.4 Model validation

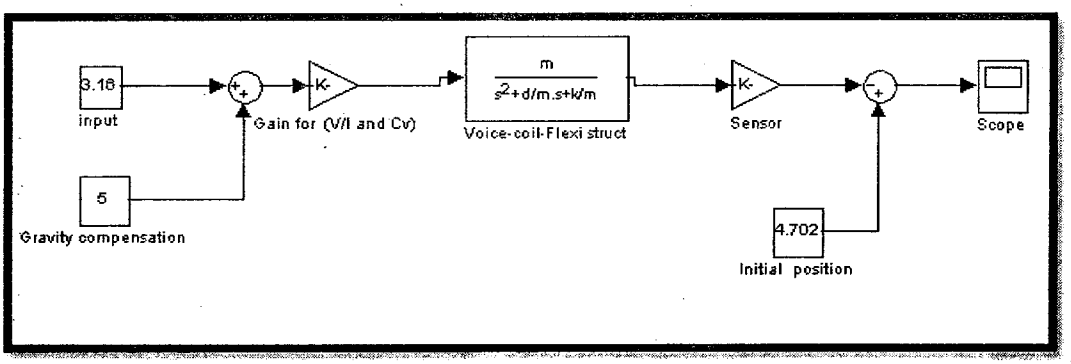

Figure 2.7-Matlab/Simulink blocks for Simulation of the identified system.

Using all the identified parameters from above it is able to simulate the step response in Matlab/Simulink. The simulink blocks are shown in figure 2.7. Data gathering from the actual step response (real-time) and the identified system simulations, figure 2.8 is

constructed. It is observed that the system is identified with an error of less than 2% (between actual and model-step response).

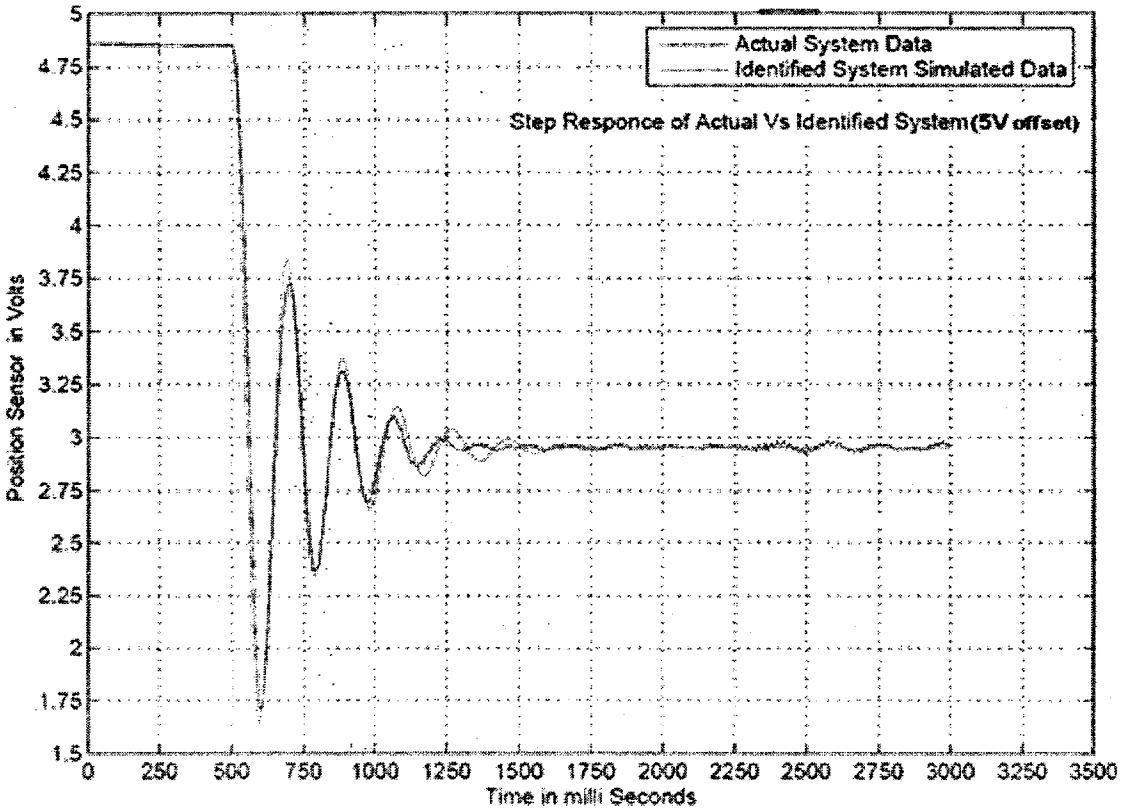

Figure 2.8- Step response of actual and simulated system.

2.4 Implementation of the position controller

The controller is realized using the hardware and software presented earlier. The structure of the implemented controller is shown in figure 2.9. The proportional gain, the integral gain and the derivative gain values are derived as follows.

The initial structure is defined and implemented such that it has very small proportional gain. Studying the response of the sensor, the value of this gain is chosen to be negative.

1. Using the Zeigler-Nichols empirical formula (table 2.2) it is able to find a first guess for the P, I & D gains. The gains were subsequently optimized for the controller.

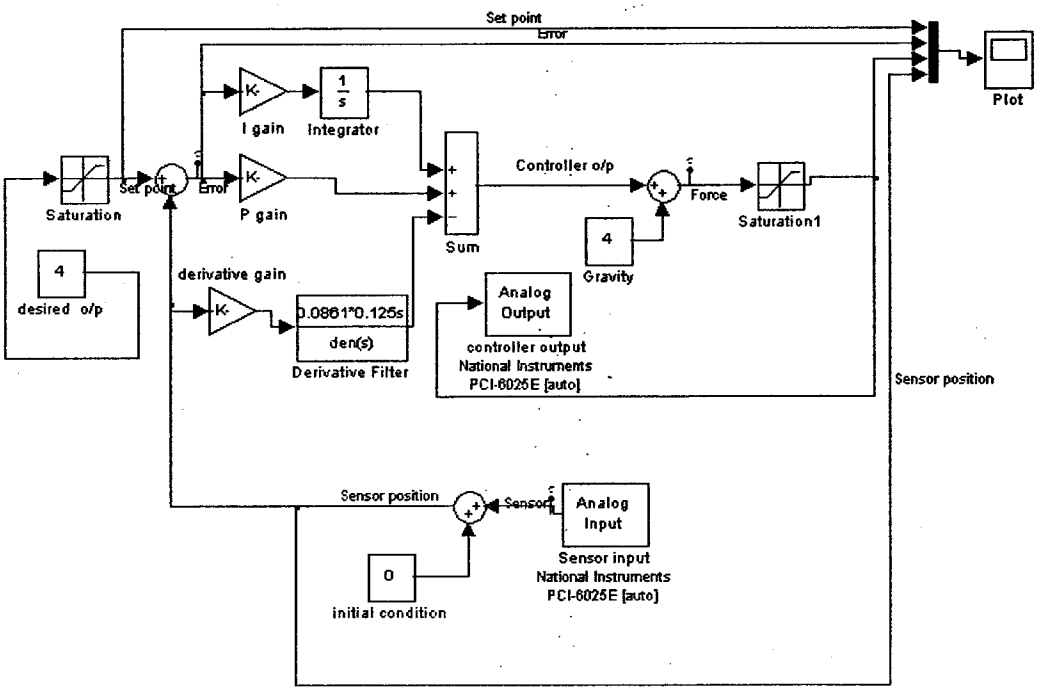

Figure 2.9-Simulink model for real time position control of the flexible structure.

Rule Name	Tuning Parameters		
Classic Ziegler-Nichols	$K_P = 0.6\ K_u$	$T_I = 0.5\ T_u$	$T_D = 0.125\ T_u$

Table 2.2- General PID parameters for Ziegler-Nichols method [34].

T_I & T_D are the integral and derivative time constants. The figure 2.9 is a structure of the implemented digital controller. The structure consists of various blocks. The system to be controlled is connected between the analog I/P and analog O/P blocks. The reference command is given through a constant block which is connected to an error computing block, where comparison between the sensor position signal to the desired value set by

user constant block is done. For the structure above, instead of feeding the error to the derivative block, direct feeding of the sensor signal is done.

Using this arrangement the signal noise reduction is achieved and amplification of noise signal is avoided. The derivative block is also implemented using a filter which will limit the high frequency noise signals. N limits the gain at high frequencies and has to satisfy the following condition [34].

$$h \times N/T_D \approx 0.2 \text{ to } 0.8 \qquad (2.4)$$

where, h = sampling time = *1* ms chosen particularly for our application.

T_D = derivative time constant.

The values of all the gains and parameters of the controller used are given in table 2.4.

Parameter	Value
K_U	-0.515
T_U	0.086 sec
K_P	-0.41
K_I	-7.907
H	0.001 sec
N	8
T_I	0.051 sec
T_D	0.010 sec

Table 2.3- Actual tuned parameters for the system.

In table 2.3, T_U = ultimate period and K_U = ultimate gain, Figure (2.10) shows the step response of the closed loop system, the initial position given by sensor is 3 V, after giving a step command it is observed that the sensor position transits to 4 V, and the error goes to 0 within 0.15 s.

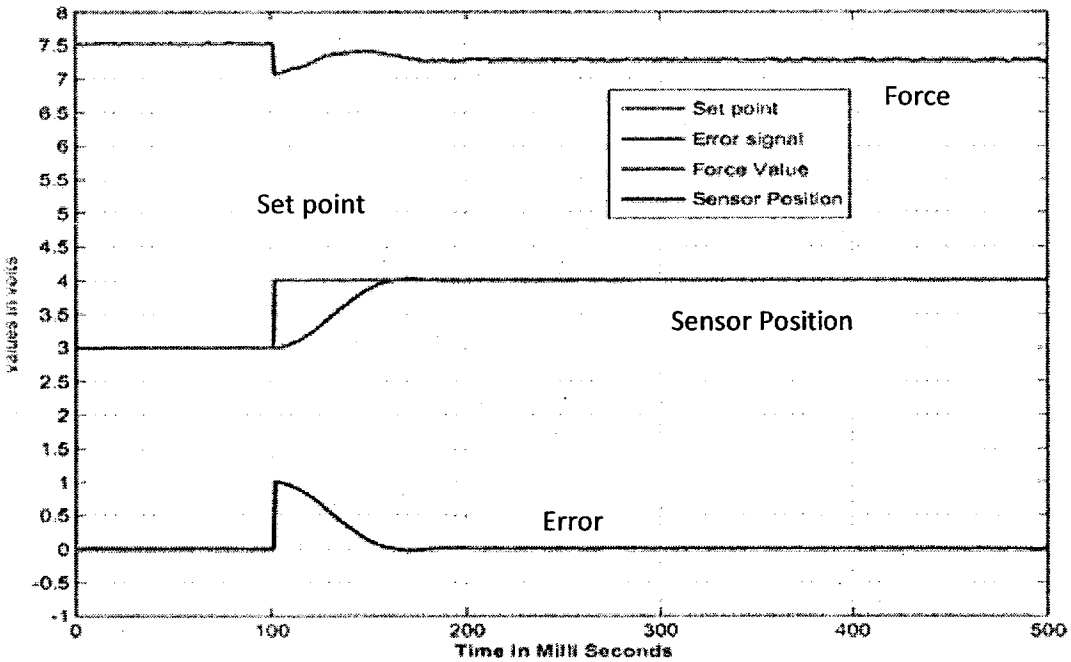

Figure 2.10-Step response of the closed loop system.

For this typical example (figure 2.10) the parameters are summarized in table (2.4)

Parameters	**Values**		**Conversion factors**
	Initial	**Final**	
Position	3 V =148 μm	4 V=0 μm	6mV/μm
Controller output	7.5 V	7.3 V	12 bit resolution
Current *(I)* from Servo amplifier	1.575 A	1.533 A	0.21 A/V
Voice coil coefficient *(Cv)*	Constant		1.05
Force at controlled positions *(F)*	1.6537 N	1.6097 N	$F= C_v \times I$

Table 2.4- Summary on step response to closed loop system

Chapter 3

Calibration, testing and characterization of the real-time force measurement setup

3.1 Optimization of the controller

The position controller discussed in the previous chapter is optimized to compensate for integral windup using back calculation [34]. When the output saturates, the integral term in the controller is re-compensated so that its new value gives and output at the saturation limit. It is found that it is advantageous not to reset the integrator instantaneously but dynamically with time T_t. The system has an extra feedback path that is generated by measuring the actual actuator output and forming an error signal (e_s) as the difference between the output of the controller (v)

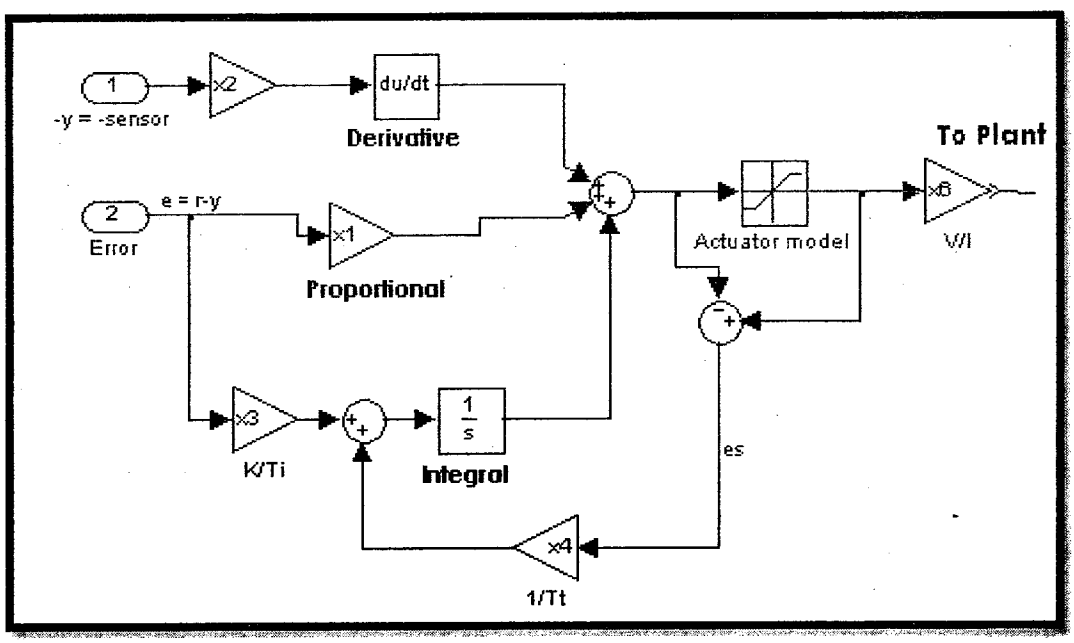

Figure 3.1- PID controller with a anti-windup based on back-calculation.

and the actuator output (u). Signal (e_s) is fed to the input of the integrator through gain $1/T_t$. The signal is zero when there is no saturation. Thus, it will not have any effect on the normal operation when the actuator does not saturate. When the actuator saturates, the signal e_s is different from zero. The rule of thumb that has been suggested, is to choose

$$Tt = (T_I T_D)^{0.5} = 0.025 \text{ s} \quad (3.1)$$

After adding the integral anti-windup block, the force measurement system turns completely ready and will be more reliable to carry out the constant velocity drilling experiments.

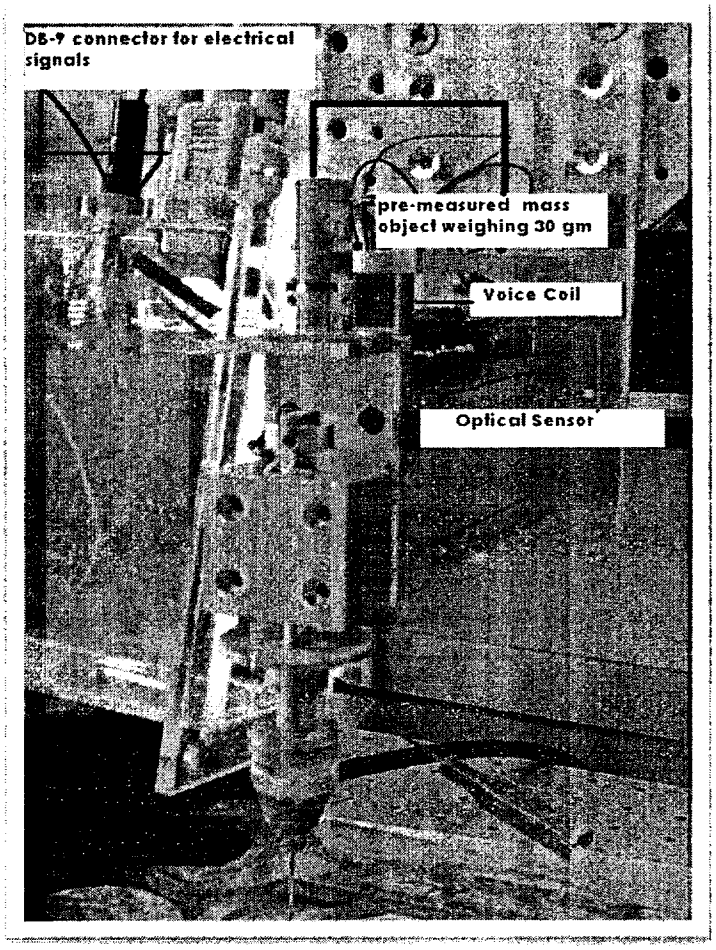

Figure 3.2-Experimental setup for calibration and testing

3.2 Experimental testing and calibration

Figure 3.2 shows a set up for the position control of the flexible structure. This set up is tested to validate its ability to measure an externally linked force or mass. The flexible structure's position is controlled at sensor output of 4 V (this position is called position at 0 μm (for reference see figure 2.4 and 2.6). It is considered that force of 0 N acts on the tip of tool at this position. The zero force displacement, principle, is validated by placing a piece of pre-measured mass weighing 30 g, on the top space available of the flexible structure. Figure 3.3 shows all

the color coded, I/O signals, in function of time, collected during this typical experiment. Between time "T = 0 s to T = 2 s", there is no extra weight. So no displacement takes place, displaying the mass = Zero Kg. After $T > 2\ s$, a pre measured object is placed manually. It can be observed that the controller starts compensating, until it minimizes the error to zero within a settling time of 150 ms, (please refer figure 2.10) and displays the mass signal as *29.5* g. The accuracy in measurement seems to be 98.3%.

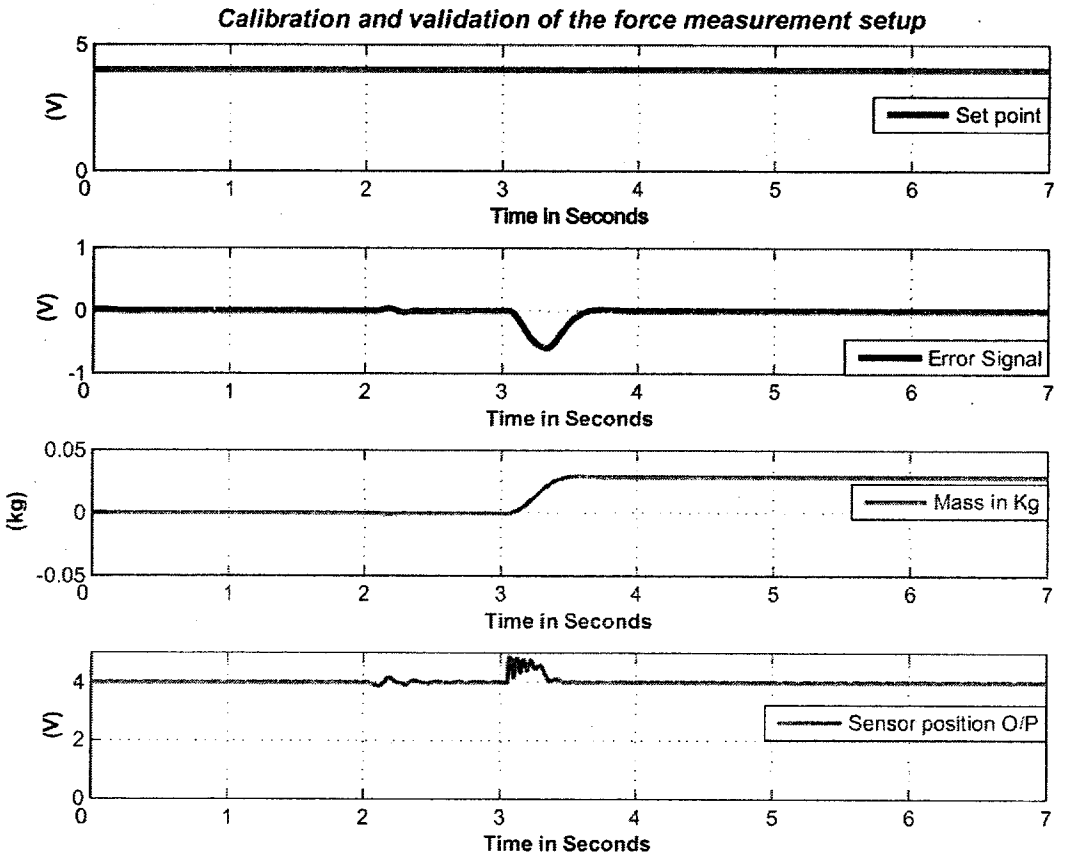

Figure 3.3-Testing and calibrating the force measurement set-up.

3.3 Characterization of the force measurement sensor.

Figure 3.4 is a plot for a real time data received from the force measurement setup during a testing experiment. The sensor o/p calibrated in Newton, is plotted against few

premeasured objects, added successively on the top of the setup. Figure 3.4 also shows the linearity of the force measurement sensor. The total range of the sensor is 0.2 N in the direction of gravity.

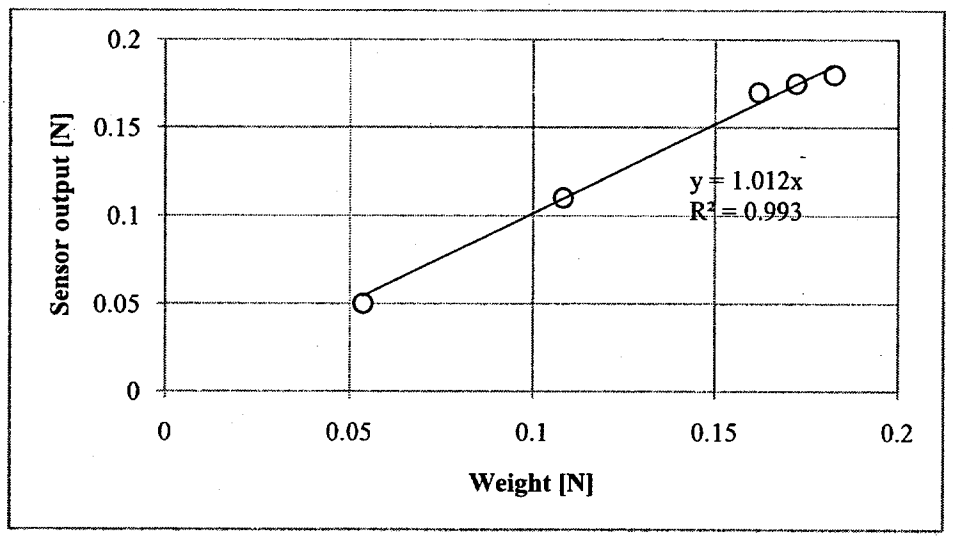

Figure 3.4 Linearity of force measurement sensor.

3.4 Validation and characterization of experimental set-up

To validate the setup for measuring force capability, during constant velocity drilling experiments, few dry-experiments (without drilling) are done. Improvements on experiment procedures are established by performing much iteration of dry experiments. For example, the procedures are optimized after each iteration, in the following steps

- Changing the orientation of work piece mounting assembly.
- Executing the motion stage software
- Plotting the gathered force and drilling depth data.
- Manually observing and discussing the plots.
- Restart with the next improved iteration until getting better.

3.4.1 Characterization of the internal stiffness of the set-up

Using dry-experiments (without drilling), the setup is capable of measuring the bending of the work-piece (see figure 3.6).

The mounting of work piece is approximated as a two end supported beam, shown in figure (3.5).

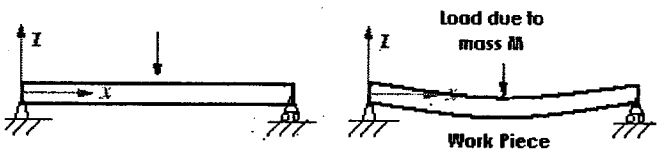

Figure 3.5- Simply supported beam (a) No load, (b) With load [44].

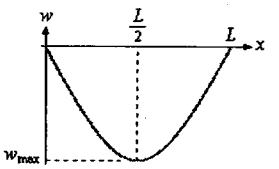

Figure 3.6- Bending characteristic [44].

$$W_{max} = -\frac{PL^3}{48EI} \qquad (3.2)$$

Where, W_{max} = max deflection at center of the beam,

Length of beam (L)	76×10^{-3} m
Load on beam (P)	1.8 N
Young modulus of work piece (E)	65×10^{9} N/m^2
Distance from neutral axis (center of beam) (L/2)	38×10^{-3} m
Moment of inertia I_m	$\frac{b \times h^3}{12} = 2.1 \times 10^{-12}$ m^4

Table-3.1 Typical values calculated for maximum deflection of work-piece

Using equation 3.2 and table 3.1 the maximum deflections W_{max} [44] of beam at the center to a point load P is estimated to be $W_{max} = -121.5\ \mu m$ (3.3), therefore due to maximum bending for center load, the stiffness can be calculated as

$$K_{the} = 1.51 \times 10^4\ \text{N/m} \qquad (3.4)$$

Based on the deflection of simply supported beam problem it is clear that the magnitude of work piece deflection is higher at center and decreases towards its edges. To minimize this variation of deflections on the surface of work-piece placing of 3 work pieces on top of each other is adopted.

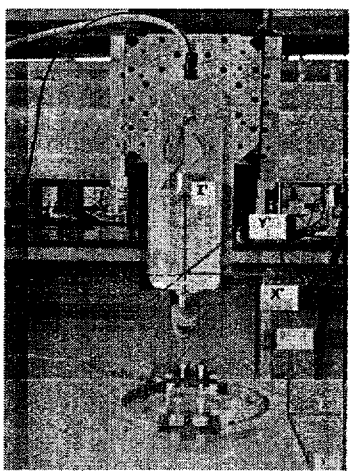

Figure3.7- Set up orientation for drilling experiments.

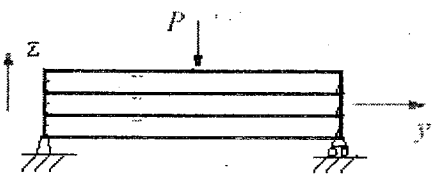

Figure 3.8- 3-workpice on the top of each other.

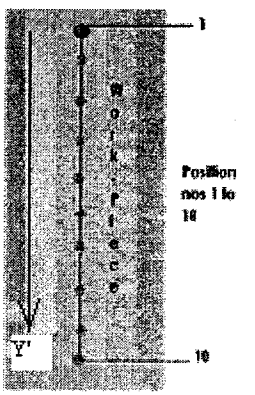

Figure 3.9- Tool moved on work-piece for 36 iterations each position.

This arrangement reduces the deflection to about 50 μm. The bending of the work-piece is expected as shown in figure 3.6.

Figure 3.10(a) shows a real sample work-piece used for a typical drilling experiment. 10 equidistant holes are drilled by moving the tool-electrode diagonally on the work-piece.

Due to mounting shortcomings, it is never possible to achieve perfection in bending symmetry as shown in figure 3.10(b).

3.4.2 Repeatability of the setup in detecting the work-piece surface

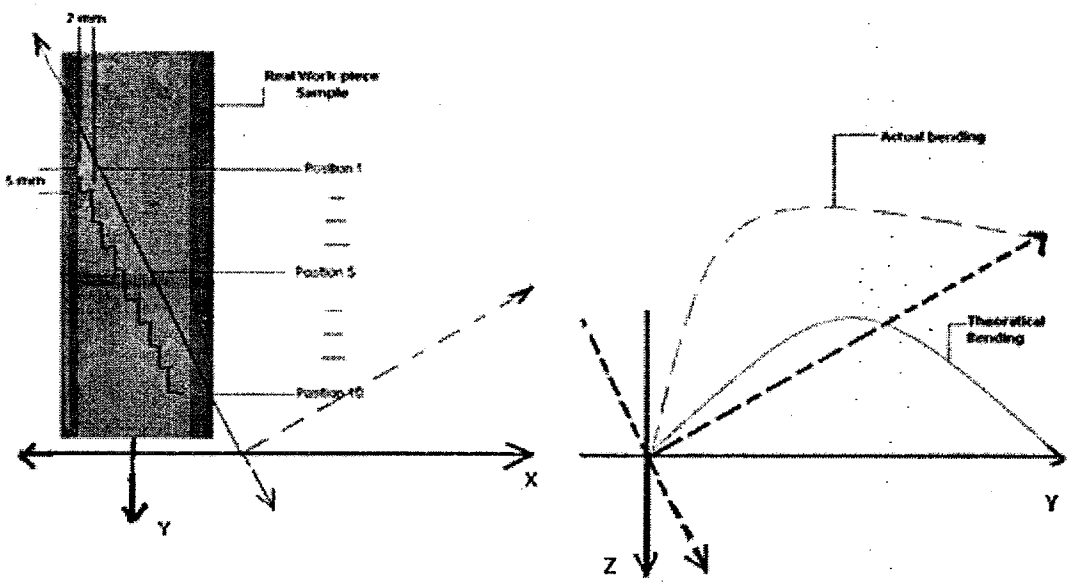

Figure 3.10- (a) Work-piece sample orientation during dry and wet experiments, (b) Expected bending.

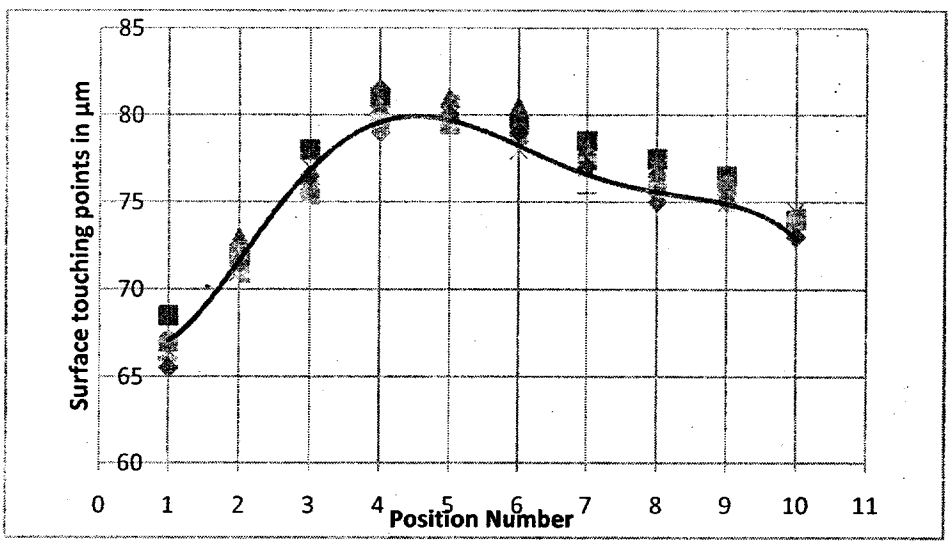

Figure 3.11-Repeatability for Surface touching at 10 different points on work-piece.

Figure 3.11 is for an experiment of 10 iterations for 10 identical positions on the same work-piece moved in the direction as specified in figure 3.10(a). It shows that the bending of work-piece and the repeatability in the measurement with respect to each position is good (better than 1 % or 5 microns)

3.4.3 Characterization of stiffness.

A final cross verification on setup's functionality is done by descending the tool ($Z = 100$ μm) on a sample work-piece, at a constant rate of (10 μm/s). (Power supply to electro-chemical cell is turned off)

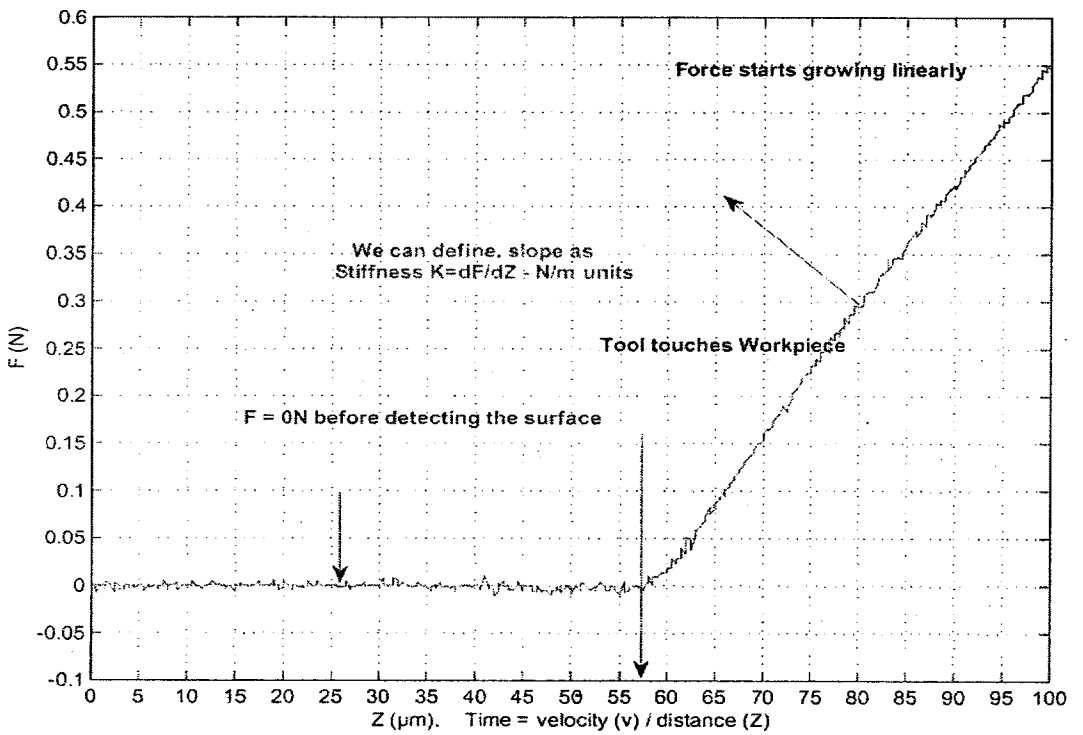

Figure 3.12- Measured force data plotted as a function of the tool moving on work-piece for z =100 μm.

Collecting the real-time force data and the relative Z-stage position data using XPS, figure (3.12) depicts the behavior of force in function to the non-drilling depth. It can be

observed that, eventually as the tool descends with a constant velocity, it touches the surface at *57* μm with respect to the start position and the contact force starts increasing linearly until *0.55* N with the end of the tool motion at $Z = 100$ μm, From the plot the overall effective stiffness can be determined as

$$K = 1.67 \times 10^4 \text{ N/m} \qquad (3.5)$$

The value in equation 3.5, is very close to the value of K_{the} (see equation 3.4) bending of work piece derived using equation (3.2) and table 3.1

3.4 Specifications of the force measurement sensor.

The Specifications of the real time force sensor is summarized as in table 3.1

S.N	Characteristics	Values
1.	Linear range	0.0 N to 2.4 N
2.	Resolution	1 mN
3.	Settling time	Less than 150 ms (Figure 2.10)
4.	Repeatability	90 %- Good
5.	Accuracy	98.3 %- Good
6.	Sensitivity	Measures force due to 1μm displacement in flexible structure.

Table-3.2 Characteristics of the real-time force measurement sensor

Chapter 4

Design of constant velocity drilling experiments

4.1 Chapter overview

This chapter is dedicated on the design aspect of constant velocity drilling experiments. The chapter starts with details on experimental apparatus and procedures. Then the choices for parameters and variables are discussed. The chapter is concluded by validating the experimental design.

Equipments	Make	Specifications
SACE Machine Head and Electrochemical cell Assembly	Made at EPFL, Switzerland	Please refer to appendix D
Voice coil	BEI Kimco	Please refer to appendix D
Optical sensor with signal conditioner	SFH 9201	Please refer to appendix D
NI DAQ PCI-6025 Card	National Instruments	Please refer to appendix D
Customized I/O connector box	Custom made at our lab	Please refer to appendix D
XPS Motion Controller	Newport corporation	Please refer to appendix D
V/I converter	Maxon motor	0-10 Volts converts to 0-2 A
Power supply	Custom made at our lab	+- 12 Volt, 2 A, +-15 Volt 2 A
Desktop Computer	Dell	2 GB Ram, Pentium dual core processor and 200 GB hard disk space
Matlab/Simulink with RTWT	Mathworks Inc.	Windows OS and Software with real time kernel for windows

Table 4.1 List of equipments for SACE Setup.

4.2 Designing the experiments

The detailed design of constant velocity drilling experiments are discussed in the following sections

4.2.1 List of apparatus/equipments.

Table 4.1 shows the list of hardware and software used to build the apparatus for the constant velocity drilling experiments.

System 1-XPS Motion Controller system		System 2- Desktop PC with NI DAQ card	
Event no.	Actions Manual/Semi-automatic	Event no.	Actions Manual/Semi-automatic
1	Initialize all functions and home search	1	Manual Loading of matlab and RTWT environment
2	Find position on work piece for hole #.	2	Manually Build and run the real time controller model
3	Move Z stage down to find the surface touching position at hole #	3	Unload the controller and reading set point
4	Moving the Z stage up 200μm	4	Load the controller and regulate the set point position
5	Turn on power supply	5	Position regulation in action
6	Start the data gathering function	6	Position regulation in action
7	Move Z position 300 μm down at constant velocity		Position regulation in action
8.	Turn Power supply off	7.	Unload and reset the controller
9.	Stop data gathering	8	Stay Idle
10	Move Z stage 3 mm up	9.	Stay Idle
11	Copy the data file to another folder	10	Stay idle
12	Repeat step number 1 – 11 for each hole	12	Repeat step number 2 to 10 for each hole

Table 4.2- Extraction of event and actions from both the systems.

4.1.2 Procedure

Events and actions from both the systems are extracted as given by the table 4.2 The work piece is mounted in the cell as described in section 3.3 The cell is filled up with 30% wt. NaOH solution until its required level (about few 100 μm above the work-piece surface)

Table 4.2 shows the experimental procedure of the actions for respective event no., (for software code please see appendix B). The data gathering is done and updated always in a new file restoring the old file. Two digital signals are used for communication between the 2 systems, one to load/unload the controller and another to read the set point. These digital signals are written from the XPS on the digital input of the DAQ card.

To measure the forces acting on the tool, for every constant velocity drilling experiment the procedure from table (4.2) is followed with 3 iterations each. Following are its details.

- Iteration I- To measure the non machining stiffness force at respective drill position.
- Iteration II- To measure the actual machining force at respective drill position.
- Iteration III- To measure the depth of the drilled hole for the respective position.

Finally the hardware and the software aspects of the complete setup are ready and can be used to carry the constant velocity drilling experiments.

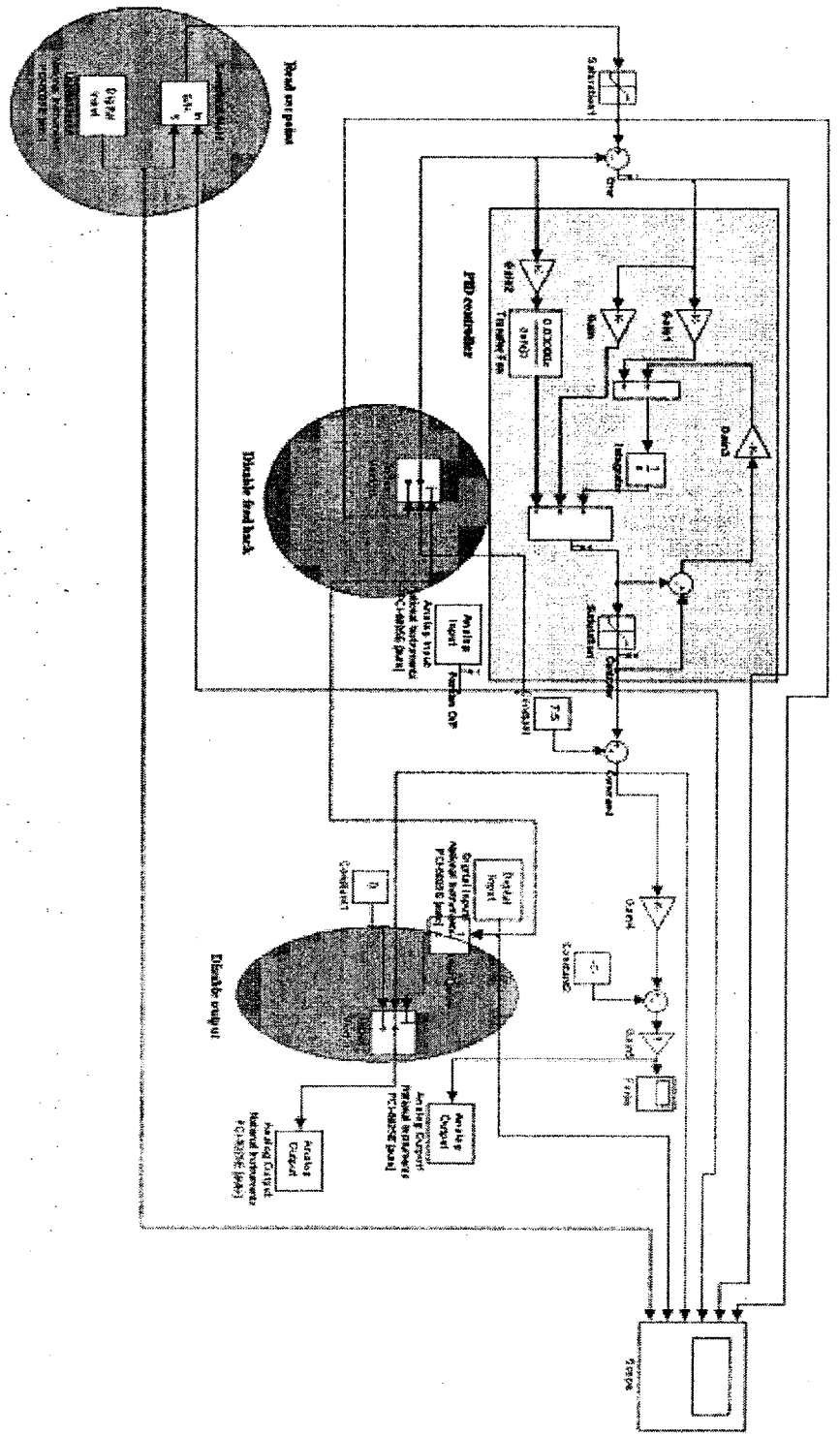

Figure 4.1 Scheme for completely automated controller.

The I/O's from controller (structure shown in figure 4.1) and XPS communication signals are shown in figure 4.2 and figure 4.3

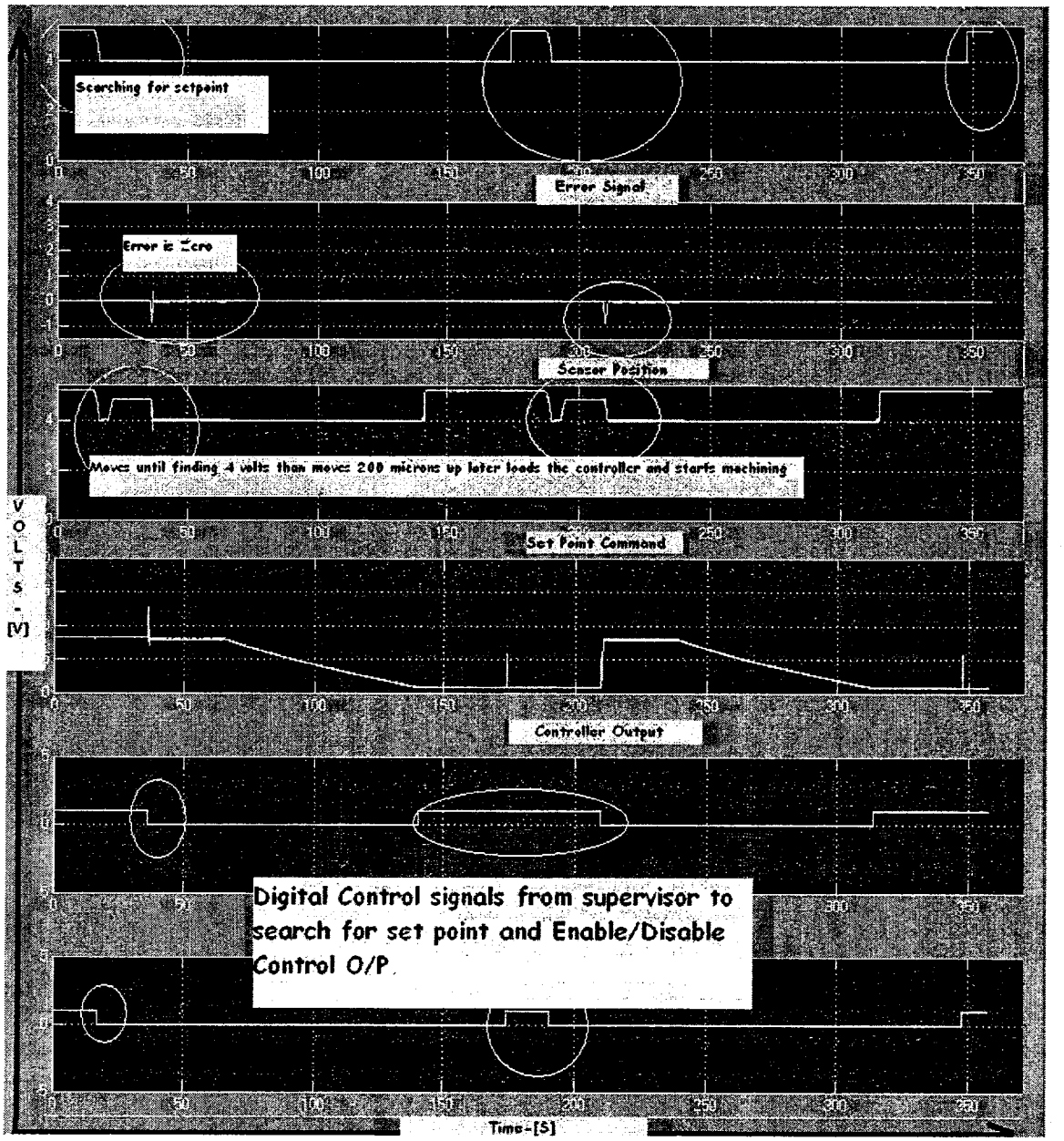

Figure 4.2- Signals for automated SACE drilling setup.

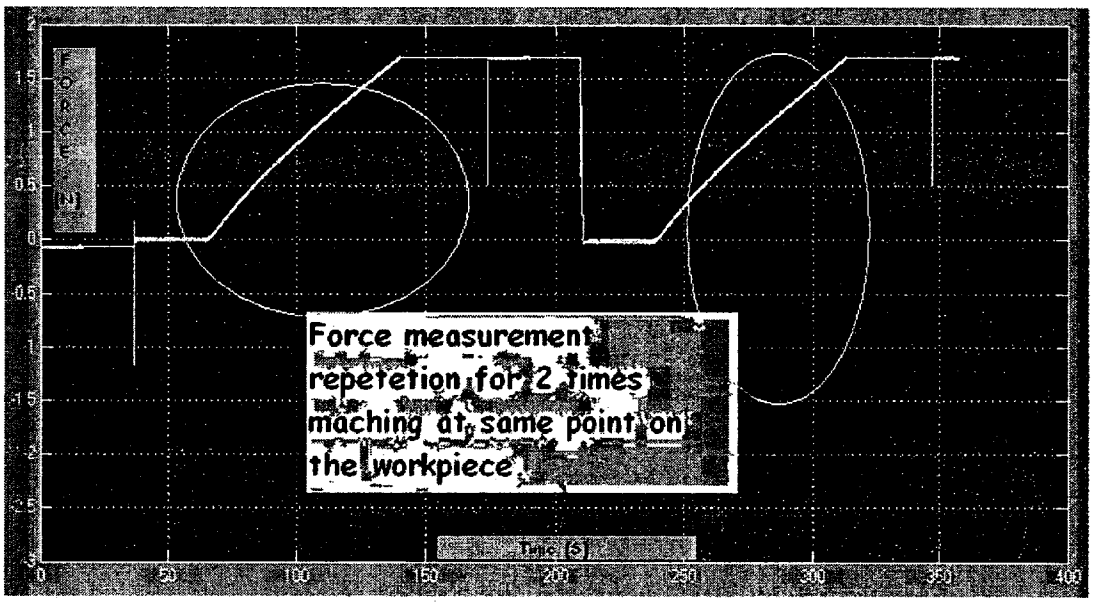

Figure 4.3- Force measurement calibrated signal for non machining experiment.

4.3 Choice of drilling velocities

Table 4.3 specifies the drilling velocities found for gravity feed drilling process. For a typical gravity feed drilling experiment, parameters were chosen as below,

- Electrolyte -NaOH-30 % wt.
- Tool – stainless steel, φ=0.4 mm
- Work piece – Glass (as mentioned in the earlier sections)

Applied voltage [V]	Data function	V_{lim}	δ[μm]
28	Mean standard deviation	1.7 1.5	70 18
30	Mean standard deviation	1.6 0.8	77 7
33	Mean standard deviation	3.1 0.7	87 20

Table 4.3- Gravity feed drilling velocities [35].

Before performing constant velocity drilling experiments table 4.3 is understood in detail.

4.3.1 Constant parameters

To minimize the issues with tool bending a thick tool (diameter of 0.7 mm) was chosen. The material of the tool was chosen to be mild steel, based on its availability at the lab facility. The work-piece chosen was the most commonly used micro-scope glass slides from Menzel Glaser. Instead of using a single work piece, 3 slides mounted on top of each other to minimize the bending affect is chosen.

4.3.2 Variables

Constant parameters	Voltages in Volts	Velocities in µm
30 % wt. NaOH, 0.7 mm C.S tool	28	1, 2
30 % wt. NaOH, 0.7 mm C.S tool	29	1, 2, 3
30 % wt. NaOH, 0.7 mm C.S tool	32	1, 2, 3, 4, 5
30 % wt. NaOH, 0.7 mm C.S tool	35	2, 3, 4, 5

Table 4.4–Parameters used for SACE constant velocity drilling experiments.

For constant velocity drilling experiments, the velocity and voltage are chosen to be variables. The measured force is presumed to be in function of these variables. Table 4.4 specifies the chosen constant velocity drilling parameters, while conducting all of the further experiments.

4.4 Validation of the experimental design

Figure 4.4 shows one sample data plot from a test experiment on constant velocity drilling, conducted on a sample work-piece.

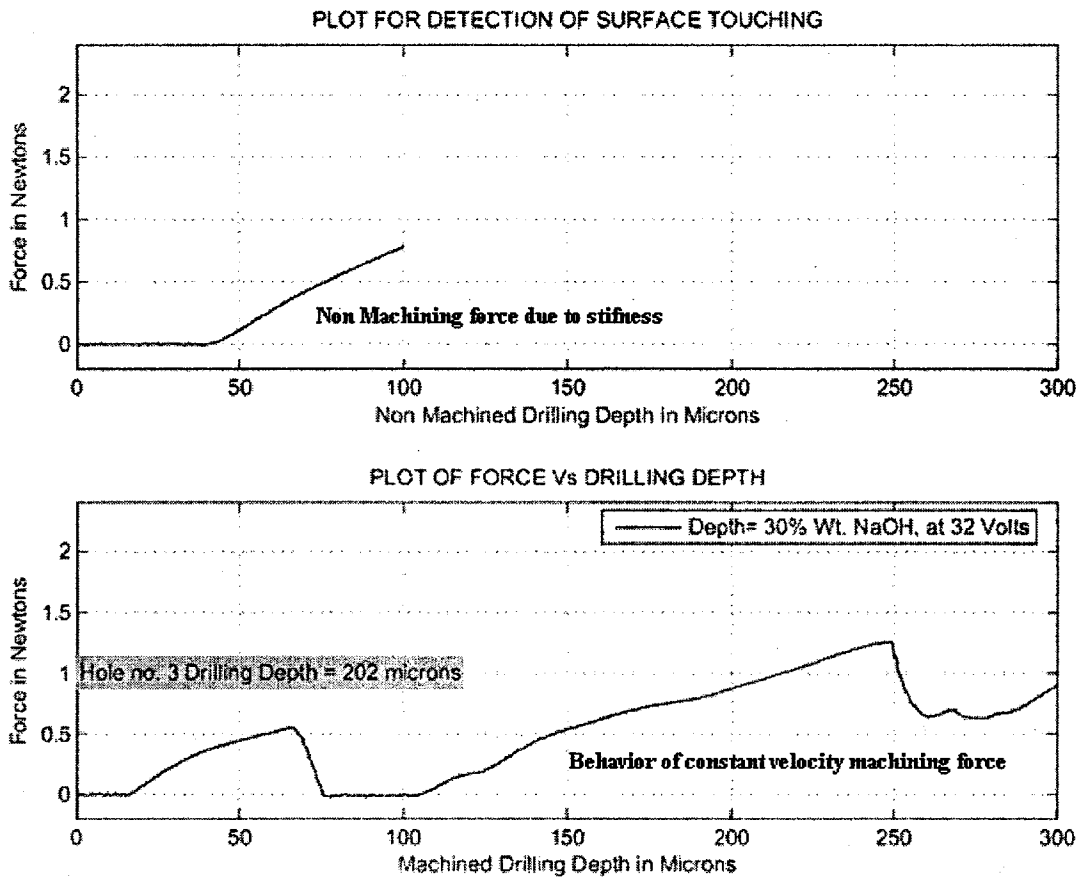

Figure 4.4- Sample plot to validate the complete automated system.

The experiment procedure was followed as mentioned in the earlier section. The experiment parameters were chosen as per the table 4.4. Validation of the experimental design is done by observing figure 4.4.

Figure 4.4 shows the details of the measured force data and proves the ability of the setup to measure force, during non-machining and machining experiments. The drilling position on the work-piece is identical for both the iterations. In the third iteration (not shown in figure) the measurement of actual drilling depth is done, illustrating a drilling depth of 202 μm in this sample experiment. It is also observed that the force is detected earlier during actual drilling experiments than to the dry experiments. Similar

observations on various identical experiments were typical (but are not presented due lack of space). The details on analysis and investigations on similar data sets, form various drilling experiments will be presented in the next chapter 5.

Chapter 5

Constant velocity drilling experiments, SACE drilling model, results and discussion

5.1 Chapter overview

This chapter presents, the details on real-time force data collected during a typical constant velocity drilling experiment including the early force detection with consequential possibility for unexpected early start to drill. It will also present a detailed investigation to confirm the possible reasons, like thermal expansion, pressure in gas film and formation of thin layer of molten NaOH. Later a discussion on accomplished drilling depths, and a crude technique to estimate the drilling depths, will be presented as well. The description on a new SACE drilling model developed for constant velocity drilling followed by its general solution and comparison with some results from the experimental data. Finally this chapter is concluded by highlighting the possible classification of forces observed in various constant velocity drilling experiments.

5.2 An example of experimental data

Figure 5.1(a) and 5.1(b) depicts change in force in real-time with respect to, non machined and machined drilling depths respectively. The data is collected during a typical constant velocity drilling experiment. (Experiment procedures for the same are described in previous section 4.1.2).

Figure 5.1(a), represents the behaviour of non-machining force in a typical dry-experiment, figure 5.1(b) represents the machining force for a typical drilling experiment at 32 V. It is observed that, in a dry experiment, the force is detected at around 42 μm,

compared to a drilling experiment where the same surface is detected at 18 μm (in both situations the origin of the z scale is the same). This shift is typical and observed in

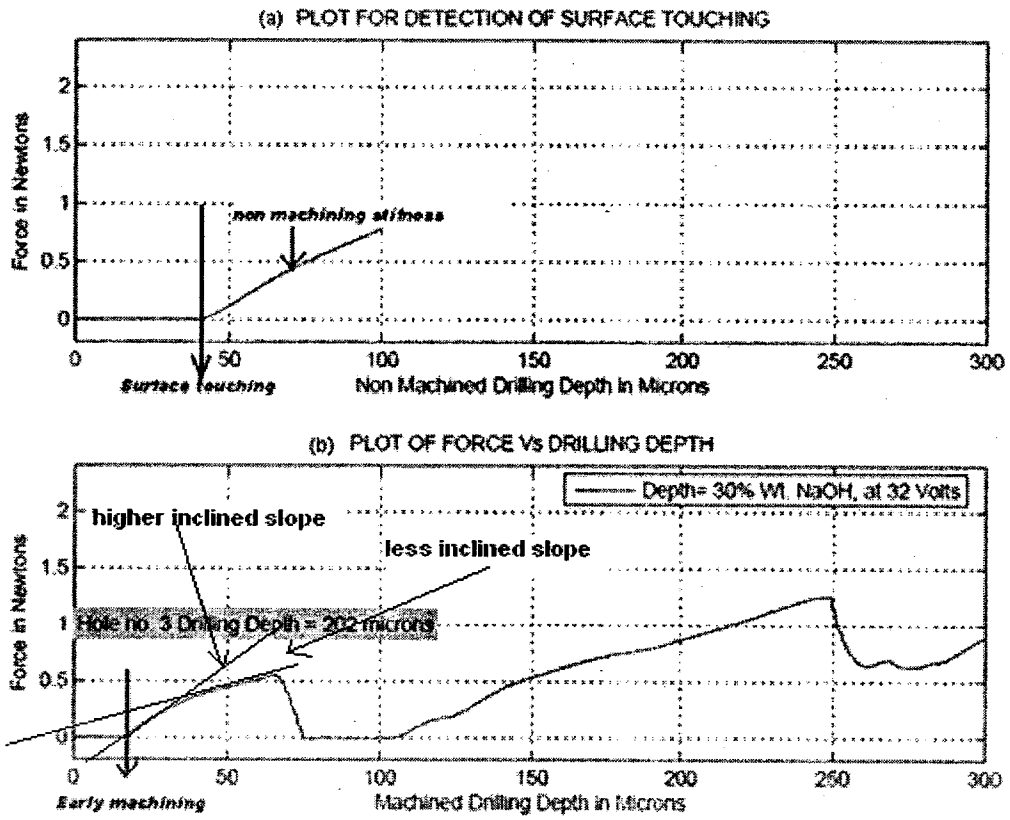

Figure 5.1- (a) and (b) Sample data plot for constant velocity drilling experiment.

all experiments. It is also observed that in a drilling experiment (fig 5.1(b)), soon after the tool appears to be touching the work-piece surface, the slope seems to be rising more rapidly and eventually reducing to a lower rate.

Thus it is observed that in actual drilling experiment the force starts with a linear increase, at faster rate and later at a smaller rate. The force also appears to be suddenly falling to some constant value or even vanishing completely. Eventually the force also

seems to be rising with random repetitions as earlier or even with few variations till it reaches the drilling depth limit (300 μm in the shown example).

Certainly a possibility in the drilling process, to start earlier than expected, cannot be mistreated by seeing the experimental fact of appearance in early force detection followed by a more rapidly rising slope. This experimental fact requires deeper analysis. Further description can be found in the following sections.

Considering these experimental facts, the forces can be characterized in association to

1. The early force detection.
2. Drilling depth,
3. Rising, falling and constant slopes.

All the possible reasons of such characterizations will be investigated and the conclusions will be presented in the further sections.

5.3 Investigations on early force detection

In figure 5.1(b) the early force detection could be combined effect of applied power and variations in level of available electrolyte. Similar kind of effect is also observed in gravity feed drilling [16-19, 37]. It can be possible, that the early force detection comes from either thermal expansion in tool and work-piece or due to formation of a molten NaOH layer or pressure due to gas film resulting in pushing the tool, or even may be combination of all. This early force detection or (probable early machining) effect is investigated to confirm the reasons. Figure 5.2 shows the typical mean values of surface

detection, at various applied voltages. It is observed that, the early force detection distance, slightly decreases linearly with increasing applied voltages.

The appearance for this slight decrease could be due to changes in tool and work-piece heights, due to thermal expansion or probably due to variations in gas film diameters, for various applied voltages or even probably due to uncontrolled level of electrolyte during each drilling experiment. Another reason for such slightly decreasing appearance can be related to decreasing damping forces acting on the tool tip, because for increase in applied voltage, the viscosity of material around the tip of tool decreases due to rising temperatures, see figure (5.11).

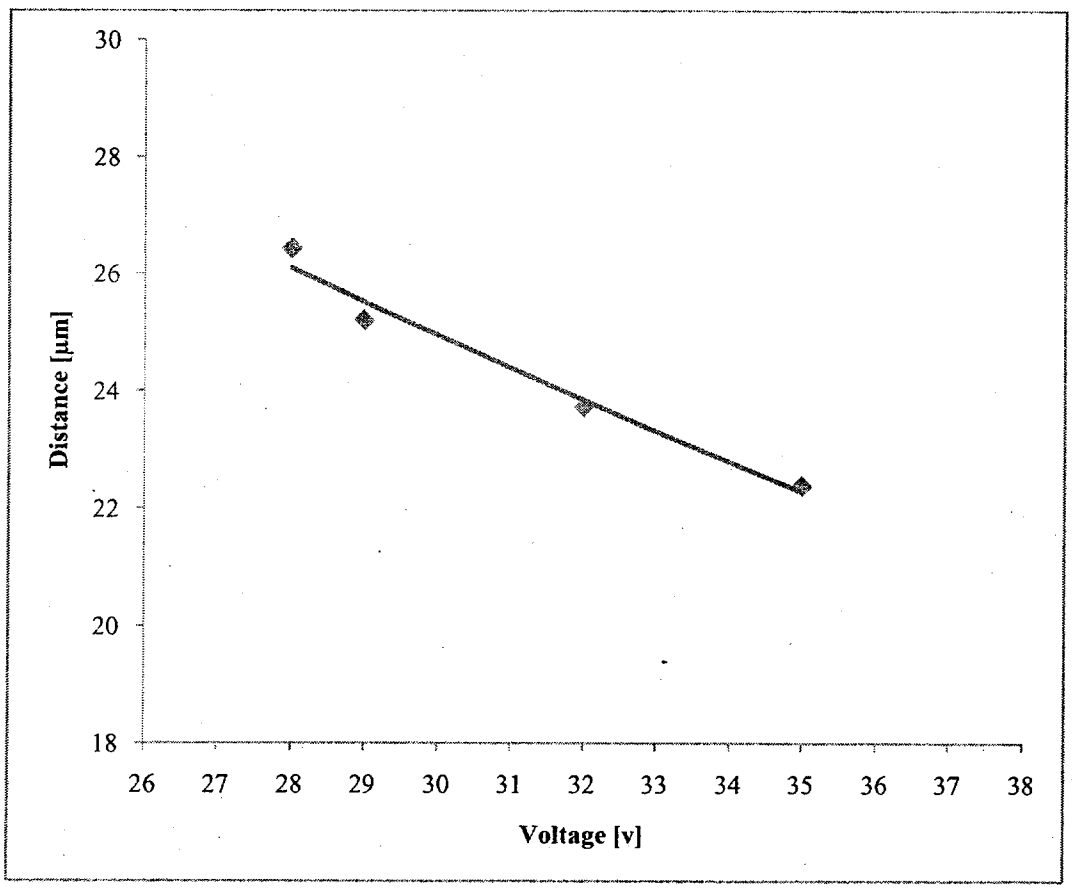

Figure 5.2- Initial error in touching surface between non-machining and machining experiments.

From figure 5.2 the mean of work-piece surface detection position lies at 24 μm.

5.3.1 Thermal expansion

Figure 5.3(a) and 5.3(b) correspond to a possible physical deformation experienced by tool and work piece during a dry and actual drilling experiment. During experiment no heat is generated, so no thermal expansion could take place.

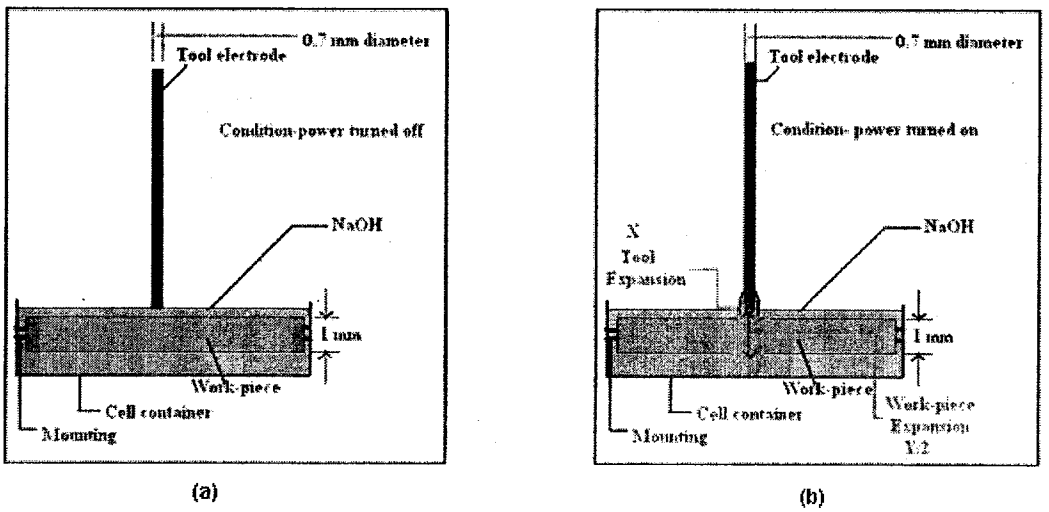

Figure 5.3-(a) and (b) Thermal expansion effect of tool and work-piece during dry and wet experiments

In a drilling experiment heat is generated due to electrochemical discharges at the contact point of tool and work-piece and the estimated temperature could be 550°C. [41] At such high temperatures, possibility of thermal expansions in materials could be prevailing. The expansion in work piece is measured on both the surfaces because the work-piece is made up of *3* slides mounted on top of each other (as mentioned formerly in section 3.4.1.) The electrolyte trapped between the 2 upper slides would definitely expand due to local surface heating of the work-piece and on top electrolyte. Thus considering the tool

expansion of L_t meters and the work piece expansion of L_w meters, the final length due to expansion together can be written as,

$$L_T = L_t + L_w/2 \qquad (5.1)$$

The potential thermal expansion of both the materials is estimated using the material parameters from table 5.1.

Component	Material	Original Dimension	Coefficient of thermal expansion	Temperature $_{max}$
Tool Electrode	Steel	$\Phi = 0.7 \times 10^{-3}$ m	13×10^{-6} m/m K	550 + 273.15 K
Work-piece	Glass (Pyrex)	$l = 76 \times 10^{-3}$ m $b = 25 \times 10^{-3}$ m, $h = 1 \times 10^{-3}$ m	4×10^{-6} m/m K	550 + 273.15 K

Table 5.1- Typical material parameters used in experiments.

The thermal expansion of the tool is calculated using the formula

$$\frac{\Delta L_t}{L0_t} = \alpha_t \Delta T_t, \qquad (5.2)$$

Where,

ΔL_t= final tool length in meters

$L0_t$= original length of tool in meters

α_t= thermal expansion coefficient of steel

ΔT_t= final temperature — initial ambient temperature

Similarly the thermal expansion of work-piece (glass) is calculated as

$$\frac{\Delta L_w}{L0_w} = \alpha_w \Delta T_w, \qquad (5.3)$$

Where,

ΔL_w= final work-piece length in meters

$L0_w$= original length of work-piece in meters

α_w= thermal expansion coefficient of steel

ΔT_w= final temperature— initial ambient temperature

Referring to figure 5.3,The expansion for the tool is

$$L_t = \Delta L_t \qquad (5.4)$$

And the expansion for work-piece is

$$L_w = \Delta L_w \qquad (5.5)$$

Note- Ambient temperature at 300 K and a partial tool-tip length of 0.5 mm is considered while doing the calculation.

Therefore using equation (5.1) the joint increase in total length can be calculated as

$$L_T \approx 7\,\mu\,m \qquad (5.6)$$

From equation (5.6), about 25% source of early machining, could be due to combined thermal expansion of work-piece and tool electrode.

5.3.2 Pressure effect due to gas film (bubble)

"The pushing on the tool, due to pressure in gas film (bubble)" is investigated in an experimental way. During each set of experiment, the tool tip was placed at distant values of 5, 10, 15, 20 and 25 μm above the work piece. The power was turned on only after confirming and recording the distance between tool and work-piece surface. The force (highest magnitude) numbers were gathered for all distant tool placement positions.

It was observed that, at instant the power was turned on, the tool started to experience a force. Figure 5.4 shows the tendency of the force experienced by the tip of the tool at a distance up to 25 μm above the work piece. The force decreases linearly as the tool is placed farther from the work-piece. This phenomenon could be assumed like growing of a bubble to variable diameters φ (assuming that after φ_{max} = 25 μm the bubble might burst). Thus the force is experienced by the tool-tip due to the sudden appearance of the bubble between the work-piece and tool. Using the linear relation between the F and ΔZ from figure 5.4 the stiffness of the bubble could be estimated as

$$K_{GF} = 1.6 \times 10^4\ N/m \qquad (5.7)$$

Also from figure 5.4 considering

$$f_{max} = 0.4\ N, \qquad (5.8)$$

The approximate pressure in the gas film (bubble) can be estimated as,

$$P_{max} = \frac{f_{max}}{A} \qquad (5.9)$$

Therefore $P_{max} = 10\ atm$ (5.10)

As of equation (5.10), the early force detection effect due to gas film (bubble) seems to be much more significant as compared to thermal expansion, but the estimated pressure inside the gas film seems kind of unrealistic. Usually the bubble created by a vaporized liquid, rise to the surface where they burst and release the gas. Usually this happens around the boiling point of the liquid where the vapor pressure is generally equal to one atmosphere [44]. Therefore it is not possible to conclude that the pressure due to gas film is responsible for the early force detection.

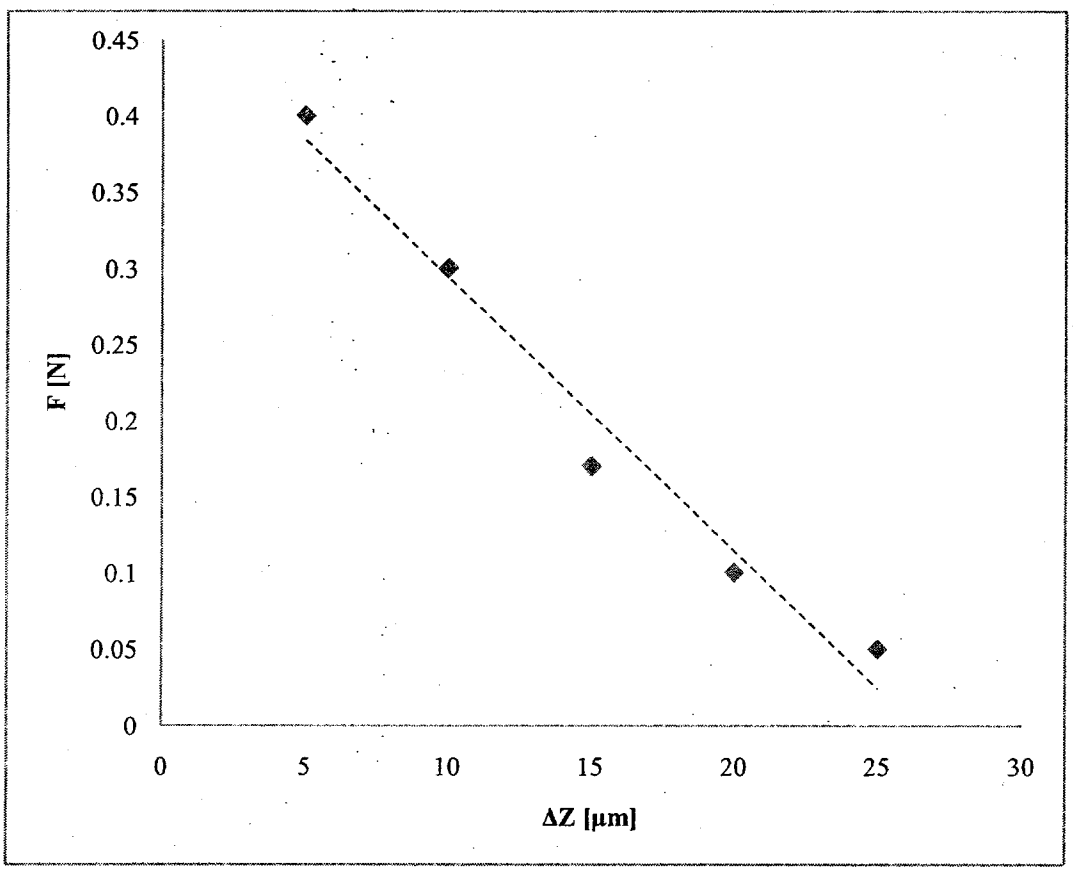

Figure 5.4- Force due to gas film as a function of distance between work piece and tool tip.

This raises the need to investigate another possible reason for early force detection, which is probably due to formation of molten NaOH.

5.3.3 Formation of molten NaOH layer.

Figure 5.5 shows the situation near the contact points of the tool electrode, work-piece and electrolyte. The electrochemical discharges, generating high heat and rising the temperature to about 550 °C [41], which is much higher than the boiling point of water (100°C) and the melting point of NaOH (323°C), it is be obvious that, from the solution surrounding this heat source, water is evaporated leaving back molten NaOH. The density of molten NaOH is about 1.04 g/cm^3, so it resides down on the work piece.

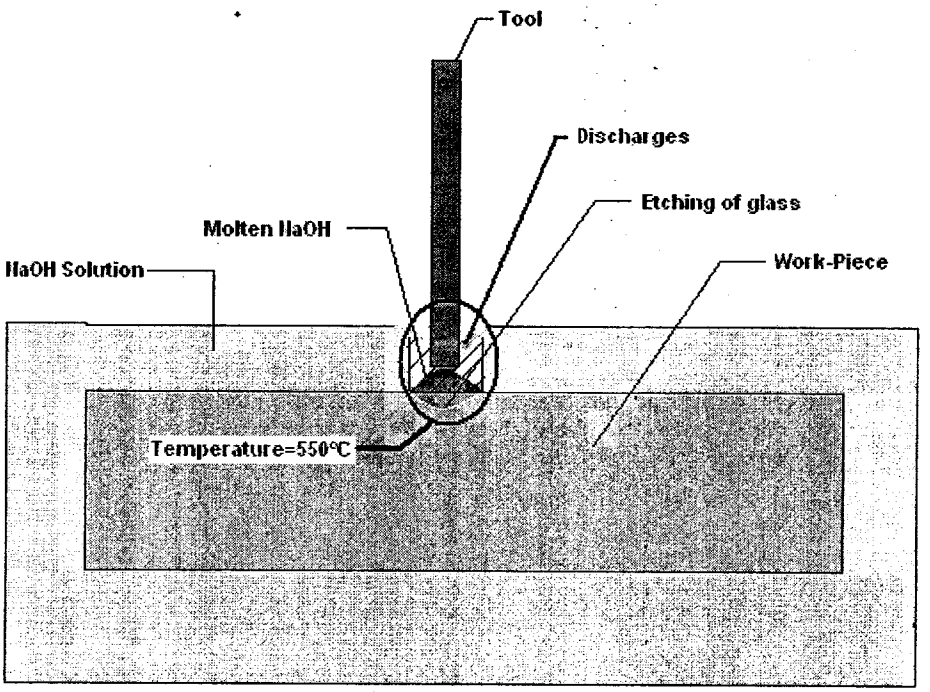

Figure 5.5- Situation between tool tip and work-piece contact point, due to heat generated by electrochemical discharge.

Based on the results from section 5.2 and 5.3.1, the possible thickness of this molten NaOH, could be around 25-7=18 μm. This deposited molten NaOH, is highly reactive with glass, thus responsible for initiating the drilling process [36].

Thus for any typical drilling experiment, the work-piece surface appears to be detected earlier compared to a typical dry experiment. The reason for such a artificial appearance, are due to thermal expansion of tool and work-piece in adjacent to the formation of a thin layer of molten NaOH, rising the height of work-piece surface and a possible pushing effect due to gas film (bubble). This early force detection could certainly lead to an early start in drilling process. The existence for such early machining can be explained, by investigating the drilling depths.

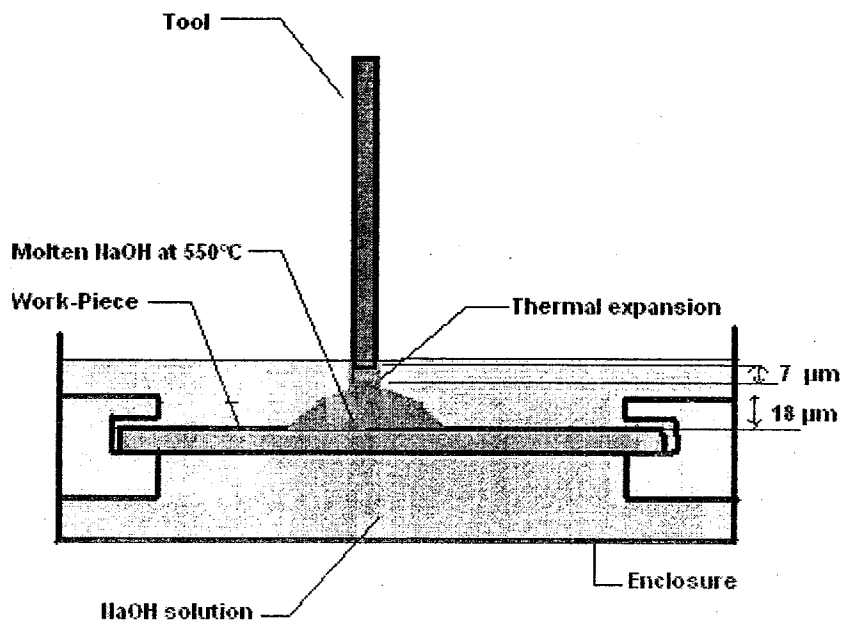

Figure 5.6- Rise in work-piece surface height due to deposition of molten NaOH after evaporation of water and partial thermal expansion in tool.

5.4 Investigation on drilling depths

Figure 5.7 depicts experimental data. (Experimental procedure as mentioned in previous section 4.1.2) The tool is moved for total depth of 375 µm, (*100* µm above surface and actual penetration in a work piece, to a maximum of 275 µm, at various constant

velocities. The drilling depths are measured in the third iteration. The drilling depths are in function of applied voltage at various velocities.

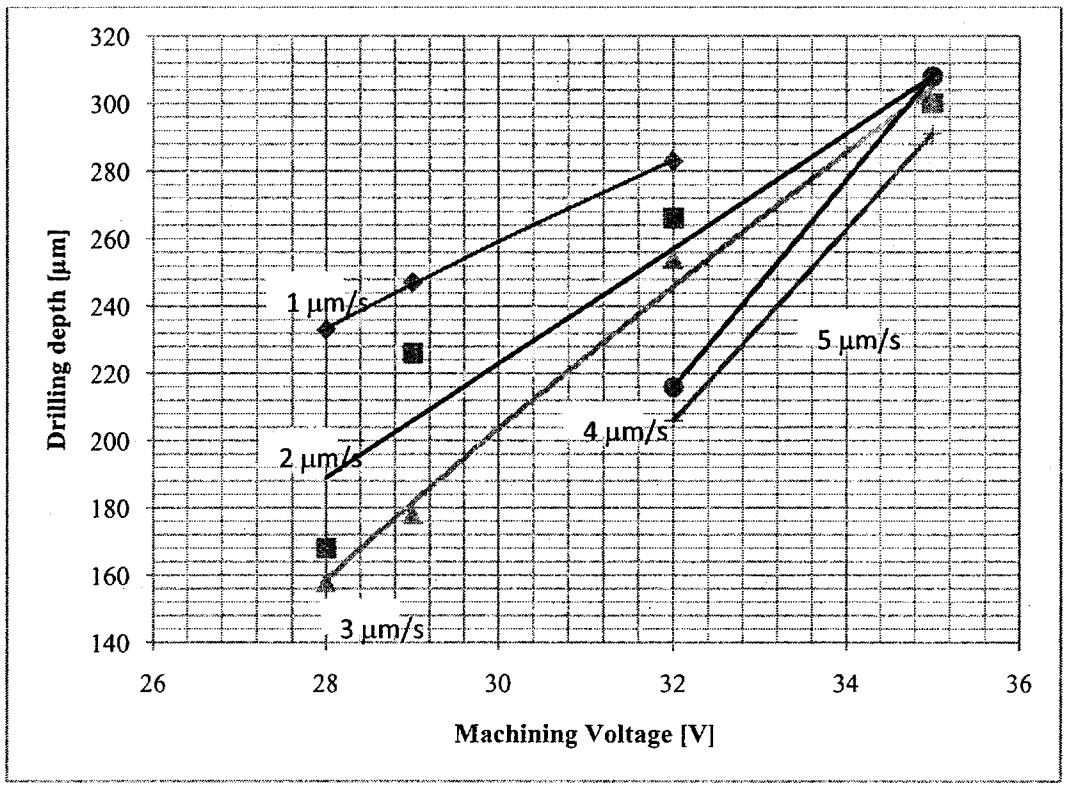

Figure 5.7- Drilling depth mean values in function of applied voltage for various velocities.

At higher applied voltages or lower drilling velocities much higher depths are accomplished. This can be compared with the gravity feed model discussed in [41]. Certainly at higher voltages more power is provided, which can surely help in removing material in the discharge regime, while at lower velocities more time is offered for material removal process.

Though the drilling depth limit was of 300 µm, in figure 5.7, drilled depths as low as 156 µm up to as high as 310 µm are observed. The extra drilling certainly can be due to the early start of machining due to the fake earlier surface detection effect, discussed earlier.

For constant velocity drilling, a comparative study on quality of hole versus drilling depths could be an interesting subject for future work; this could for sure help in implementing optimization techniques on material removal rate for SACE drilling technologies.

5.4.1 Possibility of online estimation for drilling depth.

It is very hard to control the gap between the tool and work-piece while using constant velocity drilling for SACE technology [36]. One possibility to overcome this drawback could be, using the real-time force measurement data during a typical drilling process to estimate the actual drilling depth.

Figure 5.8 illustrates an example of using this technique. In iteration-1(dry process), the first contact point (distance z_d) between tool-work-piece is recorded and starting from this point the slope (k_d) of the measured force is also recorded. Similarly, in iteration-2 (actual drilling) the same technique is applied to find z_a and k_a. Finally in iteration-3, the actual drilled depth is measured and recorded as Z_d

Here z_d, z_a, k_d and k_a are associated to a typical constant velocity drilling process (CVDP). Knowing all the values, error and the average of both slopes can be calculated as,

$$z_e = z_{d'} - z_{a'} \qquad (5.11)$$

$$k_{av} = (k_a + k_d) / 2 \qquad (5.12)$$

Using the general line equation, $y = mx + c$ and substituting the coefficients as

$$y = F(n), \quad m = k_r, \quad x = EZ(n), \quad c = z_e \qquad (5.13)$$

Where n is the drill position number (from 1 to 10 as in figure 5.6)

Using equations (5.11), (5.12) and (5.13) the drilled depth is estimated as

$$EZ(n) = \frac{F(n) - z_e}{k_{av}} \qquad (5.14)$$

Finally the estimated drilling depth can be compared to the actually measured ones (during 3rd iteration), to verify the technique.

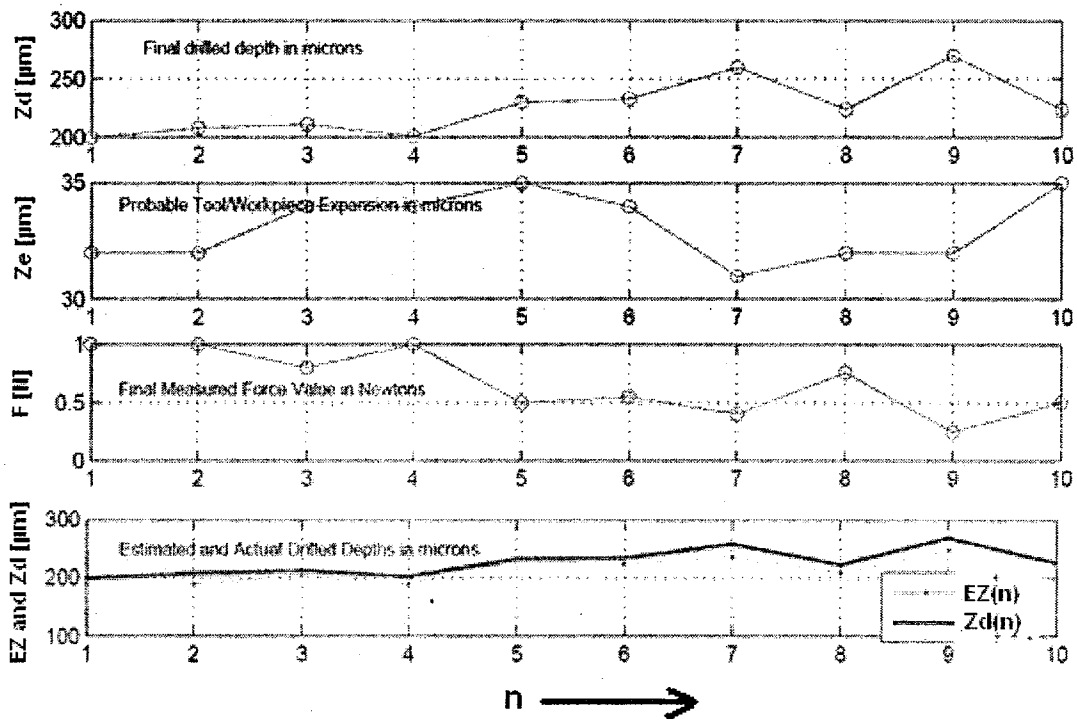

Figure 5.8- Estimation technique for drilling depths based on real-time force measurement.

Figure 5.7 illustrates the details between estimated and the actual depth. It can be clearly observed that the difference varies in a range of 10 to 25 µm, which approximately agrees with the values from early force detection, discussed earlier. It is typical that the actual drilling depths are always greater than estimated ones. This gives another evidence for the possibility of the early start in machining process.

Consequently by substituting an average position value of early force detection, the estimation could be improved by minimizing the error.

Detailed investigations on this technique, could assure accurate online monitoring of drilling depths, and sooner or later to develop supplementary gap control algorithms, for SACE constant drilling strategies.

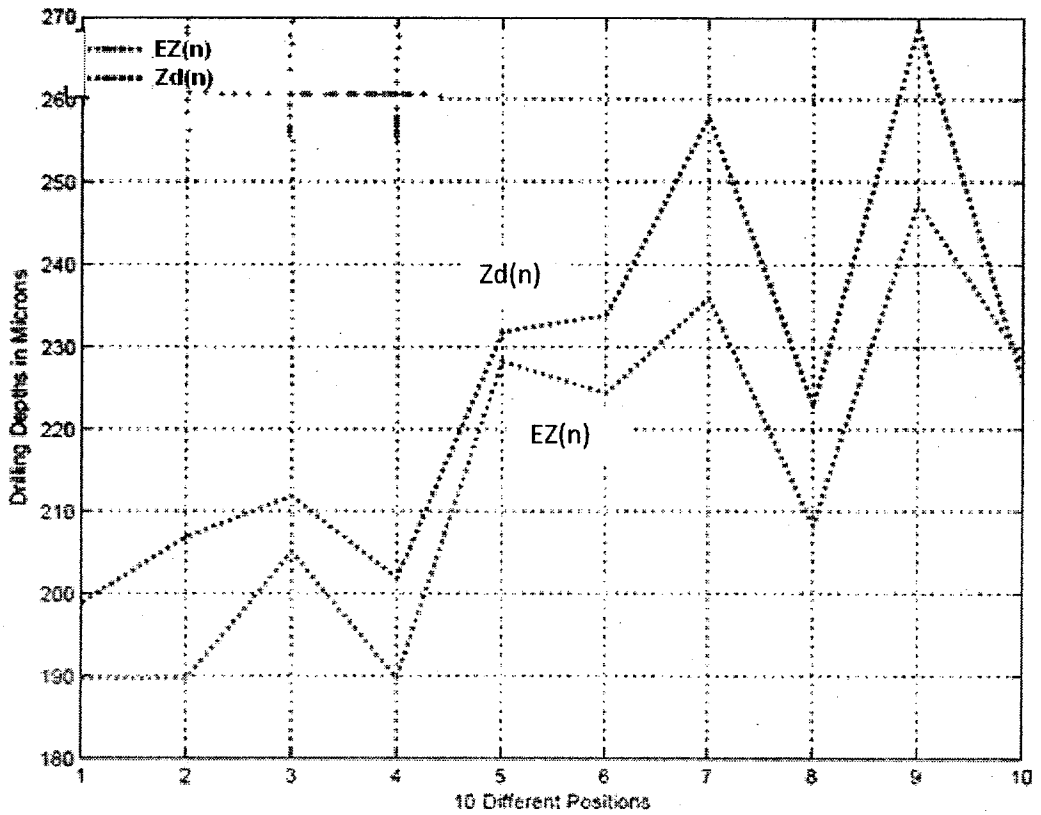

Figure 5.9- Error between estimated and actual drilling depth using the online estimation technique.

5.5 Investigation on machining forces.

As observed in figure 5.1(a) during constant velocity drilling, it is sensible, that the machining force is linked to constant, rising or diminishing slopes. These particulars are

investigated by developing a model for SACE constant velocity drilling, and further comparing the experimental data with the solution of this developed model.

5.5.1 SACE drilling model

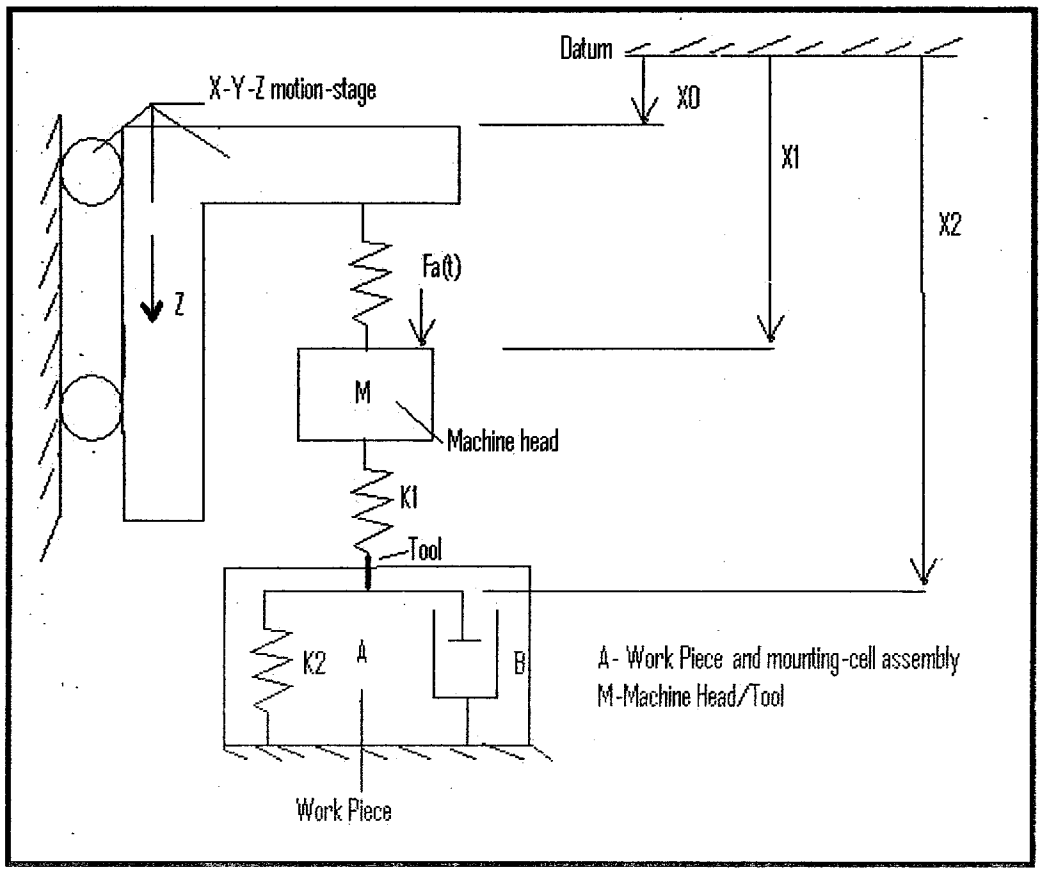

Figure 5.10- SACE drilling model.

A SACE drilling model is developed, with respect to the available information on the drilling apparatus.

The model for constant velocity drilling in SACE technology is shown in figure 5.10. Following lists the abbreviation on various used notations.

M - Mass of the machine head-tool assembly in *Kg*.

K_1 – Stiffness in *N/m* due to controller, flexible structure and tool-chuck assembly.

K_2 – Stiffness in *N/m* due to work-piece and mounting-cell.

B - Viscous damping in work-piece during machining in *N s/m.*

X_0 – Distance between the Z-motion to reference in *m.*

X_1 – Distance between mass (M) to reference in *m.*

X_2 – Distance between reference and the work-piece surface in *m.*

$F_a(t)$- Machining force measured in *N.*

5.5.2 Description of the Model

In figure 5.10 the machine head is originally positioned at a distance X_1, from the reference datum, while the work-piece and mounting cell assembly is positioned at distance X_2 with respect to the datum. The mass M and tool are assumed to be connected in series with the spring of stiffness K_1, which characterizes the upper part (tool-head assembly), whereas the work-piece and mounting cell assembly is characterized by a spring of stiffness K_2 in parallel with viscous damping B. At any time t, during machining, the distance $(X_1\text{-}X_0)$ is kept constant by applying the force $F_a(t)$. During drilling experiments the tool-head system travels at user defined velocity v in the Z direction.

5.5.3 Viscous damping (B)

Throughout dry experiments $B=0$, whereas during real drilling experiments, (with supplied power and available electrolyte). The viscosity can be estimated using Stokes equation.

$$B = 6\pi\eta r \qquad (5.14)$$

The glass viscosity is a function of temperature (Figure 5.11).

The viscosity of the material in the machining zone was estimated [41] as being

$\eta = 1.4 \times 10^8 \, [Pa \cdot s]$ (5.15)

Therefore

$B = 0.35 \times 10^6 \; Ns/m$ (5.16)

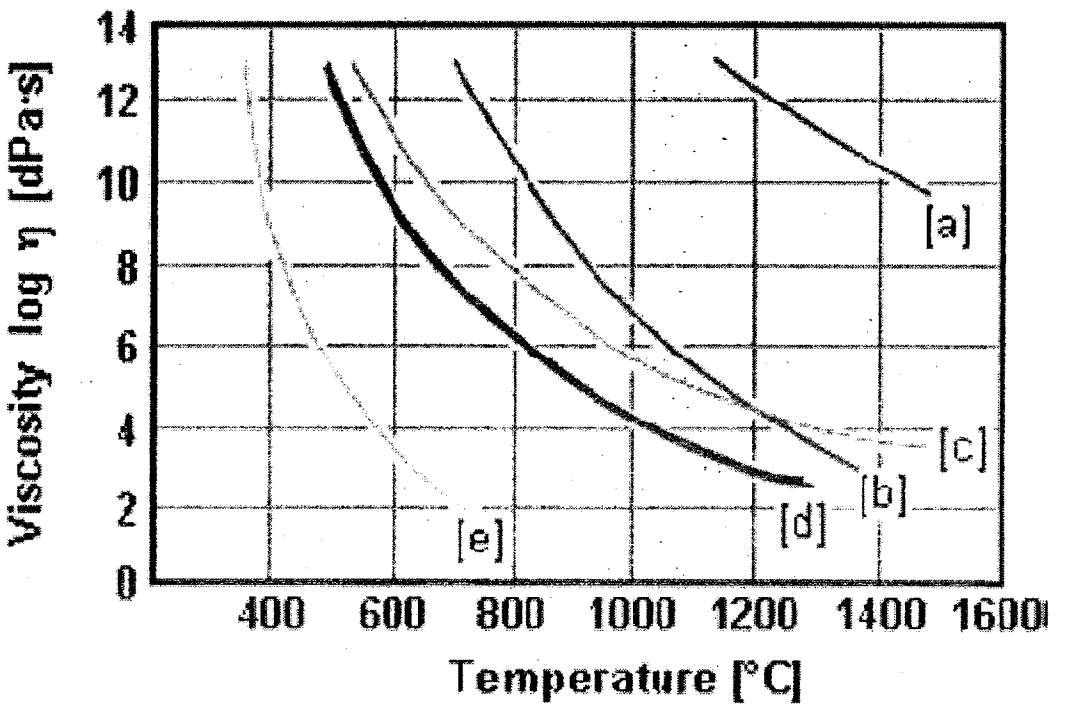

Figure 5.11-Temperature dependence of the viscosity η of technical glasses: (a) fused silica, (b) alum silicate, (c) borosilicate, (d) soda-lime-silica, (e) lead borate [35].

5.5.4 Stiffness K_1

The stiffness K_1 is the sum of stiffness due to controller, flexible structure and the tool-chuck assembly.

5.5.5 Stiffness K_2

The stiffness K_2 is the sum of stiffness due work-piece and its mounting-cell assembly.

5.5.6 Equivalent stiffness K_{eq}

The stiffness K_{eq} is the overall stiffness of the complete SACE drilling setup in the case of non-machining (i.e. $B=0$) and defined as:

$$K_{eq} = \frac{K_1 K_2}{K_1 + K_2} \qquad (5.17)$$

5.5.7 Model equations

From the model above one can write the equations of motions as:

$$M_1 \ddot{X}_1 = K_1(X_2 - X_1) + f_a(t) \qquad (5.18)$$

$$B\ddot{X}_2 = K_1 X_1 - (K_1 + K_2)X_2 \qquad (5.19)$$

Using Laplace transformations on (5.19)

$$B[SX_2(s) - \dot{X}_2(0)] = (K_1 + K_2)X_2(s) + K_1 X_1(s) \qquad (5.20)$$

As $\dot{X}_2(0) = 0$

$$X_2 = \frac{K_1}{SB + K_1 + K_2} X_1(s) \qquad (5.21)$$

Let us now consider the case of constant velocity feed drilling. In this situation

$$X_1(t) = vt \qquad (5.22)$$

with, v the imposed drilling speed, it follows using Laplace transform

$$X_1(s) = \frac{v}{s^2} \qquad (5.23)$$

$$X_2(s) = \frac{K_1}{SB + K_1 + K_2} \frac{v}{s^2} \qquad (5.24)$$

Introducing the equivalent stiffness of the model using equation 5.17

$$K_{eq} = \frac{K_1 K_2}{K_1 + K_2}$$

and the typical time constant,

$$\tau = \frac{B}{K_1 + K_2} \qquad (5.25)$$

substituting 5.25 and 5.17 in 5.24 and taking the inverse Laplace

$$X_2(t) = \frac{K_{eq}}{K_2} v \left[t + \tau \left(e^{-\frac{t}{\tau}} - 1 \right) \right] \qquad (5.26)$$

Since the driving force $f_a(t) = K_1(X_1 - X_2)$:

$$f_a(t) = K_{eq} v \left[t - \tau \frac{K_1}{K_2} \left(e^{-\frac{t}{\tau}} - 1 \right) \right] \qquad (5.27)$$

Note the following two interesting limiting cases

$$t \to \infty \quad f_a(t) = K_{eq} v t \ ({}^{K_1}/_{K_2})^2 + Bv \qquad (5.28)$$

$$t \to 0 \quad f_a(t) = \left(e^{-\frac{t}{\tau}} - 1 \right) \to -\frac{t}{\tau} \qquad (5.29)$$

$$f_a(t) = K_{eq} v \left(1 + \frac{K_1}{K_2} \right) t = K_1 v t \qquad (5.30)$$

Resemblance can be observed between figure 5.1(b) and figure 5.12

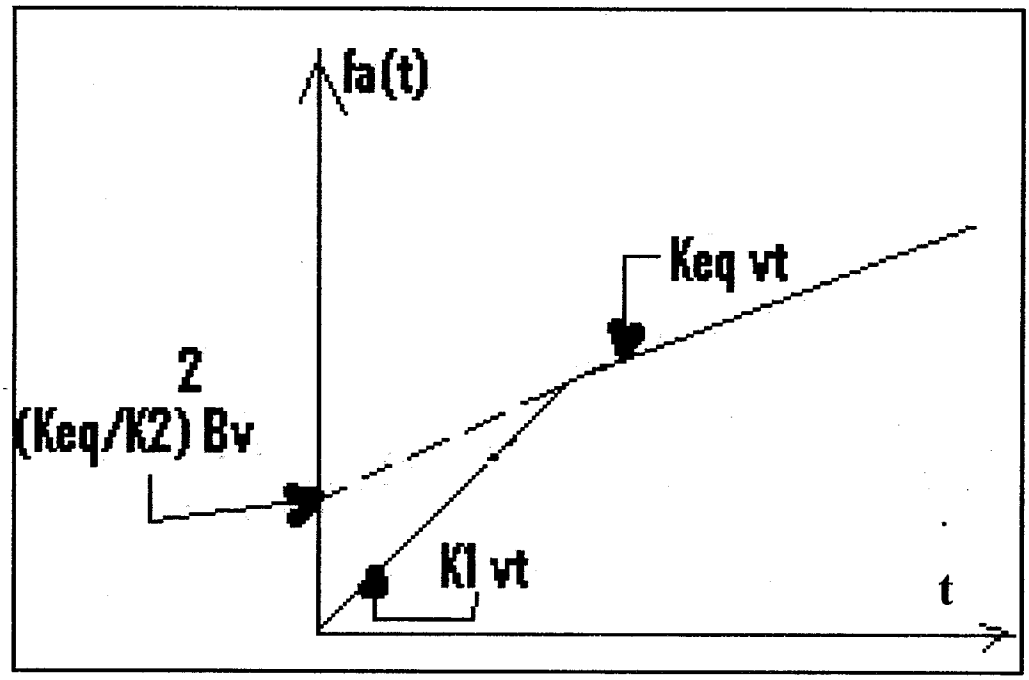

Figure 5.12- SACE drilling model solution.

5.6. Model verification

The model and its parameters discussed in the previous sections, is compared with the experimental data collected during constant velocity drilling experiments. In following sections the model verification and the experimental results will be presented.

In figure 5.13, K_1 is plotted in function to applied voltage from constant velocity drilling experiments at v=4 μm/s. The experimental value for K_1 is found to be in a range of about 17000-22000 N/m. The variation in the values of K_1 might be due presence of play in the tool chuck assembly. The dotted line shows, the stiffness value due to gas film (bubble), in function to applied voltage (see figure 5.4 for details). The gas film stiffness is observed to be constant throughout for all applied voltages.

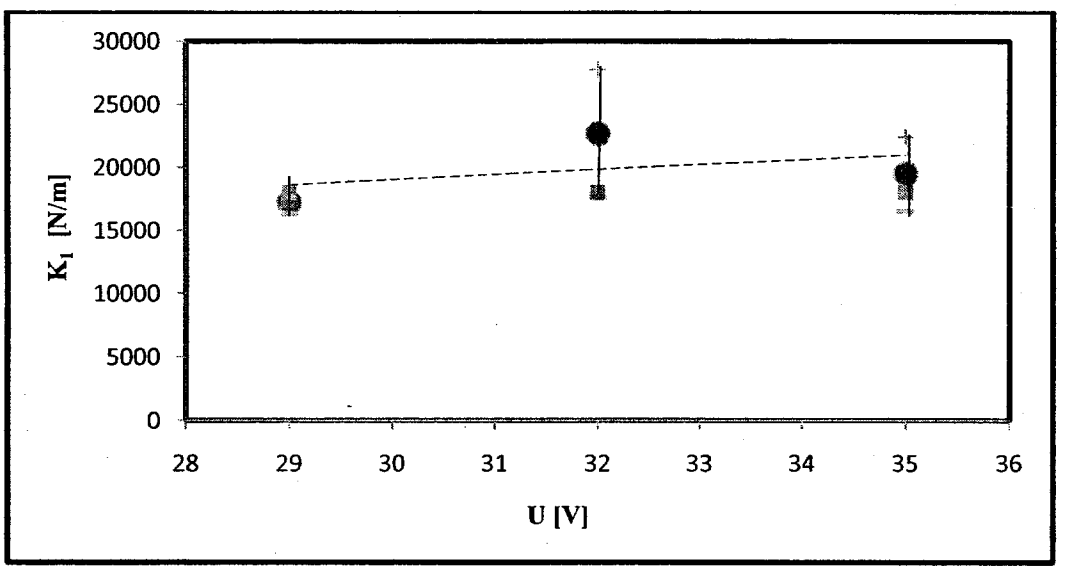

Figure 5.13- Stiffness due to gas film ('---') and the equivalent stiffness of the tool assembly K_1 ('_____') in function of applied voltages.

In figure 5.14, K_2 is plotted as a function of applied voltage, taken from constant velocity drilling experiments at v=4 μm/s. The value for K_2 is found in a range of 17000-25000 N/m. The variations in the values of K_2 might be due to the wobbling and plays present in the work-piece mounting assemblies.

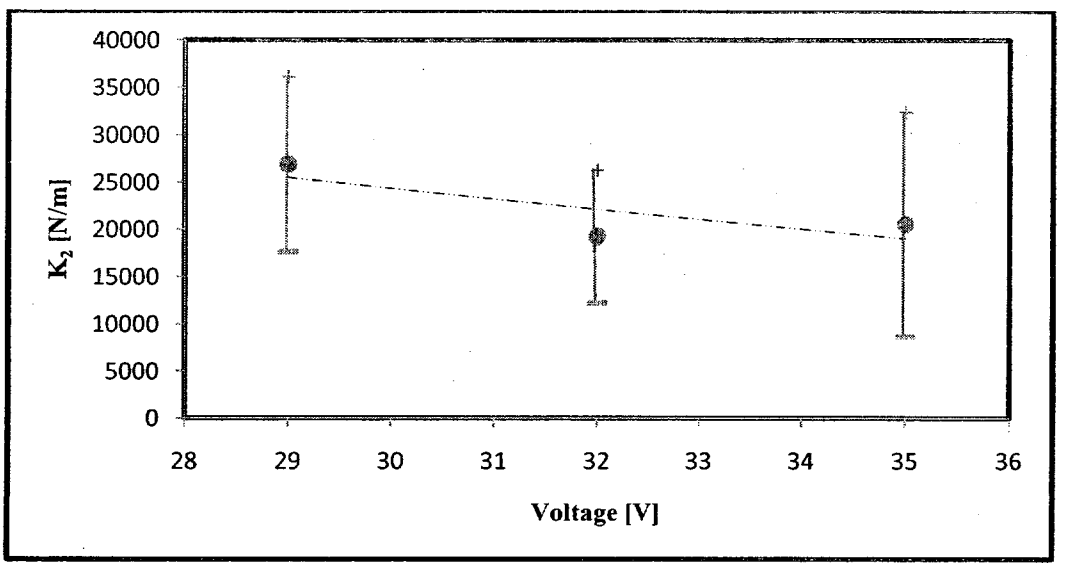

Figure 5.14-Stiffness of the work-piece assembly in function to applied voltage.

Figure 5.15 is a plot for B as a function of applied voltage, taken from constant velocity drilling experiments at v=4 μm/s, the values for B are found to be in a range of 0.20 - 0.35×10^6 N.s/m, this can be compared to equation (5.16) stated earlier. The variation in B could be due to slight temperature variations during the drilling process, affecting the material viscosity and due to un-controlled electrolyte level, during each drilling process.

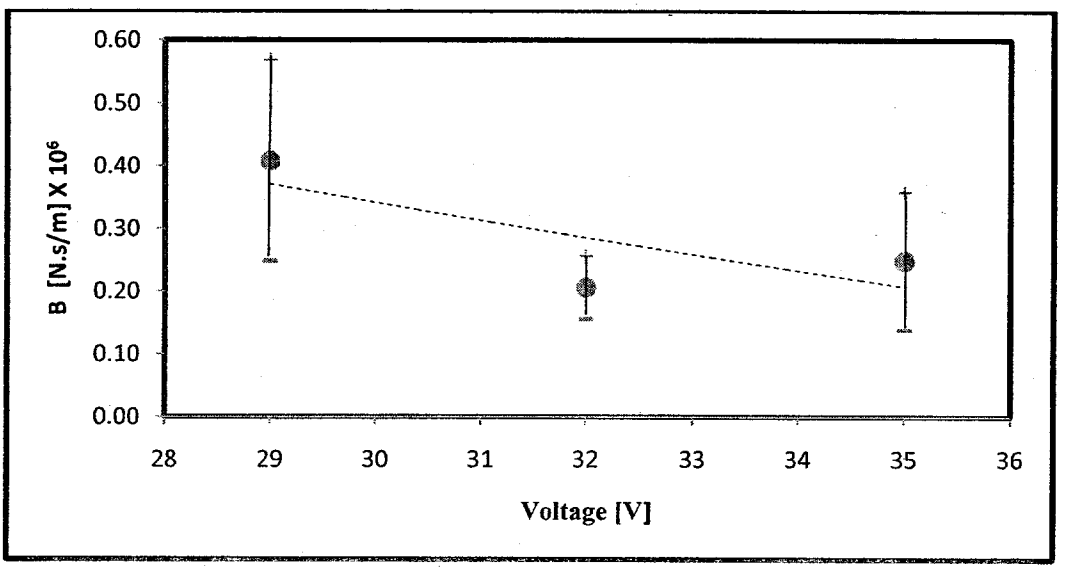

Figure 5.15-Viscous damping in function to applied voltages

Further, figure 5.16-5.19 shows the experimental values of K_1, K_2, K_{eq} and B as a function of various drilling velocities, for applied voltages at *29* V, *32* V and *35* V. It can be observed that the trends look fairly similar as well the stiffness values seem to be reducing with respect to applied drilling velocities. The stiffness's K_1 and K_2, are mostly depending on the assembly setup. The variations in K_1 and K_2 come, form considering the fact that all the experiments were not done in one shot, but in a month period and the assembly setup was disturbed between each successive experiment.

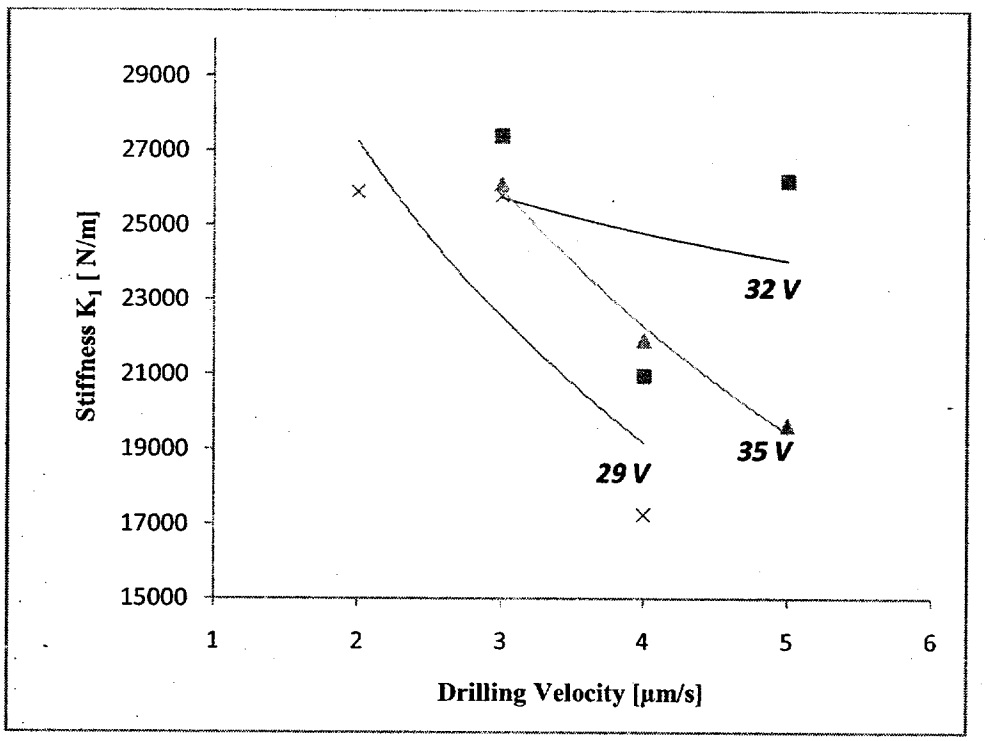

Figure 5.16- Variations in Stiffness K_1 for various drilling velocities with different applied voltages.

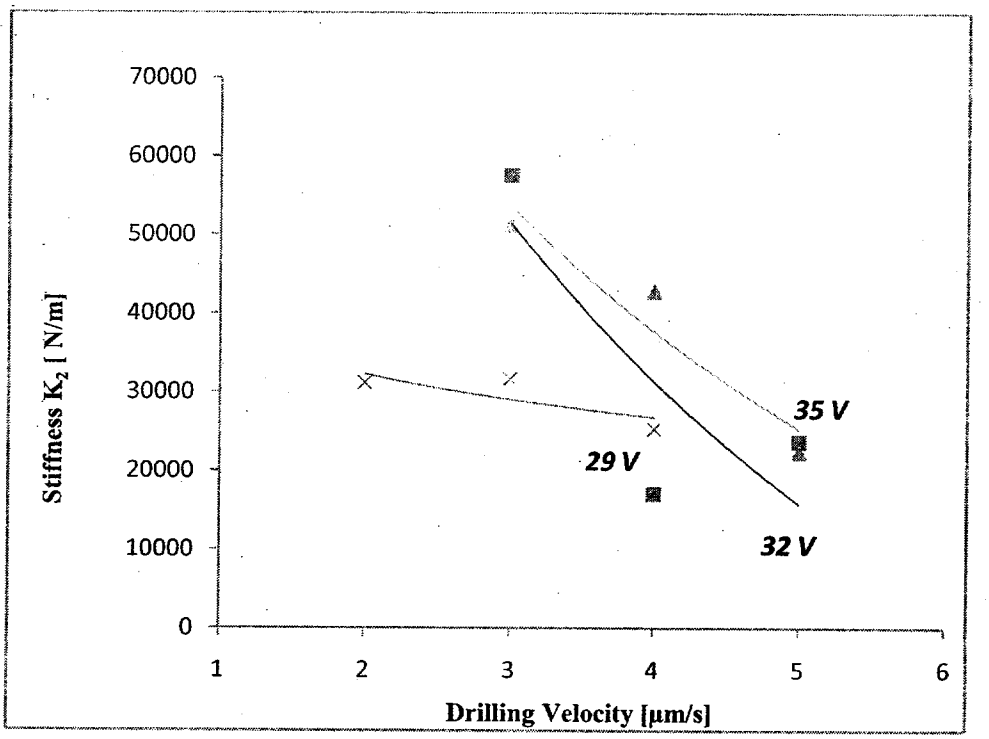

Figure 5.17- Variations in Stiffness K_2 for various drilling velocities with different applied voltages.

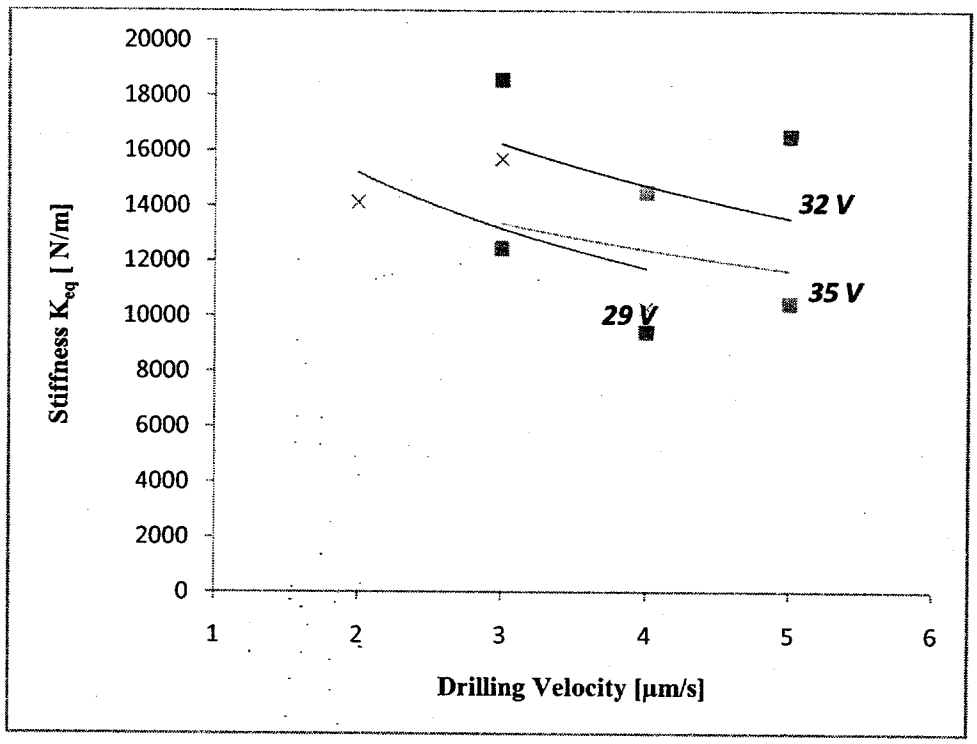

Figure 5.18- Variations in Stiffness K_{eq} for various drilling velocities with different applied voltages.

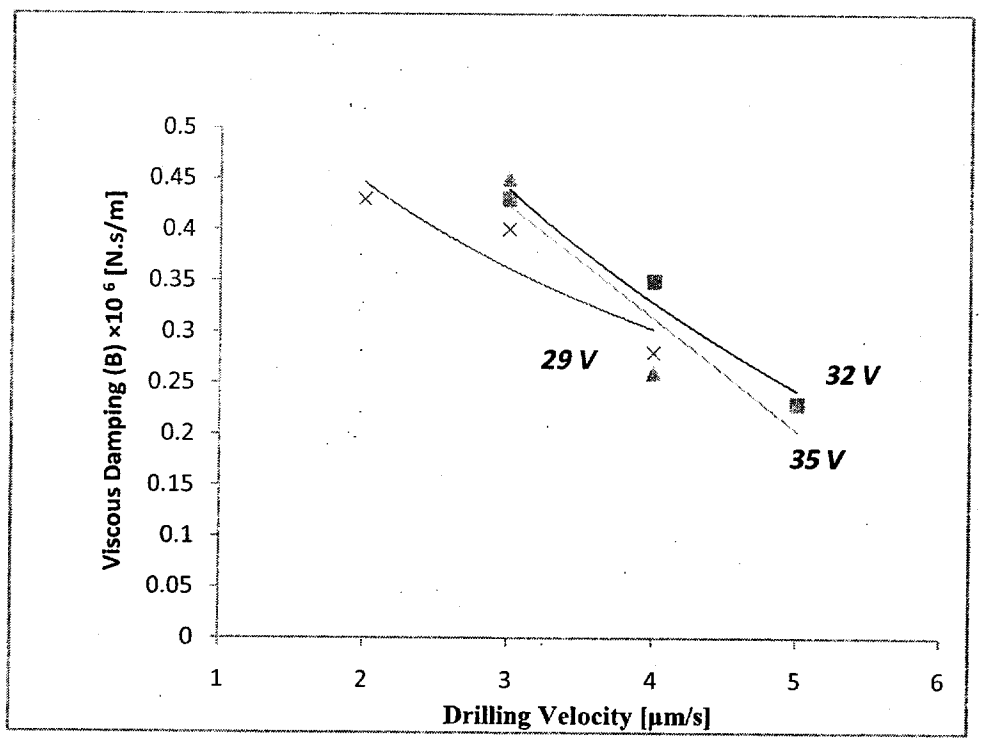

Figure 5.19- Variations in viscous damping B for various drilling velocities with different applied voltages.

In figure 5.18, it is observed that the experimental values for K_{eq} lie within the range 10000 *to* 17000 N/m. The values agree when compared to the slope of a typical dry experiment (equation (3.3) from chapter 3).

From figure 5.17, it can be observed that the experimental values for viscous damping (B) fall in the range (0.2 to 0.45)$\times 10^6$ N.s/m. Using any typical value of (B) within this range the viscosity can be calculated as $\eta = 1\times 10^8$ Pa.s., this value seems to be relatively closer to the value of η stated in equation (5.15), estimated in [41].

5.7 General observations and discussions

For constant velocity drilling experiments, the data on initial drilling depth, were analyzed using observational techniques.

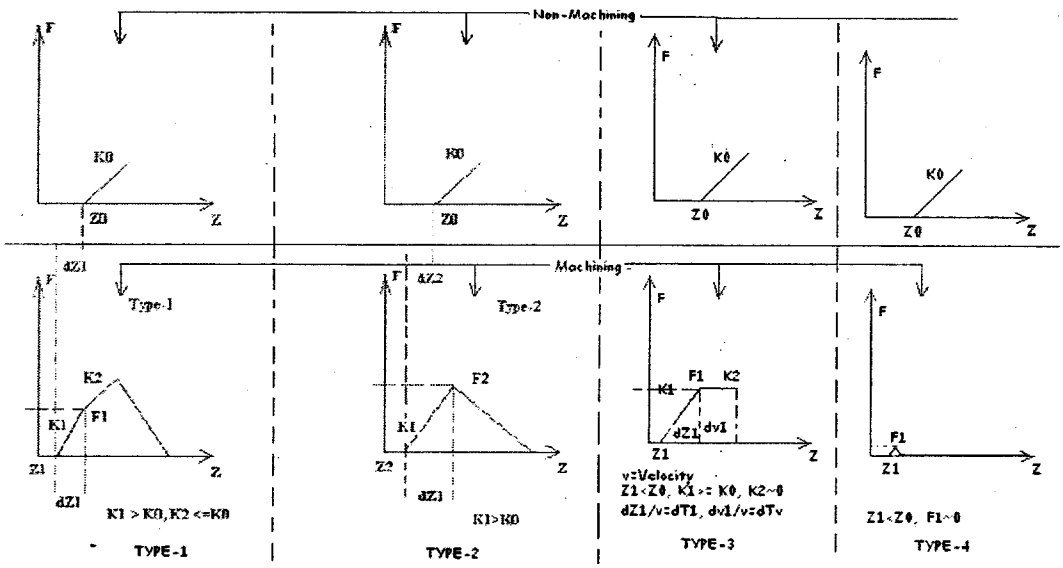

Figure 5.20- Classification of the plots for initial depth 0 > Z < 100 μm.

Never least but last, probably describing the results could help for any future work on SACE drilling technologies. Figure 5.20, shows the classification of forces based on the trends observed. The trends are summarized in table 5.2. Referring to the mechanism of

Status	Type	Stiffness	To find	To find	Force	Force detection position	Error in touching	Distance	Time constant dT
N-M	-	k_0	-	-	-	z_0	-	-	-
M	*1*	-	k_1	k_2	F_1	z_1	dz_{e1}	dz_1	dz_1/v
N-M	-	k_0	-	-	-	z_0	-	-	-
M	*2*		k_1		F_1	z_2	dz_{e2}	dz_1	dz_2/v
N-M	-	-	-	-	-	z_0	-	-	-
M	*3*	k_0	k_1	$k_2=0$	F_1	z_3	dz_{e3}	dz_3	dz_3/v
N-M	-	k_0	-	-	-	-	-	-	
M	*4*	k_0	-	-	F_{max}	-	dz_{e4}	$-dz_4$	dz_4/v

Table 5.2- Classified parameters, (N-M = non-machining, M= machining, v=drilling velocity)

SACE described in section 1.4.3, the different observed trends can be, co- related to possible cases of the model solution given in equation (5.27). Type-1 is same as the general solution shown fig 5.12; Type-2 has only one initial slope, which explains the possibility of tool touching the work-piece and is not able to remove the material., for some certain time and then suddenly boosting up the drilling process. Type-3 can be another case representing the presence of the tool in the molten viscous zone. Finally Type-4 can be one case where all the parameters are in favor to the material removal rate.

Table 5.3 is the summary for occurrence of the classified trends in function to different applied voltage. It can be observed that occurrence of trends, type-1 and type-2, are generally due to the contact between tool and work-piece surface or contacts between tool and drilling depth of the hole. These are mostly observed at higher drilling speeds. The occurrence of type-3 is typically when the tool is moving in the molten/viscous zone

of the hole and could be generally associated with rational drilling velocities equal to material removal rate.

Voltage *(V)*	Velocity *(μ/s)*	Type-1	Type-2	Type-3	Type-4
28	1	9	8	-	7
28	2	3	3	-	-
28	3	-	-	3	
29	1	9	8	-	7
29	2	7	7	1	-
29	3	6	9	-	1
29	4	-	-	-	-
32	1	1	2	-	6
32	2	1	7	-	4
32	3	3	8	-	-
32	4	3	3	7	7
32	5	5	9	3	
35	2	3	5	-	5
35	3	2	1	-	3
35	4	1	9	-	8
35	5	6	7	2	-

Table 5.3- Frequency for classified systems, Type-1 and Type -2, Type-3, Type-4.

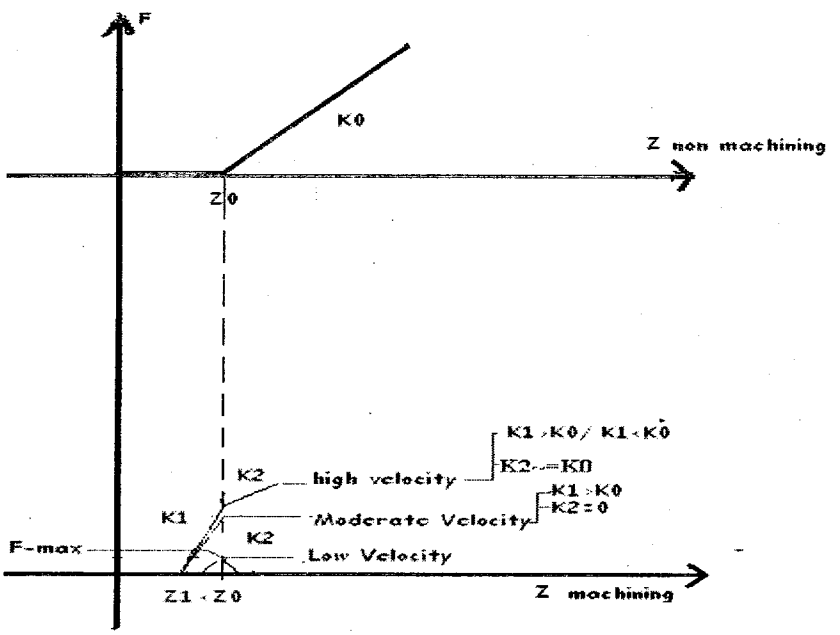

Figure 5.21- Detailed classification of the initial drilling depth for constant velocity SACE drilling.

Types of Forces	Definition of forces	Reasons
Forces due to gas film/tool expansion	Due to k_1 @ High Velocity Due to k_1 @ moderate velocity F_{max} at low velocity	Tool velocity is lagging the material removal rate capacity/Level of Electrolyte too much/or too less (observations)
Forces due to stiffness	Due to k_0 @ any velocity (non-machining)	Tool moving against after touching the surface of work-piece.
Forces due to Viscosity	Due to k_2@ moderate velocity	Tool moves with velocity against the viscous forces.

Table 5.4- Summary of the classified forces.

The occurrence of type-4 can be observed only in experiments with very low drilling velocities, where the material removal rate can be faster that the drilling speeds. Generally type-1 and type-2 are the most regular trends found in a constant velocity drilling experiments. Figure 5.22 and table 5.4 reviews the apparent relations between the observed trends at different drilling velocities

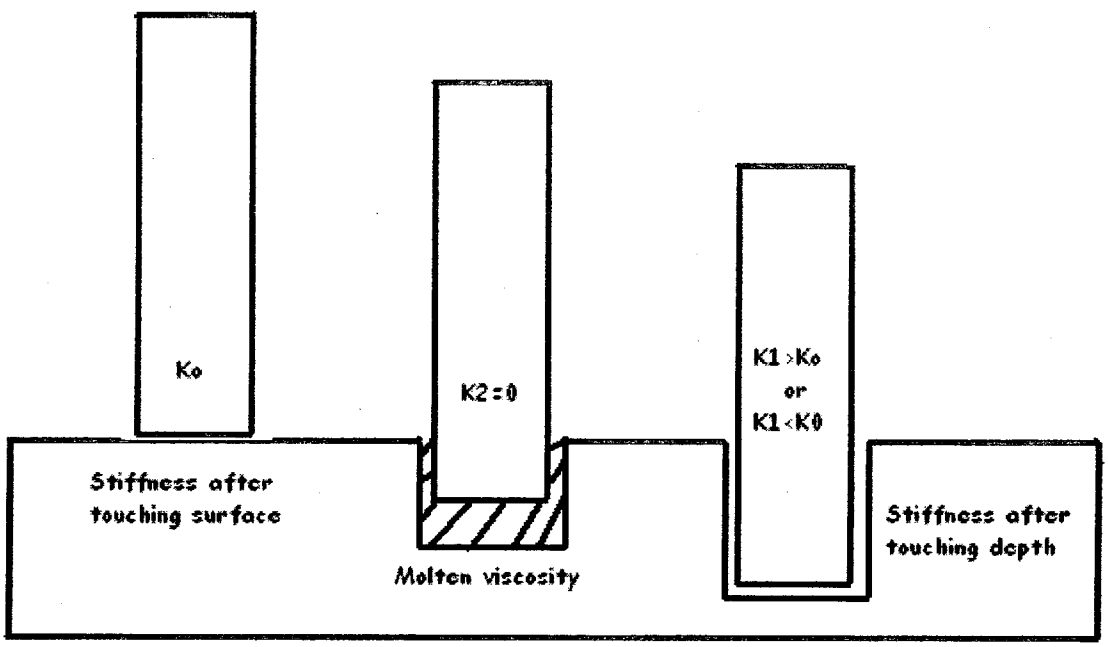

Figure 5.22- Stiffness values at different states during SACE constant velocity drilling.

Velocity	Material removal rate	Probable reasons
Low	High	Enough source of heat/ enough time for electrolyte to dissolve the melted glass
Moderate	Medium	Moderate source of heat/ adequate time for electrolyte to dissolve the melted glass.
High	Low	Fewer sources of heat/ in adequate time for electrolyte to dissolve the melted glass.
Very high	Very poor	Very less source of heat/ very inadequate time for electrolyte to dissolve the melted glass

Table 5.5- Classification based on various drilling speeds.

Figure 5.22 and table 5.5 summarizes the possible reasons and relations between machining force, drilling velocities and material removal rates.

Chapter 6

Conclusion and Future Work

6.1 Conclusion

The conclusions drawn from this thesis work are

- The early force detection is associated to the combinations of thermal expansion in tool and work piece in adjunct to formation of pure molten NaOH layer, and the possible pushing on tool effect due to gas film (bubble).
- The drilling depths have a direct relationship to applied power and an inverse relationship to the velocity of drilling. A comparative study on quality of hole against different constant velocity drilling depths could help to confirm the tradeoffs between drill-hole quality & machining time.
- Real-time force measurement setup could be used to implement gap control feedback strategies in SACE constant velocity drilling.
- With the help of SACE drilling model and the actual experimental data, it can be concluded that the machining forces associated with constant slopes appear from the moving tool in the viscous zone, the intensifying slopes are associated to the stiffness in setup and the diminishing slopes can be correlated to rapid boost in material removal rate.
- The SACE model can be the used for better understanding of the constant feed drilling process, while the investigated forces can be used as a benchmark to implement force feedback drilling strategies in SACE Technology

6.2 Discussion

Before discussing the future work, I would like to talk about the problems encountered.

- The process being much complex and exceptionally smaller amount of previous work been done, especially in the area of constant velocity drilling for SACE technology, struggling for references was very time consuming.
- Considering the fact that this process having an involvement of multi-engineering disciplines, initially it was very hard to understand.
- The SACE machine head assembly was a pre-made, readily available setup, prerequisite of certain modifications were advantageous, but were time consuming.
- It is really hard to control/maintain the electrolyte level above the work-piece in the pre-made electrochemical-cell, this could have been a source of errors, while doing the actual experiments.
- The concerned measurement scales, were in microns, many conversion factors come into the picture, due to multi engineering areas as well, and this could have also been a source of error.
- Adjacent to all these problems, Dr. Rolf Wüthrich had always been very supportive, and has given the best possible advices. His around the clock presence has been very encouraging, without which, I could have not accomplished this moment of concluding my thesis work.

6.3 Future work

I would discover myself contented to recommend few points which could be done to employ future work in the area of constant velocity drilling for SACE technology.

- The machine head assembly could be modified/re-designed with bigger size voice coil to avoid the saturation problems at higher force values.
- The SACE electrochemical cell setup could be modified/re-designed with a capability to have a level detector to control/maintain the level of electrolyte.
- The SACE cell setup could be compensated for bending, tilting or wobbling to avoid backlash and plays between different parts and assemblies, which are definitely the gigantic source of errors while dealing at scales in microns.
- Detailed investigations on quality of hole, in function to the constant velocity drilling depths can be done on different samples; this could help to confirm the tradeoffs between material removal rate and machining time.
- Development of an embedded, multi combined, real-time and smart sensor, capable to measure the parameters such as, electrolyte level, local temperature, drill-hole depth, conductivity of cell & pH, could facilitate the advancement in implementing feedback based control strategies for SACE drilling technology.

List of References

[1] V.K. Jain, S.K. Choudhury, K.M. Ramesh, "On the machining of alumina and glass", International Journal of Machine Tools & Manufacture 42 (2002) 1269-1276

[2] Y.P. Singh, V.K. Jain, P. Kumar, D.C. Agrawal, "Machining piezoelectric (PZT) ceramics using an electrochemical spark machining (ECSM) process", Journal of Materials Processing Technology 58 (1996) 24-31

[3] N.H. Cook, G.B. Foote, P. Jordan, B.N. Kalyani, "Experimental studies in electro-machining" Trans. ASME, Journal of Engineering for Industry" (1973) 945-950

[4] B. Bhattacharyya, B.N. Doloi, S.K. Sorkhel, "Experimental investigations into electrochemical discharge machining (ECDM) of non-conductive ceramic materials", Journal of Materials Processing Technology 95 (1999) 145-154

[5] R. Wüthrich, V. Fascio, "Machining of non-conductive materials using electrochemical discharge phenomenon– An overview", International Journal of Machine Tools and Manufacture, 45 (2005) 1095-1108

[6] R. Wüthrich, L.A. Hof, "The gas film in Spark Assisted Chemical Engraving (SACE) - A key element for micro-machining applications", International Journal of Machine Tools and Manufacture 46 (2006) 828-835

[7] R. Wüthrich, K. Fujisaki, Ph. Couthy, L.A. Hof, H. Bleuler, "Spark assisted chemical engraving (SACE) in micro-factory", Journal of Micromechanics and Microengineering 15 (2005) 276-280

[8] A. Kulkarni, R. Sharan, G.K. Lal, "Measurement of temperature transients in the electrochemical discharge machining process", Its measurement and Control in Science and Industry 7 (2003) 1069-1074

[9] G.W. McLellan, E. B. Shand, "Glass Engineering Handbook", McGraw-Hill, New-York, (1984).

[10] H. Kurafuji and K. Suda, "Electrical discharge drilling of glass (1968)" Ann. CIRP 16 415–9

[11] V.K. Jain, P. S. Rao, S.K.Choudhury, K.P. Rajurkar, "Experimental investigations into travelling wire electrochemical spark machining (TW-ECSM) of composites", Transaction of ASME, Journal of Engineering for Industry 113 (1991) 75-84

[12] V.K. Jain, S.K. Choudhury, K.M. Ramesh, "On the machining of alumina and glass", International Journal of Machine Tools and Manufacture 42 (2002) 1269-1276

[13] V.K. Jain, S.K. Chak, "Electrochemical spark trepanning of alumina and quartz", Machining Science and Technology 4 (2000) 277-290

[14] R. Wüthrich, V. Fascio, D. Viquerat, H. Langen, "In Situ Measurement and Microachining of Glass", International Symposium on Micromecatronics and Human Science (MHS'99), Nagoya (1999) p. 185

[15] R. Wüthrich, U. Spaelter, Y. Wu, H. Bleuler, "A systematic characterization method for gravity feed micro-hole drilling in glass with Spark Assisted Chemical Engraving (SACE)", Journal of Micromechanics and Microengineering 16 (2006) 1891-1896

[16] R. Wüthrich, B. Despont, P. Maillard, H. Bleuler "Characterization of micro-holes drilled in glass by gravity-feed with Spark Assisted Chemical Engraving (SACE)".

[17] R. Wüthrich, B. Despont, P. Maillard, H. Bleuler, "Improving drilling speed in Spark Assited Chemical Engraving (SACE) by tool vibration", J. Micromech. Microeng.

[18] P. Maillard, "Caractérisation visuelle et analyse de répétabilité de l'usinage SACE", Projet de semestre, Ecole Polytechnique Fédérale de Lausanne (2006)

[19] B. Despont, "Optimisation de performances d'usinages SACE" Projet de semstre, Ecole Polytechnique Fédérale de Lausanne (2006)

[20] Y.S. Liao, W.Y. Peng, "Study of hole-machining on Pyrex wafer by electrochemical discharge machining (ECDM)", Materials Science Forum Vols. 505-507 (2006) 1207-1212

[21] R. Wüthrich, H. Bleuler, Ph. Mandin, D. Lincot "Micro machining glass with Spark Assisted Chemical Engraving (SACE)– Applications for electrochemical micro-devices", Electrochemical Micro and Nano Systems Technology, 23th – 25th August 2006, Bad Godesberg, Germany

[22] R. Wüthrich, V. Fascio, D. Viquerat, H. Langen, "Study of Spark assisted Electrochemical Etching- Force Measurements", International Workshop on Microfactories (IWMF 2000), Fribourg (2000) 201- 204

[23] Anjali V. Kulkarni and V. K. Jain," Microfabrication using Electrochemical Spark", Mechanical Engineering Department. Indian Institute of Technology, Kanpur.

[24] V. Fascio, R. Wüthrich, D. Viquerat, H. Langen, "3D Microstructuring of Glass using Electrochemical Discharge Machining (ECDM)", International Symposium on Micromecha-tronics and Human Science (MHS'99), Nagoya (1999) 179-183

[25] H. Langen, J.M. Breguet, H. Bleuler, Ph. Renaud, T. Masuzawa, "Micro Electrochemical Discharge Machining of Glass", International Journal of Electrical Machining 3 (1998) 65-69

[26] U. Spaelter, R. Wüthrich, H. Bleuler: "Spark Assisted Chemical Engraving (SACE) machining– Haptic device for the operator", International Conference of the European Society for Precision Engineerining and Nanotechnology (EUSPEN) May 8th - 11th 2005, Montpellier, France

[27] R. Wüthrich, "Spark Assisted Chemical Engraving– A Stochastic Modeling Approach", Thèse NO2776, Ecole Polytechnique Fédérale de Lausanne (2003)

[28] R. Wüthrich, U. Spaetler, H. Bleuler "The current signal in Spark Assisted Chemical Engraving (SACE), what does it tell us?" Journal of Micromechanics and Microengineering 16 (2006) 779-785

[29] S. Henein, "Conception de guidages flexibles", Collection Meta, Presses Polytechniques et Univesitaires Romandes (2004)

[30] I. Basak, A. Gohosh, "Mechanism of material removal in electrochemical discharge machining: a theoretical model and experimental verification", Journal of Material Processing Technology 71 (1997), pp.350-359.

[31] Zhi-Ping Zheng, Hsin-Chuan Su, Fuang-Yuan Huang, Biing-Hwa Yan, "The tool geometrical shape and pulse-off time of pulse voltage effects in a Pyrex glass electrochemical discharge microdrilling process", Journal of Micromechanics and Microengineering 17 (2007) 265-272

[32] Biing-Hwa Yan, Ching-Tang Yang, Fuang-Yuan Huang, Zhe-Hong Lu, "Electrophoretic deposition grinding (EPDG) for improving the precision of microholes drilled via ECDM", Journal of Micromechanics and Microengineering 17 (2007) 376-383

[33] Amy B. Jedlicka, Alexis G. Clare, "Chemical durability of commercial silicate glasses in material characterization", Journal of Non-Crystalline Solides, 281 (2001) 6-24

[34] K.J. Åström, B. Wittenmark "Computer-Controlled Systems– Theory and Design", Third Edition, Prentice Hall (1997)

[35] P. Millard, "Investigation on material removal process in SACE glass machining - Design of a force measuring set-up", Master's Thesis at Ecole Polytechnique de Lausanne (EPFL), Swiss Federal Institute of Technology.

[36] R. Wüthrich, "Micromachining Using Electrochemical Discharge Phenomenon- Fundamentals and Applications of Spark Assisted Chemical Engraving", First Edition, William Andrew (2009)

[37] M. Mousa, A Allagui, H D Ng and R Wuthrich, "The effect of thermal conductivity of the tool electrode in spark-assisted chemical engraving gravity-feed micro-drilling", Journal of Micromechanics and Microengineering, 19 (2009) 015010.

[38] Tohid Fatanat Didar, "Micro-fabrication with Spark Assisted Chemical Engraving (SACE) Technology", Master's Thesis in The Department of Mechanical and Industrial Engineering, Concordia University, Montreal, 2008.

[39] Andrew Morrison, Luis Rodrigues, Rolf Wüthrich, " Reducing Variablity in Spark Assisted Chemical Engraving Gravity Feed Drilling of Glass", Department of Mechanical and Industrial Engineering, Concordia University, Montreal, Canada. 1st Microsystems and Nanoelectronics Research Conference (MNRC 2008).

[40] Malek Mousa, "Quality Assessment and Improvement on Spark Assisted Chemical Engraving the Gravity Feed Micro-drilling", Master's Thesis in The Department of Mechanical and Industrial Engineering, Concordia University, Montreal, 2008.

[41] M. Jalali, P. Maillard, R. Wüthrich,"Towards a better understanding of glass gravity-feed micro-hole drilling with electrochemical discharges", Journal of Micromechanics and Microengineering(2007)

[42] J. West, A. Jadhav, "ECDM methods for fluidic interfacing through thin glass substrates and the formation of spherical microcavities", Journal of Micromechanics and Microengineering 17 (2007) 403-409

[43] A.Morrison, L.Rodrigues, R.Wuthrich, "Stochastic Staircase Model for Spark Assisted Chemical Engraving Gravity Feed Drilling of Glass", 1st Workshop on Multi-physics, Concordia University March 2 and March 3, Room EV 2.184.

[44] www.google.ca

[45] www.youtube.ca

[46] http://library.concordia.ca/

Appendix A

Matlab code

Bending of work-piece:

```
clc
rho=(2.23)*(1/100)*(1/10^6);        % Density - in Kg/m^3
l=76/1000;                          % Length-in m
h=1/1000;                           % Height-in m
b=25/1000;                          % Breadth-in m
m= rho*l*b*h;                       % Mass- in Kg
F =1.8;                             % Force n Newtons
I= b*h^3/12;                        % moment of inertia in m^4
E=65*10^9;                          % Youngs Modulus- N/m^2
z = -(F*l^3)/(48*E*I)               %Maximum bending of work-piecein m,
(N*m^3)/(m^4*N/m^2)
```

Estimation for viscous damping:

```
clc
pi=3.142;                           % Constant
eta=7.6*10^7;                       % estViscosity in Pa.s
r=0.35*10^-3;                       % Radius  of tool-tip in m
v=1*10^-6;                          % Velocity in m/s
B=6*pi*eta*r;                       % Viscous damping
f=B*v                               % Viscous force Pa.s.m.m/s = N..... Pa=N/m^2
f=0.5                               % Force in N
eta=f/(6*pi*v*r)                    % Viscosity in Pa.s
```

Thermal expansion of tool and work-piece:

```
Lot=0.5*10^-3;                      % Original length of tool in m.
ALPHAt=13;                          %Coefficient of thermal expansion of tool.
dT=823.15;                          % Final temperature of tool in Kelvin.
dLt=Lot*ALPHAt*dT*10^-6             % Change in length of tool.

Low=1*10^-3;                        % Original height of work-piece in m.
ALPHAw=4;                           %Coefficient of thermal expansion of glass
dT=823.15;                          % Final temperature of tool in Kelvin.
dLw=Low*ALPHAw*dT*10^-6             % Change in length of tool.

dLt+dLw/2
```

Estimation of pressure due to gas film(bubble)

```
f=0.4                    % Force in N
pi=3.142                 % Constant
r=0.35*10^-3             % Radius of tool-tip in m
a=pi*r*r                 % Area of tool tip in m^2
p=f/a                    % pressure due to gas film(bubble) in N/m^2
```

Estimation of drilling depths

```
A=[200 208 211 201 230 233 260 224 270 224];
A1=[63 53 52 52 50 50 52 50 50 50];
B1=[31 21 18 18 15 16 21 18 18 15];
F1=[1 1 0.8 1 0.5 0.55 0.4 0.76 0.25 0.5];
T=1:1:10;
X1(:,:) = 300-(A1-B1);
X2(:,:) = 10^-6*(X1(:,:)-A(:,:))
slope=1.2958e+004;  % slope = m taken from the mean values of non machining stifness
incpt(:,:) = 10^-6*mean(A1-B1);
Y(:,:)=F1(:,:);                  % Y-Y1=m(X-X1)+C
X(:,:)=Y(:,:)/slope - incpt/slope

subplot(5,1,1);plot(T,A,'-bo');
xlabel('10 different random positions')
ylabel('Final drilled depth in microns')
title('TO SEE DEPTH VERSES MEASURED FINAL FORCE VALUE')
grid on
subplot(5,1,2);plot(T,A1-B1,'-bo');
xlabel('10 different random positions')
ylabel('Probable Tool/Workpiece Expansion')
grid on

subplot(5,1,3);plot(T,F1,'-bo');
xlabel('10 different random positions')
ylabel('Final Measured F Value in Newtons')
grid on

subplot(5,1,4);plot(T,F1,'-bo');
xlabel('10 different random positions')
ylabel('Final force Measured Value')
grid on

subplot(5,1,5);
plot(300-mean(A1-B1)-1000000*X,'-r');
```

```
hold on;
plot(300-mean(A1-B1)-1000000*X2,'-b')
xlabel('10 different random positions')
ylabel('Estimated and Actual Drilled Depths in microns')
grid on
plot(T,1000000*X2,'--ro');
hold on;
plot(T,1000000*X,'--bo');
ylim([0,100])
grid on;

plot(300-mean(A1-B1)-1000000*X,'--r');
hold on;
plot(300-mean(A1-B1)-1000000*X2,'--b')

B=[200 206 278 149 233 256 251 252 208 192 249 201 273];
C=[249 201 273 255 287 237 287 283 288 311 265 264 249];
t=1:1:13;
plot(t,A,'--ro')
hold on
plot(t, mean(A),'--ro')
hold on
plot(t,B,'--bs')
hold on
plot(t, mean(B),'--bs')
hold on
plot(t,C,'--gd')
hold on
plot(t, mean(C),'--go')
grid on

mean(A)
mean(B)
mean(C)
```

Appendix B

List of .tcl script programs

Name of file: C_V_Drill.tcl

Purpose: Program for Constant velocity Drilling

```
#Display error and close procedure
proc DisplayErrorAndClose {socketID code APIName} {
global tcl_argv
if {$code != -2 && $code != -108} {
set code2 [catch "ErrorStringGet $socketID $code strError"]
if {$code2 != 0} {
puts stdout "$APIName ERROR => $code - ErrorStringGet ERROR => $code2"
set tcl_argv(0) "$APIName ERROR => $code"
} else {
puts stdout "$APIName $strError"
set tcl_argv(0) "$APIName $strError"
}
} else {
if {$code == -2} {
puts stdout "$APIName ERROR => $code : TCP timeout"
set tcl_argv(0) "$APIName ERROR => $code : TCP timeout"
}
if {$code == -108} {
puts stdout "$APIName ERROR => $code : The TCP/IP connection was closed by an
administrator"
set tcl_argv(0) "$APIName ERROR => $code :  The TCP/IP connection was closed by
an administrator"
}
}
set code2 [catch "TCP_CloseSocket $socketID"]
return
}
```

```
#Main process

set TimeOut 3000
set code 0
puts stdout ">>> Constant velocity drilling  process starts now!"

# load the FindZero function
```

```
source //Admin//Public//Scripts//FindZero.tcl #(please check the next .tcl script on page no.for details)

#Open TCP socket

OpenConnection $TimeOut socketID
if {$socketID == -1} {
puts stdout "OpenConnection failed => $socketID"
return
}
```

```
# Initialization and homing all three  axis

puts stdout "Have you Initialized before?"
```

```
set m 1                          # ... counter to increment  the file number  during data saving.
puts stdout "Move Y axis up to start..."
puts stdout "Move Z axis up to start..."
#puts stdout " You have 10 seconds, Please load and build the controller file in Matlab/Simulink"
```

```
# Moving  X`axis

set code [catch "PositionerSGammaParametersSet $socketID XYZ.X 2 400 0.001 0.001"]
if {$code != 0} {
DisplayErrorAndClose $socketID $code "PositionerSGammaParametersSet"
return
}
set code [catch "GroupMoveRelative $socketID XYZ.X -12"]
if {$code != 0} {
DisplayErrorAndClose $socketID $code "GroupMoveRelative"
        return
}
```

```
# Moving Y`axis

set code [catch "PositionerSGammaParametersSet $socketID XYZ.Y 2 400 0.001 0.001"]
if {$code != 0} {
DisplayErrorAndClose $socketID $code "PositionerSGammaParametersSet"
```

```
return
}

set code [catch "GroupMoveRelative $socketID XYZ.Y 4"]
if {$code != 0} {
DisplayErrorAndClose $socketID $code "GroupMoveRelative"
return
}
```

 # Moving Z`axis up

```
set code [catch "PositionerSGammaParametersSet $socketID XYZ.Z 2 400 0.001 0.001"]
if {$code != 0} {
DisplayErrorAndClose $socketID $code "PositionerSGammaParametersSet"
return
}

set code [catch "GroupMoveRelative $socketID XYZ.Z 6"]
if {$code != 0} {
DisplayErrorAndClose $socketID $code "GroupMoveRelative"
return
}
```

 # Start the For Loop (for iteration)

```
for {set j 1} {$j<2} {incr j} {      # ..... 1 iteration for one work
piece
for {set i 1} {$i<11} {incr i} { # ..... 10 iterations for 10 hole
positions
for {set k 1} {$k<4} {incr k} { # ..... 3 iterations for same hole
position
puts stdout "Starting Fabrication of the $m.$k hole"
```

```
# Digital signals from XPS to NI DAQ for event action communication purpose
set code [catch "GPIODigitalSet $socketID GPIO3.DO 1 6"]
if {$code != 0} {
DisplayErrorAndClose $socketID $code "GPIODigitalSet"
return
}
set code [catch "GPIODigitalSet $socketID GPIO3.DO 2 0"]
if {$code != 0} {
DisplayErrorAndClose $socketID $code "GPIODigitalSet"
```

```
return
}
puts stdout "Controller o/p Disabled"
after 500
```

 # Finds the first surface point on work-piece

```
puts stdout ">>> Finding location of the $m th hole"
FindZero $socketID Z
```

 # Sampling and holding position set point by the NI DAQ card

```
set code [catch "GPIODigitalSet $socketID GPIO3.DO 1 0"]
if {$code != 0} {
DisplayErrorAndClose $socketID $code "GPIODigitalSet"
return
}
puts stdout "Sampled Set Point"
after 1000
set code [catch "GPIODigitalSet $socketID GPIO3.DO 1 5"]
if {$code != 0} {
DisplayErrorAndClose $socketID $code "GPIODigitalSet"
return
}
puts stdout "Holding Set Point"
after 2500
```

 # Move up Z axis for correction purpose due to work piece bending

```
puts stdout "Moving Z axis up  by 0.200 mm "
set code [catch "PositionerSGammaParametersSet $socketID XYZ.Z 0.1 400 0.001
0.001"]
if {$code != 0} {
DisplayErrorAndClose $socketID $code "PositionerSGammaParametersSet"
return
}
set code [catch "GroupMoveRelative $socketID XYZ.Z -0.200"]
if {$code != 0} {
DisplayErrorAndClose $socketID $code "GroupMoveRelative"
```

```
return
}
```

 # Find the Start position value of Z axis

```
set code [catch "GroupPositionCurrentGet $socketID XYZ.Z  Z2"]
if {$code != 0} {
DisplayErrorAndClose $socketID $code "GroupPositionCurrentGet"
return
}
puts stdout "Start position=$Z2"
set code [catch "GPIODigitalSet $socketID GPIO3.DO 2 6"]
if {$code != 0} {
DisplayErrorAndClose $socketID $code "GPIODigitalSet"
return
}
puts stdout " Controller o/p  Enabled "
after 1000
```

 # Iteration for measuring the non-machining force for the stiffness measurement purpose

```
if {$k == 1} {
puts stdout "power is turning off"
set code [catch "GPIOAnalogSet $socketID GPIO2.DAC4 0.00"]
if {$code != 0} {
DisplayErrorAndClose $socketID $code "GPIOAnalogSet"
return
}
}
```

 # Iteration for measuring the-machining force

```
if {$k == 2} {
puts stdout "power is turning on"
set code [catch "GPIOAnalogSet $socketID GPIO2.DAC4 2.00"]
if {$code != 0} {
DisplayErrorAndClose $socketID $code "GPIOAnalogSet"
return
}
}
```

```
# Iteration for measuring the final drilling depth

if {$k == 3} {
puts stdout "power is turning off"
set code [catch "GPIOAnalogSet $socketID GPIO2.DAC4 0.00"]
if {$code != 0} {
DisplayErrorAndClose $socketID $code "GPIOAnalogSet"
return
}
}
puts stdout " You have 1.5 seconds, Position Controller is enabled"
after 150
```

```
#Initializing Data Gathering function

puts stdout "Gathering Start"

set code [catch "EventExtendedConfigurationTriggerSet $socketID
XYZ.Z.SGamma.MotionStart 0 0 0 0"]
if {$code != 0} {
DisplayErrorAndClose $socketID $code "EventExtendedConfigurationTriggerSet"
return
}
set code [catch "GatheringReset $socketID "]
if {$code != 0} {
DisplayErrorAndClose $socketID $code "GatheringReset"
return
}
set code [catch "GatheringConfigurationSet $socketID  XYZ.Z.CurrentPosition
GPIO2.ADC1  GPIO2.ADC2 GPIO2.ADC3  GPIO2.ADC4"]
if {$code != 0} {
DisplayErrorAndClose $socketID $code "GatheringConfigurationSet"
return
}
set code [catch "EventExtendedConfigurationTriggerSet $socketID
XYZ.Z.SGamma.MotionStart 0 0 0 0"]
if {$code != 0} {
DisplayErrorAndClose $socketID $code "EventExtendedConfigurationTriggerSet"
return
}
set code [catch "EventExtendedConfigurationActionSet $socketID GatheringRun 22000
1000 0 0"]
if {$code != 0} {
DisplayErrorAndClose $socketID $code "EventExtendedConfigurationActionSet"
return
```

```
}
set code [catch "EventExtendedStart $socketID arg1"]
if {$code != 0} {
DisplayErrorAndClose $socketID $code "EventExtendedStart"
return
}
```

 # Moving Z down axis for non-machining iteration

```
if {$k == 1} {
puts stdout "Starting to move down with constant Velocity to find the touching surface"
puts stdout "Moving 0.090 mm down "
set code [catch "PositionerSGammaParametersSet $socketID XYZ.Z 0.010 400 0.001
0.001"]
if {$code != 0} {
DisplayErrorAndClose $socketID $code "PositionerSGammaParametersSet"
return
}
set code [catch "GroupMoveRelative $socketID XYZ.Z 0.080"]
if {$code != 0} {
DisplayErrorAndClose $socketID $code "GroupMoveRelative"
return
}
puts stdout "Done finding the touching surface for hole  $m.$k"
}
```

 # Moving Z down axis for actual machining iteration

```
if {$k == 2} {
puts stdout "Starting to Drill with constant Velocity"
puts stdout "Moving 0.300 mm down "
set code [catch "PositionerSGammaParametersSet $socketID XYZ.Z 0.001 400 0.001
0.001"]
if {$code != 0} {
DisplayErrorAndClose $socketID $code "PositionerSGammaParametersSet"
return
}
set code [catch "GroupMoveRelative $socketID XYZ.Z 0.300"]
if {$code != 0} {
DisplayErrorAndClose $socketID $code "GroupMoveRelative"
return
}
```

```
puts stdout "Done with drilling hole no = $m.$k"
}
```

```
# Moving Z down axis for finding final drilling depth iteration

if {$k == 3} {

puts stdout "Starting to move down with constant Velocity to find the depth of the hole"
puts stdout "Moving 0.010 mm down "
set code [catch "PositionerSGammaParametersSet $socketID XYZ.Z 0.010 400 0.001
0.001"]
if {$code != 0} {
DisplayErrorAndClose $socketID $code "PositionerSGammaParametersSet"
return
}
set code [catch "GroupMoveRelative $socketID XYZ.Z 0.010"]
if {$code != 0} {
DisplayErrorAndClose $socketID $code "GroupMoveRelative"
return
}
puts stdout "Done finding the touching surface for hole  $m.$k"
}
```

```
# Stop and gathering data save function

set code [catch "GatheringStopAndSave $socketID "]
if {$code != 0} {
DisplayErrorAndClose $socketID $code "GatheringStopAndSave"
return
}
puts stdout "Gathering Stop and Saving Data"
puts stdout "Power Turning Off"
set code [catch "GPIOAnalogSet $socketID GPIO2.DAC4 0"]
if {$code != 0} {
DisplayErrorAndClose $socketID $code "GPIOAnalogSet"
return
}
```

```
puts stdout " Controller is disabled and you can save the Simulink Data"

set code [catch "GPIODigitalSet $socketID GPIO3.DO 2 0"]
if {$code != 0} {
```

```
DisplayErrorAndClose $socketID $code "GPIODigitalSet"
return
}
puts stdout " Controller o/p  Disabled "
after 1000
```

```
#Movin up the Z axis

set code [catch "PositionerSGammaParametersSet $socketID XYZ.Z 1 400 0.001 0.001"]
if {$code != 0} {
DisplayErrorAndClose $socketID $code "PositionerSGammaParametersSet"
return
}
set code [catch "GroupMoveRelative $socketID XYZ.Z -3"]
if {$code != 0} {
DisplayErrorAndClose $socketID $code "GroupMoveRelative"
return
}
puts stdout "The $m th hole has been finished"
puts stdout " you have 10 seconds remaining, please Save your data and get ready for the
next activity"
after 5000
```

```
#Change the gathered file name

set new_name //Admin//Public//$m.dat
puts stdout "$new_name"
file copy -force -- //Admin//Public//Gathering.dat $new_name
puts stdout " Copied  $m file of saved data"
incr m
}
```

```
#Moving X axis left for the next channel

puts stdout "Move X axis to drill the next hole"
set code [catch "PositionerSGammaParametersSet $socketID XYZ.X 3 400 0.1 0.1"]
if {$code != 0} {
DisplayErrorAndClose $socketID $code "PositionerSGammaParametersSet"
return
                }
set code [catch "GroupMoveRelative $socketID XYZ.X 5"]
if {$code != 0} {
```

```
DisplayErrorAndClose $socketID $code "GroupMoveRelative"
return
 }
```

```
#Moving Y axis Front for the next channel

puts stdout "Move Y axis to drill the next hole"

set code [catch "PositionerSGammaParametersSet $socketID XYZ.Y 3 400 0.1 0.1"]
if {$code != 0} {
DisplayErrorAndClose $socketID $code "PositionerSGammaParametersSet"
return
                        }
set code [catch "GroupMoveRelative $socketID XYZ.Y -2"]
if {$code != 0} {
DisplayErrorAndClose $socketID $code "GroupMoveRelative"
 return
                    }
}
```

```
# If end of all iterations moving all axis back to origin
 if {$i==10} {
puts stdout "Move X axis Back to origin"
set code [catch "PositionerSGammaParametersSet $socketID XYZ.X 3 400 0.001 0.001"]
if {$code != 0} {
DisplayErrorAndClose $socketID $code PositionerSGammaParametersSet"
return
                        }
set code [catch "GroupMoveAbsolute $socketID XYZ.X -12"]
if {$code != 0} {
DisplayErrorAndClose $socketID $code "GroupMoveAbsolute"
return
                    }
set code [catch "PositionerSGammaParametersSet $socketID XYZ.Y 3 400 0.001 0.001"]
if {$code != 0} {
DisplayErrorAndClose $socketID $code "PositionerSGammaParametersSet"
return
                        }
set code [catch "GroupMoveAbsolute $socketID XYZ.Y 4"]
if {$code != 0} {
DisplayErrorAndClose $socketID $code "GroupMoveAbsolute"
return
                    }
```

```
puts stdout "Moving Y axis towards the Origin"

}
```

```
set code [catch "GPIODigitalSet $socketID GPIO3.DO 1 6"]
if {$code != 0} {
DisplayErrorAndClose $socketID $code "GPIODigitalSet"
return
}
```

```
puts stdout ">>>> Constant Velocity Feed Drilling for 10 holes, using SACE technology
has  been successfully finished"


# Close TCP socket
TCP_CloseSocket $socketID
```

Name of file: findzero.tcl

Purpose: Program to find zero position (work-piece surface touching at 4 V position)

```
proc FindZero {socketID Z} {
puts "start FindZero"
upvar $Z Zfinal
puts stdout "Searching for the glass surface until position at 4 V is found"

# Change velocity to slow one
set code [catch "PositionerSGammaParametersSet $socketID XYZ.Z 0.2 400 0.001
0.001"]
if {$code != 0} {
DisplayErrorAndClose $socketID $code "PositionerSGammaParametersSet"
return
}

# Configure Event
set code [catch "EventExtendedConfigurationTriggerSet $socketID
GPIO2.ADC1.ADCLowLimit 4.8 0 0 0 XYZ.Z.SGamma.MotionState 0 0 0 0"]
if {$code != 0} {
DisplayErrorAndClose $socketID $code "EventExtendedConfigurationTriggerSet"
```

```
return
 }
set code [catch "EventExtendedConfigurationActionSet $socketID XYZ.MoveAbort 0 0
0 0" ]
if {$code != 0} {
DisplayErrorAndClose $socketID $code "EventExtendedConfigurationActionSet"
return
}

# Start event
set code [catch "EventExtendedStart $socketID EvID"]
if {$code != 0} {
DisplayErrorAndClose $socketID $code "EventExtendedStart"
return
}

# Start Z motion to touch the glass surface
set code [catch "GroupMoveRelative $socketID XYZ.Z 5"]
if {$code != 0} {
if {$code == -27} {
puts stdout "Glass surface detected"
} else {
puts stdout "ERROR Glass surface not detected"
DisplayErrorAndClose $socketID $code "FindZero"
return -1
                }
}

# Gets the surface position at 4 V
set code [catch "GroupPositionCurrentGet $socketID XYZ.Z  Zfinal"]
if {$code != 0} {
DisplayErrorAndClose $socketID $code "GroupPositionCurrentGet"
return
 }
set code [catch "EventExtendedRemove $socketID $EvID"]
if {$code != 0} {
DisplayErrorAndClose $socketID $code "EventExtendedRemove"
return
puts stdout "Glass surface detected at Z=$Zfinal"
}
```

Appendix C

Pictures and diagrams

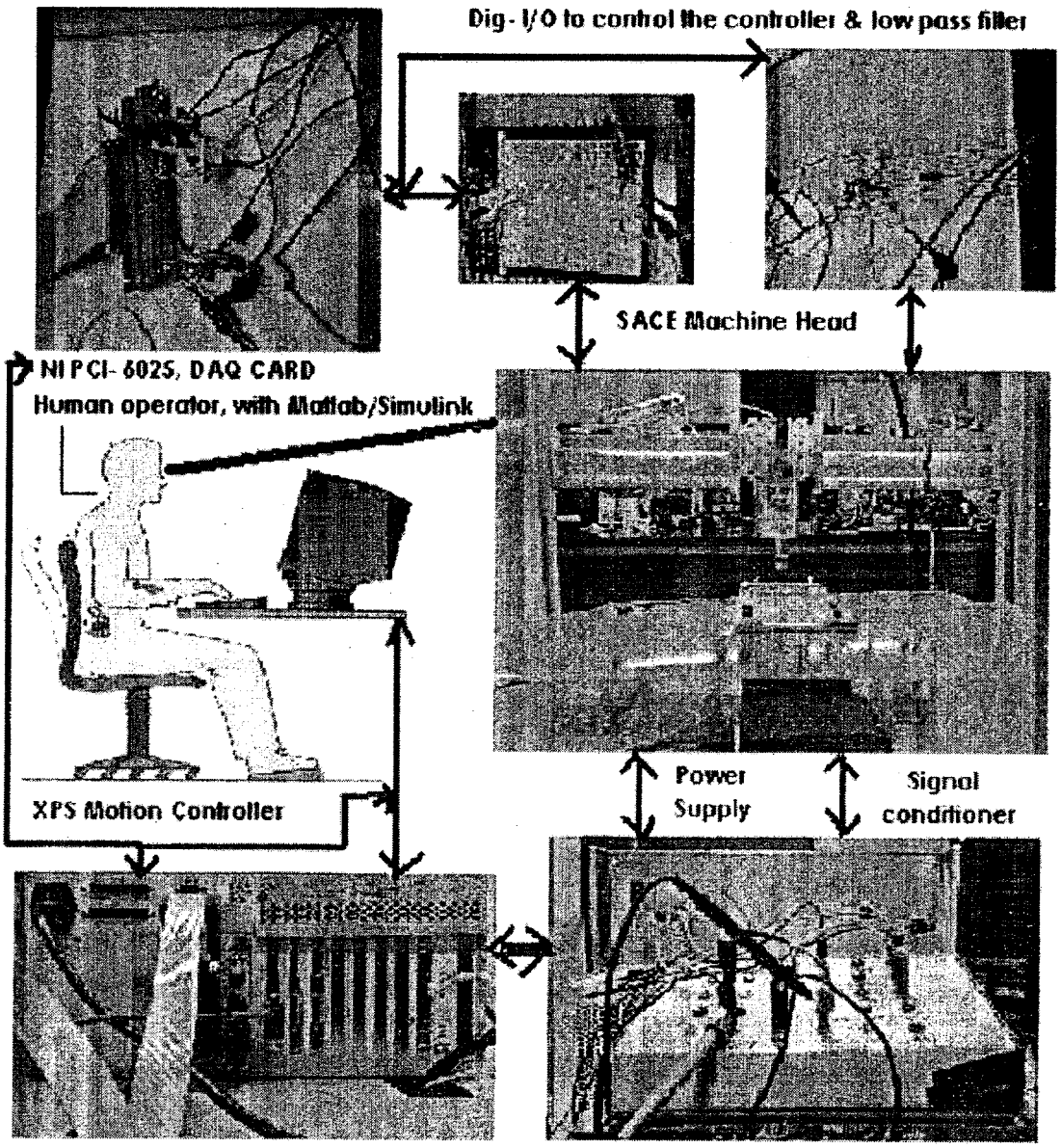

Experiment setup for SACE's Constant velocity Drilling (Courtesy Concordia University EV-014.205)

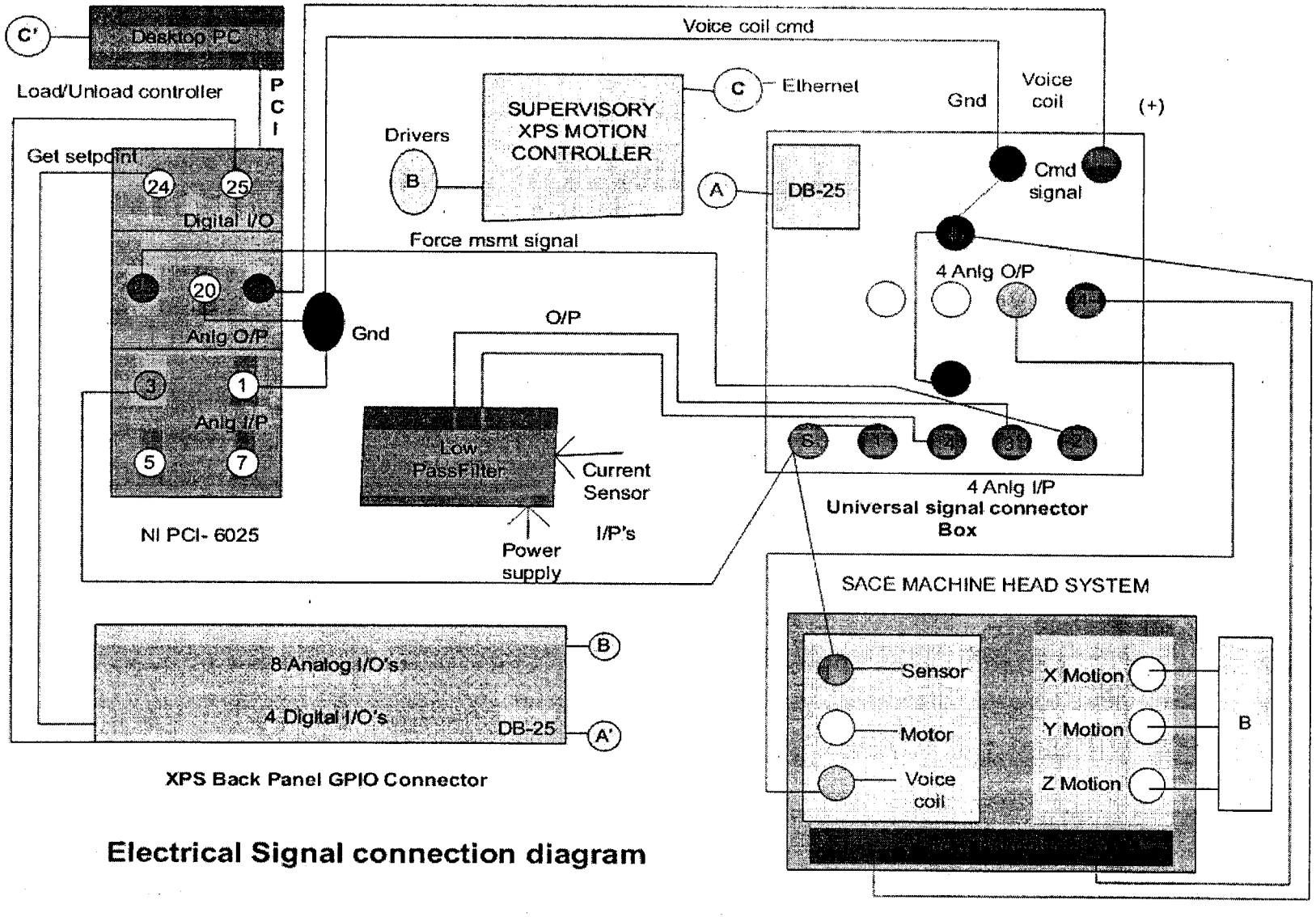

Electrical Signal connection diagram